

**Measurement of advection and surface-atmosphere  
exchange in complex terrain.**

**Kevin H. Jones**



**Thesis submitted for the degree of Master of Philosophy  
The University of Edinburgh**

**2008**

## **Declaration**

I declare that this thesis represents my own work, and that where the work of others has been used it has been duly accredited. Chapter 2 of this thesis is based on a collaborative experiment with CSIRO, Australia, which resulted in the publication of Leuning *et al.* (2008), (see appendix to this thesis).

Kevin H. Jones

October 2008

## **Acknowledgements**

Many thanks for helpful discussions and advice during the work for this thesis are due to:

Prof. John Moncrieff

Dr. Ray Leuning

Dr. Rob Clement

&

Prof. John Finnigan

This research was supported by NERC grant NER/S/J/2004/13118.

Thanks also to my parents Nanette Betty Jones and Haydn Towyn Jones, without the moral support of which the completion of this project would not have been possible.

## Abstract

Accurate observations of the carbon cycle are essential as inputs to global climate models. Observations made by the micrometeorological technique of eddy covariance, whilst widespread, may be incorrect if air is advected away from below the sensor system. This is potentially a serious issue for FLUXNET, a global network of eddy flux sites. The approach in this thesis to investigate this problem was twofold:

A full micrometeorological mass balance using an instrumented 50 m long by 50 m wide by 6 m high Cartesian control volume (CV) covering the understorey vegetation of a 40 m high Eucalyptus forest was carried out; situated adjacent to the Tumbaruma eddy covariance site in Australia. At night positive (into the atmosphere) advection fluxes caused by down-slope katabatic drainage within the forest trunk space, dominated the CO<sub>2</sub> flux budget of the CV, with both vertical and horizontal advection terms having predominantly positive values. The nighttime estimates of advection were subject to large systematic errors that were of the same order of magnitude as the advection signal. Nevertheless, the nocturnal respiration flux of the understorey vegetation was clearly resolved by the diurnal full mass balance flux curve that resulted from the experiment, having a typical value of 5  $\mu\text{mol m}^{-2} \text{s}^{-1}$ .

A second experiment carried out at the Griffin forest in Scotland demonstrated the presence of sub-canopy katabatic/gravity flows at night that would be likely to cause scalar advection resulting in underestimation of the nocturnal respiration flux of CO<sub>2</sub>. Finally, it is recommended that the micrometeorological mass balance technique should not be deployed across FLUXNET because of financial cost and issues of systematic error.



Copyright of this thesis is retained by the author and The University of Edinburgh. Ideas contained in this dissertation remain the intellectual property of the author and their supervisors, except where explicitly otherwise referenced.

All rights reserved. The use of any part of this dissertation reproduced, transmitted in any form or by any means, electronic, mechanical, photocopying, recording, or otherwise or stored in a retrieval system without the prior written consent of the author and The University of Edinburgh is not permitted.

# Table of Contents

<b>Declaration</b>	.....	<b>i</b>
<b>Acknowledgements</b>	.....	<b>ii</b>
<b>Abstract</b>	.....	<b>iii</b>
<b>Table of Contents</b>	.....	<b>v</b>
<b>1 The advection problem in eddy flux measurements</b>	.....	<b>1</b>
1.1	Introduction	1
1.2	The eddy covariance flux method	4
1.3	Missing fluxes at eddy covariance sites	10
1.4	Energy balance closure and mechanisms for missing fluxes	12
1.5	Measuring the advection flux terms	15
1.6	Canopy flow models for complex terrain	21
1.7	Data assimilation models	28
1.8	Chapters 2 and 3 of this thesis	29
<b>2 The Tumbarumba Advection Experiment</b>	.....	<b>32</b>
2.1	Experimental Setting	32
2.1.1	Methodology	34
2.2	Experimental results	41
2.2.1	The eddy flux ‘lid’ calculation for the control volume	49
2.2.2	The discovery of a maxima in the nighttime wind profile	57
2.2.3	Other results from the CV faces and 6 m central mast	64
2.2.4	Vertical velocities within the CV	67
2.2.5	The final CO <sub>2</sub> flux components for the CV	70

2.3	Conclusions	75
<b>3</b>	<b>Griffin forest wind transect &amp; profile experiments</b>	<b>77</b>
3.1	Introduction	77
3.2	Site description	79
3.3	Experimental setup and results	81
3.3.1	The horizontal transect experiment	81
3.3.2	Transect experiment results and discussion	84
3.3.3	The tower profile experiment	90
3.3.4	The profile experiment results	92
3.3.5	Discussion of the profile experiment results	100
3.3.6	The tower profile cross correlation study	101
3.3.7	Discussion of the profile cross-correlation study	119
3.4	Conclusions	120
	<b>Conclusions</b>	<b>123</b>
	<b>References</b>	<b>127</b>
	<b>Appendix Leuning <i>et al.</i> (2008)</b>	<b>133</b>

# 1 The advection problem in eddy flux measurements

## 1.1 Introduction

Rising atmospheric CO<sub>2</sub> concentrations in the earth's atmosphere from anthropogenic sources are now an established fact (Keeling & Whorf, 2004), as is the likelihood that they will cause environmentally harmful effects (Pachauri *et al.* 2007). Houghton *et al.* (1990) showed that there was likely to be an unaccounted for or 'missing' sink for CO<sub>2</sub> on land in the earth's environment, since not all the annual anthropogenic emissions of CO<sub>2</sub> were absorbed by the oceans or went into the atmosphere. This encouraged the world's scientific community to attempt to quantify the earth's carbon cycle by direct measurement

FLUXNET is one such initiative (Baldochi *et al.* 2001), taking the form of a global network of 'eddy covariance towers', measuring turbulent CO<sub>2</sub> exchange fluxes between ecosystems and the atmosphere by using the micrometeorological technique of eddy covariance (Moncrieff *et al.* 1997). A review by Houghton (2003) has placed the likely location of the unaccounted for sink in the northern mid-latitudes with a particular emphasis on temperate forests. FLUXNET exists to try and locate the missing sinks or identify the major sources of carbon on land.

For more than twenty years the eddy covariance method (also referred to as the eddy correlation method) has been the preferred micrometeorological technique of measuring fluxes of scalar quantities such, as carbon dioxide (CO<sub>2</sub>) and water vapour, from vegetated surfaces in to the atmosphere, although the technique dates back to the work of Swinbank (1951). The exchange rate of CO<sub>2</sub> across the interface between the atmosphere and a plant canopy is measured as the covariance between fluctuations in vertical wind velocity and CO<sub>2</sub> mixing ratio (Baldochi 2003). The interface in question is a notional horizontal flux plane at the same height as the eddy covariance system, which usually consists of a 3 component ultrasonic anemometer and the sampling point for an infrared gas analyser (IRGA), as described by Moncrieff *et al.* (1997), and illustrated in figure 1.1. This equipment is usually situated on a mast or tower above the ecosystem under investigation.



**Figure 1-1** Eddy covariance sensor, consisting of a 3-axis ultrasonic anemometer and open path infrared gas analyser (IRGA), capable of measuring turbulent fluxes of carbon dioxide, latent heat, sensible heat and momentum. *Photo courtesy of S.Dengel.*

The first field studies over relatively long periods using the method took the form of field campaigns in the mid 1980s, initially conducted over short vegetation such as grass or crops during the summer in order to estimate CO<sub>2</sub> uptake during the growing season (Anderson *et al.* 1984). The first eddy covariance CO<sub>2</sub> flux measurements over a deciduous forest were done by Verma *et al.* (1986). These early campaigns were limited in duration due to instrumental limitations such as the inability of the ultrasonic anemometers used to operate during rain, and problems of maintaining instrumental calibration over long periods. The 1990s saw these problems substantially solved and, combined with the availability of cheap portable data storage, led to extended experiments in tropical and temperate forests and for periods of a growing season or longer. Examples of these being Grace *et al.* (1996), who measured 10 weeks of eddy flux data on a tower above the Amazon forest in Brazil, scaling up the results to estimate the annual carbon balance of the tropical forest ecosystem, and Wofsy *et al.* (1993) who measured CO<sub>2</sub> fluxes from a mixed deciduous forest in Massachusetts, USA, for a period of almost 2 years, estimating annual carbon balance for a temperate forest. The BOREAS study (Sellers *et al.* 1997) included the use of the eddy covariance method to study boreal ecosystems, including forests, at several sites during an international collaborative experiment in Canada, over several years.

The success of these finite duration experiments inspired researchers to consider a global network of eddy covariance sites continuously measuring Earth's ecosystems, in much the same way as weather stations monitor the world's weather. The components of this global network were organised on a regional basis, with the Euroflux/CarboEurope network being initiated in 1996 (Aubinet *et al.* 2000), and the AmeriFlux network in 1997 (Running *et al.* 1999). Other regional networks followed, including OzFlux (Australia), ChinaFLUX, AsiaFlux and Fluxnet-Canada. In 1998 the FLUXNET project was set up by the American National Aeronautics and Space Administration (NASA), in order to offer worldwide coordination and a data repository for these regional networks (Baldocchi *et al.* 2001). As of the end of March 2008 there were 543 eddy flux sites contributing to the FLUXNET project (FLUXNET website 2008), providing data from a wide range of land ecosystem

types, spread around the globe, albeit with a rather *ad hoc* spatial distribution (Baldocchi *et al.* 2001).

There are some still outstanding issues concerning CO<sub>2</sub> flux estimates obtained by eddy flux sites, especially those fluxes measured over tall vegetation such as forests, that must be resolved before FLUXNET can be considered a global operational network in the manner of the International Weather Organisation (IMO), weather station network (Baldocchi *et al.* 2001, Baldocchi 2003). FLUXNET at present provides outputs the validity of which are still, to some extent, open to debate by members of the scientific community. Methodological standardisation between eddy flux site operators can help resolve some of these issues (Aubinet *et al.* 2000, Baldocchi *et al.* 2001, Baldocchi 2003). However, some problems concerning the eddy flux method are still subjects of active scientific research, and until they are resolved standardisation of methods across eddy flux site networks cannot be completed.

A particular outstanding problem concerning the eddy flux method is the so called ‘advection problem’ (Feigenwinter *et al.* 2004) which can occur at any eddy flux site that is not topographically flat and level (although even at sites considered ‘ideal’, advection may result as a function of passing large convective cells), and can be particularly severe at forested sites. In order to understand this problem and possible solutions, it is first necessary to describe the eddy flux method in detail.

## **1.2 The eddy covariance flux method**

Moncrieff *et al.* (1997) demonstrate that the turbulent flux  $F_c$ , of a scalar with concentration  $c$ , through the horizontal flux plane coincident with the eddy covariance sensors (sonic and IRGA), is given by the working equation for eddy covariance (equation 1.1):

$$F_c = \overline{w'c'} + \text{correction terms} \quad (1-1)$$

where  $w$  is the vertical wind velocity, and standard Reynold’s notation (Reynolds 1895) is used with prime denoting departure from the mean, and overbar representing

the time averaging operator. A typical averaging period would be an hour, giving a series of 24  $F_c$  flux density values over a diurnal cycle. A positive  $F_c$  value indicates transport of the scalar from the ecosystem into the atmosphere. The ‘correction terms’ in equation 1.1 include one to correct for changes in air density (Webb *et al.* 1980), required if  $c$  is measured as a concentration or partial pressure, rather than a mixing ratio. Other correction terms include those concerning the response of the eddy covariance system (sonic, IRGA and other system components). These corrections are described by Moncrieff *et al.* (1997).

Use of the eddy covariance equation (equation 1.1) gives satisfactory estimations of net ecosystem exchange (NEE) of CO<sub>2</sub> over short vegetation such as crops and grasslands, situated in flat areas. However, to attempt the calculation of NEE over tall vegetation, such as forests, other factors must be taken into account.

Equation 1.2 is adapted from Feigenwinter *et al.* (2004), and provides a more generalised description for using the eddy covariance flux to estimate the NEE of CO<sub>2</sub> between any given ecosystem and the atmosphere above:

$$NEE = \int_0^h \frac{\partial \bar{c}(z)}{\partial t} dz + \overline{w'c'}(h) + \int_0^h \bar{w}(z) \frac{\partial \bar{c}(z)}{\partial z} dz + \int_0^h \left( \bar{u}(z) \frac{\partial \bar{c}(z)}{\partial x} + \bar{v}(z) \frac{\partial \bar{c}(z)}{\partial y} \right) dz \quad (1-2)$$

where  $u$ ,  $v$  and  $w$  are wind velocity components in the  $x$ ,  $y$  and  $z$  directions, respectively of the Cartesian volume (CV) shown in figure 2.1. The perpendicular height above the ground of the eddy covariance sensor, which consists of a 3 axis ultrasonic anemometer and IRGA (see figure 1.1), is represented by  $h$ , which is also the height of the CV. Height within the CV is represented by  $z$ , and  $t$  represents time. The value  $c$  is the CO<sub>2</sub> concentration in  $\mu\text{mol m}^{-3}$ . It should be noted that mole fraction (mixing ratio) values of CO<sub>2</sub> relative to dry air (units,  $\mu\text{mol mol}^{-1}$ , often written as ppmv) common in the literature, would have to be multiplied by the mean molar concentration of dry air within the CV (units,  $\text{mol m}^{-3}$ ), to get  $c$  values in units of  $\mu\text{mol m}^{-3}$  suitable for use in equation 1.2. The units of NEE, the measured CO<sub>2</sub> flux from the ecosystem into the air are  $\mu\text{mol m}^{-2}\text{s}^{-1}$ .

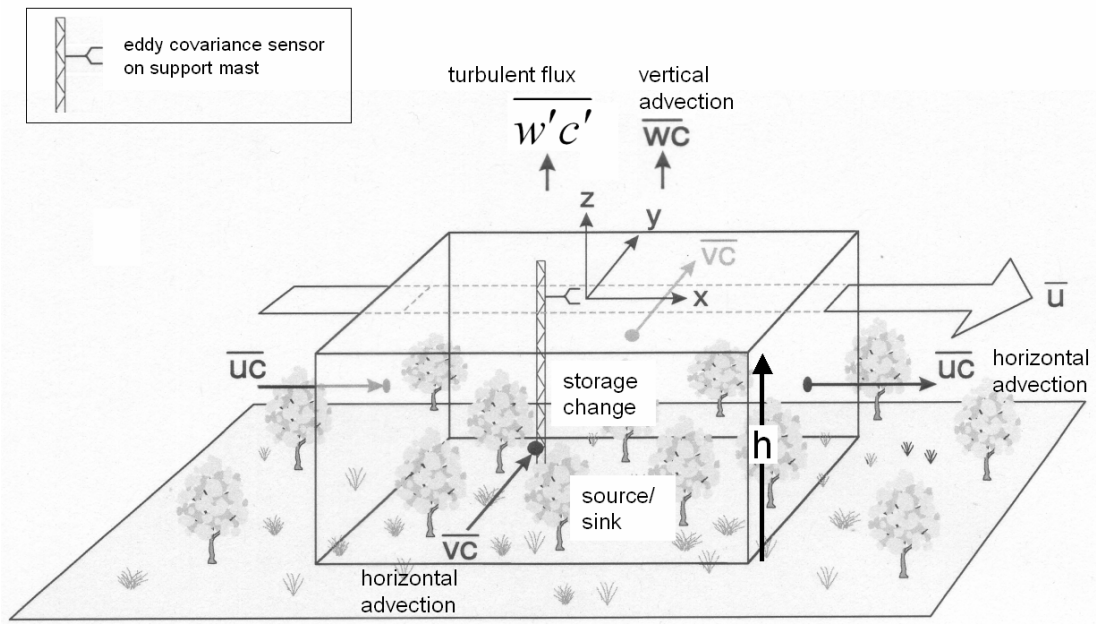


Referring to figure 1.2, the terms on the right hand side (RHS) of equation 1.2 can be described as follows:

- I Change in storage of the scalar  $c$  below the height  $h$ , during the averaging period.
- II The vertical turbulent flux of  $c$ , as given by  $F_c$  in equation 1.1.
- III The vertical advection flux of  $c$  through the lid of the CV (at height  $h$ ), which exists if a residual mean vertical wind velocity,  $\bar{w}$ , is present over the averaging period.
- IV The net horizontal advection flux of  $c$  through the side walls of the CV. This can be calculated as the sum of horizontal flux divergences across the CV, in the  $x$  and  $y$  directions respectively.

With regard to term IV of equation 1.2 for the net horizontal advection flux (often referred to as simply the ‘horizontal advection’ in the literature), it is quite possible for a significant horizontal advection flow of scalar rich air (say a high CO<sub>2</sub> concentration) to be flowing horizontally across the CV and for term IV to be zero. This will be the case if the horizontal advection flux of CO<sub>2</sub> entering one side of the CV is the same as that leaving on the opposite side (note: this would require no respiration flux within the CV), resulting in no horizontal flux divergence across the CV, and hence zero net horizontal advection flux.

In the context of equation 1.2 and figure 1.2, the ideal forest site over which to measure NEE of CO<sub>2</sub> using the eddy covariance method, would be topographically horizontal, homogeneous and infinite in extent. Under such conditions the vertical and horizontal advection terms (III and IV) should be zero, and NEE values for each time averaging period can be calculated using just terms I and II, the change in storage term (storage term), and the turbulent flux from eddy covariance.



term I	term II	term III	term IV
$NEE = \int_0^h \frac{\partial \bar{c}(z)}{\partial t} dz + \overline{w'c'}(h) + \int_0^h \bar{w}(z) \frac{\partial \bar{c}(z)}{\partial z} dz + \int_0^h \left( \bar{u}(z) \frac{\partial \bar{c}(z)}{\partial x} + \bar{v}(z) \frac{\partial \bar{c}(z)}{\partial y} \right) dz$			
storage change	turbulent flux	vertical advection	horizontal advection

**Figure 1-2** Cartesian volume (CV) for an eddy covariance mast situated above a forest ecosystem.  $u$ ,  $v$  and  $w$ , are the wind components in the  $x$ ,  $y$  and  $z$  directions.  $c$  is the scalar concentration and  $h$  is the height of the CV (and eddy covariance sensor). Reynold's notation is used to indicate means taken over the averaging period. *Schematic courtesy of Finnigan, J., & Leuning, R., (pers comm.). Equation modified from Feigenwinter et al. (2004).*

The storage term is calculated from the differences in CO<sub>2</sub> profiles measured within the CV at the beginning and end of the averaging period (Finnigan 2006).

Consequently, the support tower of the eddy flux sensors (sonic anemometer and IRGA) at eddy flux sites are often equipped to measure CO<sub>2</sub> concentration profiles from ground level up to the sensor height,  $h$ . The resulting NEE values for each averaging period will then be formally correct, allowing graphs of diurnal NEE exchange between the ecosystem and atmosphere to be constructed. The storage term is usually greatest at night under stable atmospheric conditions when there is a tendency for CO<sub>2</sub> concentrations to build up within the canopy. At dawn the onset of solar heating tends to break down stability within the forest canopy, resulting in ‘flushing’ of stored CO<sub>2</sub> from the canopy into the atmosphere above, through the lid of the CV (height  $h$ ). This flushing is especially efficient if accompanied by windy conditions. As a consequence of this flushing effect, annual measures of NEE over forests are not significantly affected by the storage term, since its annual mean value should be close to zero. Thus, researchers interested in only annual NEE, or carbon sequestration at a forest site over a period of months or years, will often ignore it and use just equation 1.1 to get their NEE estimate.

The advection terms of equation 1.2 will need to be taken in to account if the forest site is somehow ‘non ideal’, either if it is not horizontal and flat, or if the forest is non homogeneous in the vicinity of the eddy covariance tower. By ‘in the vicinity’ one means within the ‘flux footprint’ of the of the eddy covariance sensors at the top of the tower. The flux footprint concept is discussed by Schmid (1994) and describes the ‘catchment area’ of forest that is ‘seen’ by the eddy covariance sensors. The size of the flux footprint is proportional to the tower height,  $h$ , the wind speed and is a function of atmospheric stability. Also the orientation and length of the flux footprint will vary as the wind direction and strength vary at the flux tower site. The choice of  $h$ , the height of the tower is determined by aerodynamic considerations relating to the forest canopy height, such that the eddy covariance sensors (sonic and IRGA) must be situated in the so called ‘constant flux layer’ above the canopy. As a consequence, if a heterogeneity such as a clearing or change in vegetation type falls within the flux footprint of the tower, then a horizontal flux divergence of CO<sub>2</sub> may

come into existence across the CV (see figure 1.2), resulting in a finite net horizontal advection flux (term IV in equation 1.2). The magnitude of the net horizontal advection flux would tend to be larger, the closer the clearing or change in vegetation was to the base of the tower. Marcolla *et al.* (2005) were able to measure such a net horizontal advection flux of CO<sub>2</sub> caused by a forest edge. Unfortunately, current eddy covariance towers reporting to the FLUXNET network are not equipped to measure the data required to calculate the horizontal advection term. Such data would take the form of CO<sub>2</sub> concentration profiles measured at the faces or corners of the CV, plus a vertical profile of horizontal wind speed within the CV, both from ground level up to the height,  $h$ .

Lee (1998) published an approximate method for estimating the vertical flux term (term III in equation 1.2) at an eddy covariance tower, using just the standard instrumentation normally used to obtain the eddy flux (term II, eq. 1.2) and storage term (term I, eq. 1.2), i.e. the sonic anemometer and IRGA, and tower CO<sub>2</sub> concentration profile respectively. Lee uses the implicit assumption that the vertical advection velocity,  $\bar{w}$ , will decrease linearly from the top of the CV at height,  $h$ , down to zero at ground level. Lee's approximation to vertical advection is given in equation 1.3:

$$\overline{w_h}(\overline{c_h} - \langle \bar{c} \rangle) \quad (1-3)$$

where  $\overline{w_h}$  and  $\overline{c_h}$  are temporal means of vertical velocity and CO<sub>2</sub> concentration measured over the averaging period, at the sonic anemometer and IRGA at height,  $h$ , and  $\langle \bar{c} \rangle$  represents the vertically integrated values of  $\bar{c}$  measured on the tower CO<sub>2</sub> profile. Equation 1.3 can be used to replace term III in equation 1.2 and has been used in several studies involving advection (Feigenwinter *et al.* 2004, Marcolla *et al.* 2005), however the method is the subject of controversy in the literature and has been criticised by Finnigan (1999). Leuning *et al.* (2008) carried out an experiment involving a fully instrumented control volume (CV) and found that Lee's equation (eq. 1.3) gave results favourably comparable to a vigorous numerical implementation of term III in equation 1.2, provided that the vertical advection

velocity,  $\overline{w_h}$ , was estimated using the horizontal divergence method of Vickers and Mahrt (2006) and Heinesch *et al.* (2007).

### **1.3 Missing fluxes at eddy covariance sites**

Researchers such as Malhi *et al.* (1998) and Andreae *et al.* (2002) reported large uptakes CO<sub>2</sub> by the Amazonian tropical forest, indicating these forests were a larger sink of CO<sub>2</sub> than had been previously indicated by chamber measurements. Miller *et al.* (2004) discusses how these results indicating a large carbon sink, were probable due to a failure to account for an underestimation of forest respiration during calm nights. During such calm nights the formation of a stable layer beneath the eddy covariance sensor was leading to removal of CO<sub>2</sub> from the site by some process, probably advection (terms III and IV in equation 1.2).

Goulden *et al.* (1996) observed similar effects at a temperate forest (Harvard forest, USA) leading to a systematic underestimation of NEE values derived from eddy covariance (equation 1.1), caused by an underestimation of the nighttime respiration flux, in comparison with the daytime flux (photosynthesis and respiration). Goulden *et al.* (1996) noted that the eddy covariance flux (equation 1.1) was positively correlated with the friction velocity,  $u^*$ , despite there being no reason in plant physiology for respiration or photosynthesis to be correlated with this micrometeorological quantity. It was concluded that the true CO<sub>2</sub> flux out of the forest was being underestimated at low  $u^*$  (roughly corresponding to low wind speeds), and a  $u^*$  threshold was proposed based on where the eddy covariance flux versus  $u^*$  graph flattened out. For the Harvard forest for example, this threshold was 0.17 m s<sup>-1</sup> during the nighttime. For nocturnal  $u^*$  values less than this threshold and when data was missing, eddy covariance flux values were replaced by values derived from a plant respiration model and photosynthesis model, driven by measured soil temperature and photosynthetically active radiation (PAR), the model having been calibrated using fluxes measured above the  $u^*$  threshold.

Similar  $u^*$  threshold models are now used for many eddy covariance flux sites in the FLUXNET network, replacing eddy covariance and change in storage fluxes with modelled fluxes, when  $u^*$  drops below the threshold determined for the site, or when data is missing due to equipment failure.

The  $u^*$  threshold approach has been criticised for circularity, and the relatively arbitrary way in which the threshold is chosen, with its determination being impossible for some sites (Ruppert *et al.* 2006). If incorrectly applied at sites without a CO<sub>2</sub> profile to measure storage, the threshold approach can actually lead to serious over estimation of diurnal NEE, due to double counting of fluxes (Aubinet 2008).

A six year study of carbon sequestration at the Niwot Ridge forest flux site in the USA, carried out by Yi *et al.* (2008) indicated another flaw in the  $u^*$  approach. Namely, that  $u^*$  is measured at the top of the eddy covariance tower above the canopy using a sonic anemometer (see figure 1.1), but that on calm nights it is possible for stable (low  $u^*$ ) conditions to exist in the forest canopy, while  $u^*$  at the sonic anemometer is above the threshold. This leads to an underestimation of the nocturnal flux and an overestimate of carbon sequestration for the site.

Kutch *et al.* (2008) similarly found that for the Hainich forest in Germany,  $u^*$  threshold corrected flux values were less than NEE values indicated by bottom-up modelling and direct aerodynamic measurements of the advection terms, even in daytime when good mixing was expected.

During very stable conditions within a forest canopy, which can occur on a calm night, a condition known as intermittent turbulence can occur (Aubinet 2008). This consists of mostly calm conditions (low  $u^*$ ) associated with CO<sub>2</sub> storage within the canopy, punctuated by intermittent surges of turbulence known as intermittent turbulent events (ITEs), which are associated with high  $u^*$  and ejection of stored CO<sub>2</sub> from the canopy past the eddy covariance sensors. If the turbulent fluxes associated with such ITE storage ejections are included in the calibration of the

respiration models used to obtain fluxes below the  $u^*$  threshold, then a significant overestimation of nocturnal respiration flux can result.

Thus the  $u^*$  threshold method can significantly overestimate and significantly underestimate NEE, depending how it is applied or where the  $u^*$  value is measured.

A possible way out of this impasse is the so called ‘super-site’ (Ohkubo *et al.* 2007) where very extensive traditional field measurements of ecosystem fluxes (such as chamber measurements) are used to cross constrain the very best daytime eddy covariance flux data. Unfortunately, the ‘super-site’ approach is very manpower intensive and expensive, thus being unsuitable for the majority of FLUXNET sites.

Another alternative approach is to attempt to directly measure the missing fluxes aerodynamically, i.e. the vertical and horizontal advection terms, terms III and IV in equation 1.2. However, as we shall see later, this too is probably too manpower intensive and expensive for deployment generally across FLUXNET.

#### **1.4 Energy balance closure and mechanisms for missing fluxes**

The energy balance at Earth’s surface is often not closed in practise. Net radiation and ground heat flux typically exceed the total turbulent fluxes of sensible and latent heat by about 20% (Foken and Oncley 1995). This strongly suggests that other turbulent fluxes such as CO<sub>2</sub> measured at eddy covariance towers may suffer from a similar lack of closure that may manifest itself as ‘missing flux’. Foken (2008) reviewed publications concerning the energy balance closure problem from the past 20 years and came to the conclusion that the energy balance can probably only be closed on the larger landscape scale in heterogeneous landscapes. This is strongly suggestive of the existence of large-scale horizontal advective processes or large scale eddies transporting scalars away from eddy covariance towers.

Aubinet (2008) lists three principal processes as being likely for the underestimation of fluxes at eddy covariance sites, mostly at night.

- 1) Intermittent turbulent events (ITEs)

- 2) Land breezes
- 3) Gravity/katabatic flows

Intermittent turbulent events (ITEs), have been discussed earlier with respect to the  $u^*$  threshold. However, because of the short duration of ITEs they may not satisfy the stationarity requirement of the eddy covariance method and may require the use of variable length averaging periods to resolve the scalar fluxes they are transporting.

Land breezes are generated by a different process to gravity flows but have a similar effect in removing scalars from the vicinity of an eddy covariance tower by advection (Aubinet 2008), see equation 1.2, terms III and IV.

Gravity or katabatic type density flows are believed to be the most important mechanism for causing the ‘missing respiration flux’ at night, and is probably the most important factor in the underestimation of NEE when averaged over the whole diurnal cycle (Goulden *et al.* 2006, Belcher *et al.* 2008).

During nighttime, the atmospheric boundary layer is typically stably stratified, with a temperature inversion often existing within a few 10’s of metres of the surface (Belcher *et al.* 2008). This is especially true under anti-cyclonic conditions with clear skies and slack winds (Mahrt 1999). In hilly terrain the denser air at the bottom of the inversion can flow downhill under gravity to form a katabatic drainage flow. Mahrt (1981) has suggested that such drainage flows can form on slopes as low as 1 degree, and Belcher *et al.* (2008) demonstrate that for a forested slope the tendency for a drainage flow to form is dependant on overall slope length rather than slope angle, with the consequence that almost all forested land surfaces are potentially affected by horizontal advection of scalars at night (term IV in equation 1.2).

Katabatic flows within forests are often channelled by the trunk space below the canopy (Aubinet *et al.* 2003, Aubinet 2008), as was observed in the experiment carried out in the Tumbarumba forest, Australia, described in chapter 2 of this dissertation, and Leuning *et al.* (2008).



Belcher *et al.* (2008) describe the typical onset of a katabatic flow within a sloping forest at night as follows. After sunset the soil surfaces and foliage of the canopy cool by radiative cooling, hence cooling the air within the canopy itself, resulting in a collapse of turbulent mixing within the canopy. The resultant situation is cooler strongly stratified air within the canopy overlain by moderately stable warmer air above the canopy. The decoupling caused by the end of turbulent exchange stops heat being moved downwards by turbulence from the warmer upper layer, giving rise to acceleration in subsequent cooling by radiation. The final result is a deep, relatively dense stable layer within the canopy. This layer will flow down hill by gravity as a katabatic flow.

Assuming a homogenous forest of infinite extent, let us consider such a nocturnal katabatic flow flowing left to right with a constant velocity,  $\bar{u}$ , through the CV as shown in figure 1.2. Let us further assume that the collapse in turbulence in the forest canopy has completely decoupled the eddy covariance sensor at height,  $h$ , from the soil and vegetation respiration of the forest. The respiration flux will enter the katabatic flow as it crosses the CV causing an increase in CO<sub>2</sub> concentration,  $c$ , resulting in a higher advection flux ( $\bar{uc}$ ) leaving on the right-hand side of the CV than entered on the left-hand side. This will result in the entire respiration flux of the forest being removed from the forest by horizontal advection (see term IV in equation 1.2). In this particular case change in storage (eq. 1.2 term I) in the CV will be zero, as will the eddy covariance flux (eq. 1.2 term II) and vertical advection flux (eq. 1.2 term III). This extreme hypothetical example illustrates the effective manner in which a gravity flow can make the nocturnal respiration flux of a forest ‘go missing’.

The ultimate fate of CO<sub>2</sub> removed from the CV in the way just described, is to flow down slope to a low point such as a lake or river, where it will form a nocturnal ‘pool’ of CO<sub>2</sub> (Goulden *et al.* 2006, de Araujo *et al.* 2008). This pool will be mixed back into the atmospheric boundary layer during mid-morning by the onset of turbulent mixing. In geographical terms the distribution of these mixing ‘events’ can be thought of as being like isolated ‘chimneys’ or ‘walls’ within the landscape, such

that a randomly located eddy covariance tower is unlikely to encounter one. Thus the flux remains missing.

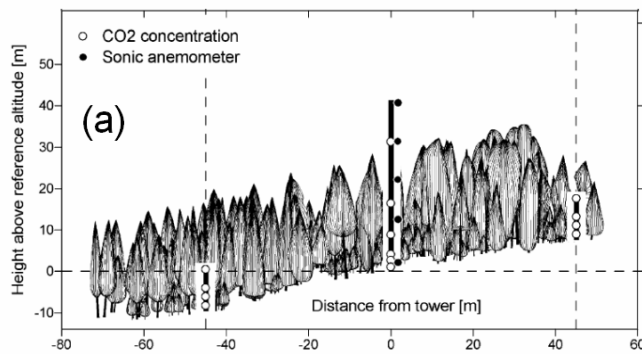
Referring again to figure 1.2 the horizontal flux divergence (eq. 1.2 term IV) across the CV will be increased if the wind accelerates across the box. Thus the horizontal flux divergence can be affected by the shape or curvature of the terrain surface around the eddy covariance tower or mast. The horizontal flux divergence can also be affected by heterogeneities within the forest such a nearby forest edge or change in vegetation type (Marcolla *et al.* 2005).

### **1.5 Measuring the advection flux terms**

Aubinet (2008) defines two distinct ways of overcoming the problem of the missing nocturnal respiration flux of CO<sub>2</sub>. Firstly there is the ‘filtering approach’ where problematic periods of eddy covariance data are removed and replaced by ‘good’ values, normally derived from some sort of respiration model. The  $u^*$  threshold method discussed earlier (Goulden *et al.* 1996) is the most widely used method of the filtering approach. The super-sites method (Ohkubo *et al.* 2007) can also be thought of as a filtering approach.

The other approach is the ‘correction approach’ where the missing fluxes are corrected for by direct measurement of the missing CO<sub>2</sub>. This means direct measurement of the vertical and horizontal advection terms in equation 1.2 (terms III and IV, respectively). Experiments to obtain these advection terms usually attempt to directly measure the advection fluxes through the faces of the CV shown in figure 1.2. As discussed earlier with reference to Leuning *et al.* (2008) this entails an experimental setup capable of measuring horizontal flux gradients. Figure 1.3 shows the experimental set-up for two recent advection experiments.

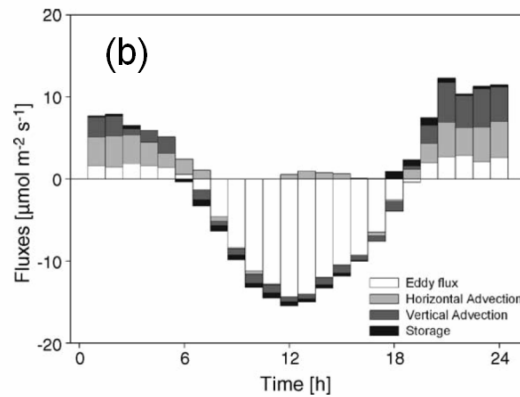
Figure 1.3a shows a side view of a 2D transect advection experiment done by Marcolla *et al.* (2005) in a spruce forest, near Renon, Italy, with a moderately steep topographic slope of 11 degrees. During nighttime stable conditions, gravity flows in the down slope direction (along the line of the transect) were the dominant form of airflow within the canopy, thus allowing the 2D approach to be used. The central



Renon (Italy)  
Norway spruce  
Italian Alps, 1730 m asl  
Slope 11 degrees

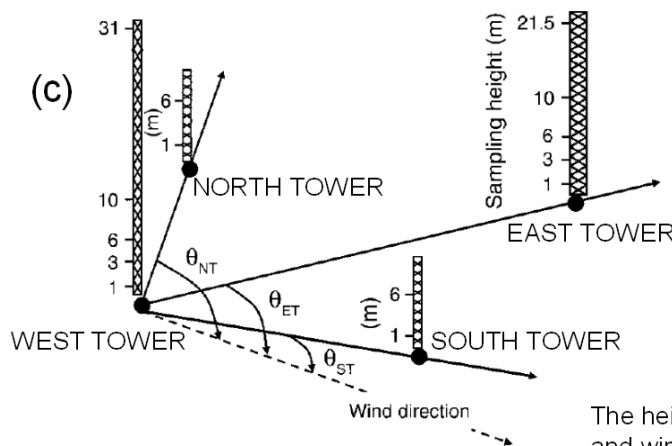
2D linear setup

Marcolla *et al.* 2005



Mean diurnal variation of eddy flux, horizontal and vertical advection flux and storage change, derived from 35 days of data.

Marcolla *et al.* 2005



Niwot Ridge (USA)  
Mixed subalpine forest  
3050 m asl  
Slope 4 degrees  
(west-to-east)

3D rhomboid setup

Yi *et al.* 2008

The heights used for CO<sub>2</sub> concentration and wind speed measurements are shown on each tower.  
The eddy covariance term was measured on the east tower.

**Figure 1-3** Examples of 2D and 3D experimental setups used to investigate advection fluxes at sloping eddy covariance sites. *Source for figures, Marcolla et al. (2005), Yi et al. (2008).*

tower in figure 1.3a measures eddy covariance and storage, whilst the two towers at either end of the transect measure the horizontal CO<sub>2</sub> flux gradient along the 2D CV, allowing term IV of equation 1.2 to be calculated (a constant wind profile was assumed along the 2D CV). Marcolla *et al.* (2005) collected 35 days of data in the summer of 2002, resulting in the mean diurnal flux curve shown in figure 1.3b. This clearly shows that advection dominates the site at night (fluxes of between 5 and 10  $\mu\text{mol m}^{-2} \text{s}^{-1}$ ), with both horizontal and vertical advection fluxes acting in the same direction (out of the CV). The inclusion of the advection terms for the Renon site reduced the apparent carbon sink of the forest by 65% (from 3.29 to 1.15  $\text{g C m}^{-2} \text{d}^{-1}$ ) compared to using the standard Euroflux  $u^*$  threshold method.

Figure 1.3c shows a schematic view of a 3D rhomboid setup used by Yi *et al.* (2008) in their experiment to measure the horizontal and vertical advection terms at the Niwot Ridge Ameriflux site, in the Rocky Mountains, USA. The topographic slope of the site was 4 degrees. Only three of the four towers shown in figure 1.3c were used in any particular measuring campaign, but the east tower (the eddy covariance tower) was always included. The horizontal advection flux was calculated by a form of ‘triangulation’ between CO<sub>2</sub> concentration and horizontal wind speed values between the three towers as described in Yi *et al.* (2008), using the angles annotated in figure 1.3c. Vertical advection was calculated according to Lee (1998).

For the Niwot Ridge site, Yi *et al.* (2008) determined that mean summertime advection fluxes at night were, 2.76  $\mu\text{mol m}^{-2} \text{s}^{-1}$  for horizontal advection (out of the CV), and  $-1.46 \mu\text{mol m}^{-2} \text{s}^{-1}$  for vertical advection (into the CV). The inclusion of the advection terms for Niwot Ridge reduced the apparent annual carbon sink of the forest by 65% compared to using the standard AmeriFlux  $u^*$  threshold method.



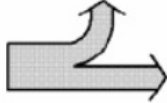
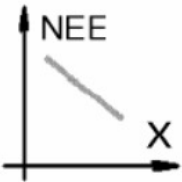
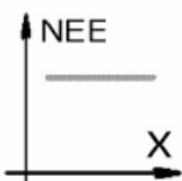
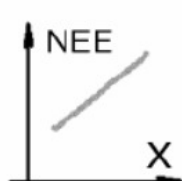
Similar advection experiments have been carried out at other sites, including by Feigenwinter *et al.* (2004) who used a three tower 3D array to determine that using the advection terms resulted in a 15% reduction in the apparent carbon sink of the Tharandt forest, Germany (sink reduced from 1.84 to 1.56  $\text{g C m}^{-2} \text{d}^{-1}$ ) compared to eddy covariance and storage change estimates alone (without  $u^*$  threshold filtering).

The vertical and horizontal advection terms at the Tharandt site were found to have opposite signs but similar magnitude (mean  $2.4 \text{ g C m}^{-2} \text{ d}^{-1}$ ), with the vertical term slightly dominating giving a mean flux out of the CV of  $0.28 \text{ g C m}^{-2} \text{ d}^{-1}$  for the 20 duration of the experiment.

Staebler *et al.* (2004) investigated horizontal advection in Harvard forest, USA, using a complex 3D array of  $\text{CO}_2$  sensors surrounding a central eddy covariance tower. The resulting advection correction reduced the apparent carbon sink of the forest by between 30 and 70% on calm nights when gravity flows were likely, compared to eddy covariance and storage change estimates alone (without  $u^*$  threshold filtering).

Aubinet (2008) has developed a classification scheme to make sense of the diverse results coming from advection experiments. This classification scheme is shown in figure 1.4. The scheme relates the presence of convergence or divergence within a notional 2D CV (figure 1.4, row 1) and the  $\text{CO}_2$  source/sink distribution within the CV (column 1), to the sign of the horizontal and vertical advection terms within the CV (i.e. whether the advection term is positive and thus removing  $\text{CO}_2$  from the CV, or negative and adding  $\text{CO}_2$  to the CV). It should be noted that because vertical  $\text{CO}_2$  concentration profiles within a forest are usually negative at night, a downward vertical air movement will give rise to a positive vertical advection, as is seen in column 1 of figure 1.4.

Figure 1.4 correctly predicts that for the Renon site (Marcolla *et al.* 2005) (column 1, row 4) to have both positive values of horizontal and vertical advection (see figure 1.3b) there must be an increase in the  $\text{CO}_2$  source going across the CV towards the downwind direction. Information given in Marcolla *et al.* (2005) does indeed indicate more vegetation (and hence a larger source of nighttime  $\text{CO}_2$  respiration) towards the downwind end of the Renon CV. Figure 1.4 predicts that the site of the Tumbarumba advection experiment, described in chapter 2 and Leuning *et al.* (2008), will have a similar positive gradient of respiration flux source density across the CV. However, this has yet to be checked.

Source intensity	Convergence 	Constant mass flow 	Divergence 	
Decreasing 	$VA > 0$ $HA < 0$ $ HA  <  VA $ Vielsalm (B) Aubinet et al. (2003) Tharandt (D) Feigenwinter et al. (2004)	$VA = 0$ $HA > 0$  Hesse (F) Aubinet et al. (2005)  Harvard (USA) Staebler and Fitzjarrald (2004)	$VA < 0$ $HA > 0$ $ HA  >  VA $  Niwot Ridge (USA) Turnipseed et al. (2003)	
Constant 	$VA > 0$ $HA = 0$  Browns River (CND) Prince Albert (CND) Lee (1998)		Harvard (USA)	Niwot Ridge (USA) Turnipseed et al. (2003)
Increasing 	$VA > 0$ $HA > 0$ Renon (I) Marcolla et al. (2005) <b>Tumbarumba</b> <b>Leuning et al. (2008)</b>		Harvard (USA)	Niwot Ridge (USA) Turnipseed et al. (2003)

**Figure 1-4** A classification scheme for different advection patterns in relation to CO<sub>2</sub> source intensity distributions and mass flow characteristics. *Taken from Aubinet (2008).*

Abbreviations are: HA, horizontal advection; VA, vertical advection; NEE, biological source/sink; B, Belgium; D, Germany; CND, Canada; I, Italy; and F, France. In the source intensity column, X represents the downwind position. *Taken from Aubinet (2008).*

N.B reference to Tumbarumba has been added as a modification.

Sites shown in figure 1.4, column 2, row 2, and figure 1.4, column 4, have horizontal and vertical advection terms with opposite signs. This gives rise to the likelihood of a large relative error resulting after they are added together in term IV of equation 1.2.

The advection approach shows promise, but the manpower and expense required to continually make advection measurements at a significant proportion of FLUXNET sites, would be prohibitive. Also results of an advection study carried out by Leuning *et al.* (2008) and reported in this thesis, suggest that the standard errors associated with advection fluxes measured at night, are of the same order as the fluxes themselves. On the other hand, the  $u^*$  threshold methods, despite being cheap enough to deploy across FLUXNET, tend to systematically underestimate nocturnal respiration fluxes at night. Super-site approaches are promising, but again, far too expensive to be used at anything but a tiny fraction of sites (Finnigan 2008).

One method that shows promise, but which has not been discussed widely thus far, is that of van Gorsel *et al.* (2007) who have developed a method that estimates the nocturnal respiration flux from the maximum eddy covariance flux plus change in storage measured after sunset but before the onset of advection fluxes. This method has been tested successfully at the Tumbarumba forest eddy covariance site (van Gorsel *et al.* 2008). When this method is used to provide the advection terms in equation 1.2 (terms III and IV) the resulting NEE is in good agreement with flux chamber measurements from the Tumbarumba site. The method resulted in a 280% increase in the nocturnal CO<sub>2</sub> fluxes detected at the site compared with the traditional  $u^*$  threshold method. Nocturnal fluxes using the  $u^*$  method with a  $u^*$  threshold of 0.25 m s<sup>-1</sup> were 1.63 +/- 0.3 μmol m<sup>-2</sup> s<sup>-1</sup>, whereas the new method gave fluxes of 4.6 +/- 0.3 μmol m<sup>-2</sup> s<sup>-1</sup> for the same period. This resulted in a 5.6 +/- 0.5 t C ha<sup>-1</sup> y<sup>-1</sup> reduction in the estimated carbon sink of the Tumbarumba forest compared with the  $u^*$  threshold method. If this method can be made to work at other FLUXNET sites it could represent a major breakthrough in solving the ‘missing flux’ problem, since it would be relatively cheap to deploy across FLUXNET.

## 1.6 Canopy flow models for complex terrain

Finnigan (2008) divides the roles mathematical models can play in surface flux measurement into two distinct groups:

- 1) Relatively simple analytical and numerical models that can assess the likely severity of advection at a given flux site, and also help in the planning of measurement strategies.
- 2) Data assimilation models.

At present only models of type 1 exist so we will discuss them first. Included in this first type are a number of simple canopy flow models that can describe air flow through a dense canopy over gently sloping 2-dimensional (2D) terrain.

One example is the analytical model of Finnigan and Belcher (2004) who use linearised dynamics and ‘perturbation pressure’ to describe air flow above and below a forest canopy over a shallow Gaussian hill (shallow meaning the ratio of height over length being a lot less than unity) in neutral conditions, with a dense homogeneous canopy (dense means the momentum flux is totally absorbed within the canopy before reaching the ground). Output from Finnigan and Belchers model is shown in figure 1.5a, which shows normalised horizontal wind velocity profiles across a 2D Gaussian hill of width  $2L$ , covered in a dense canopy of height,  $h$ . The above canopy wind blows from left-to-right over the entire width of the hill.

However, due to pressure perturbation effects, the airflow in the lower part of the canopy becomes reversed in the immediate lee of the hillcrest. This reversed airflow has the important consequence of causing flow convergence at the hillcrest and the possible ejection of scalars such as  $\text{CO}_2$  from the forest canopy. To demonstrate this point, figure 1.5b shows output from a model by Katul *et al.* (2006) that uses Finnigan and Belchers wind field from figure 1.5a, to drive an eddy diffusion model of turbulent fluxes (Belcher *at al.* 2008). Figure 1.5b shows flow convergence along the hillcrest has indeed created a plume of  $\text{CO}_2$  that appears to be emerging from the canopy. Clearly the hillcrest would not be a wise choice of location for an eddy covariance tower, as it would be likely to suffer from vertical advection. In addition,



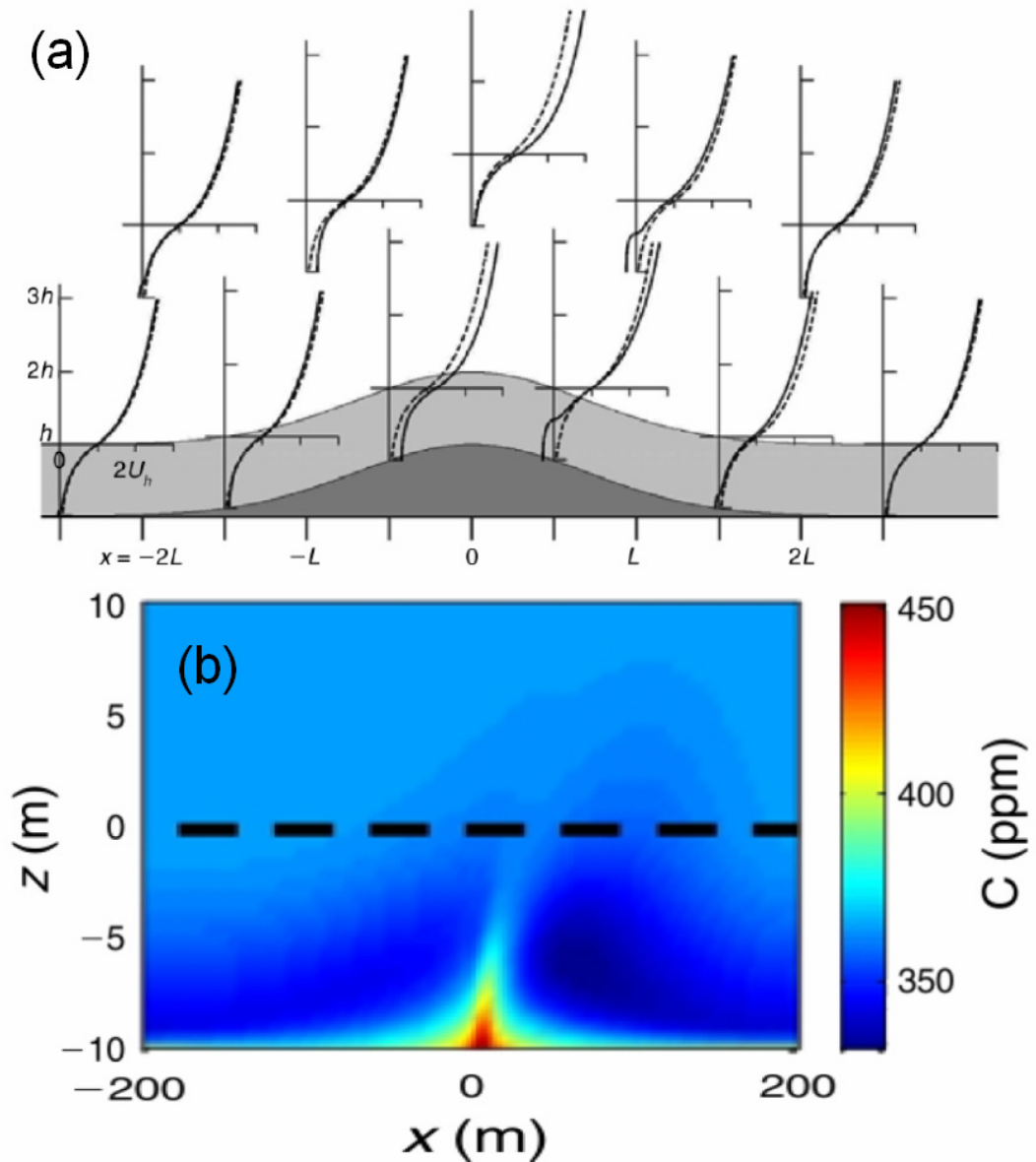


**Figure 1-5** Effects of an isolated Gaussian hill on wind speeds and scalars within and above a canopy. (a) Normalised wind speed profiles across the hill, with a canopy of height,  $h$ . The solid lines are wind speed profiles above the hill calculated using the model of Finnigan and Belcher (2004). The dashed lines are wind profiles for a canopy without the hill. Taken from Belcher *et al.* 2008. (b) Concentration values of  $\text{CO}_2$  calculated for the wind field shown in (a) using the model of Katul *et al.* (2006). Taken from Belcher *et al.* 2008, Katul *et al.* 2006. Note: for (b) the canopy occupies  $-h$  to  $0$ , and the width of the hill is  $200$  m. In (a) the width of the hill is  $2L$ .

other results from Katul's model (not shown) indicate large changes in the turbulent eddy covariance flux as one crosses the hill crest, that would render the site unsuitable as a source of representative ecosystem flux values.

The Finnigan and Belcher (2004) model demonstrates that even gently rolling terrain can have serious implications for conventional eddy covariance measurements as currently made by FLUXNET stations.

Rob Clement (*pers comm.*) has implemented Finnegan and Belcher's (2004) model as a computer programme that can be run on a personal computer (PC). Figure 1.6 shows some 'screen shots' generated using the programme. The upper two panels illustrate the idealised situation of wind flow across a forested Gaussian hill and gives similar results to figure 1.5a. However, the lower two panels show outputs for a real topographic transect, across the Griffin forest eddy covariance site in Scotland (a detailed topographic description of which is given in chapter 3). The 2D transect used in this case goes down the axis of the valley in which the tower is situated. Here we start to see some of the problems of using such a model on real topography. The valley profile has been de-trended to allow the computer model to run on the residual topography. Also, if one attempted to run the model for the across valley direction, errors would result since the slopes would be too steep, and violate the assumptions behind the model. It can be concluded that to be really useful in complex terrain such a model would have to be implemented fully in 3-dimensions rather than just two. Also, the slope constraint of the model limits its use to less steep terrain. However, in certain types of rolling terrain, with moderate slope, Clement's computer model in its present form could be very useful in aiding the location of future eddy covariance sites.

In addition to Finnegan and Belcher's (2004) model, hill canopy models have been developed by other researchers, such as similar 2D numerical canopy model by Ross and Vosper (2005).

Wind flow and scalar transport at forest edges has been modelled by Sogachev *et al.* (2008). The modelling of such discontinuities is particularly important in

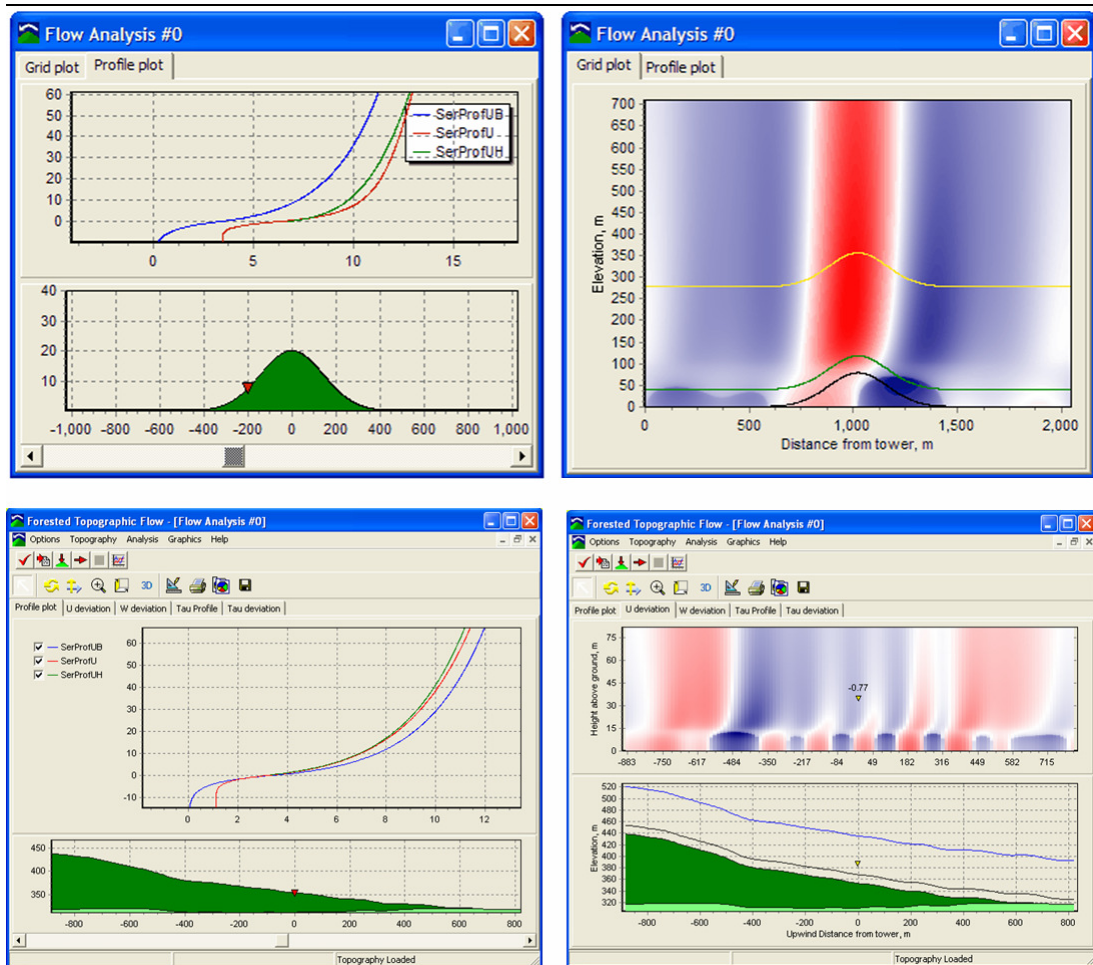


**Figure 1-6** Shows screen shots from the Hill Flow computer programme written by Rob Clement (Clement *pers comm.*), based on Finnigan and Belcher's (2004) model. The top left panel shows a model run across a Gaussian hill. In this panel the blue profile is for just the canopy assuming no topography. The red profile is from Finnigan and Belcher's model, and the green profile is based on a model by Hunt *et al.*, both for canopy and topography. The position of the profile on the topography transect is indicated by the red triangle. The top right panel shows a 'wind velocity deviation profile colour grid' across the hill, where blue represents wind speeds less than the background flow and red represents wind velocities higher than the background flow. The bottom two panels show the same outputs as the top two panels, but for a real topographic transect across the Griffin forest eddy covariance tower in central Scotland. The tower is situated at the zero position on the transect.

determining the fetch of homogeneous forest that an eddy covariance tower must have in order to avoid advection affects from the forest edge (the fetch must be at least 40 times the canopy height according to Sogachev *et al.*).

Belcher *et al.* (2008) have extended the concepts used in Finnegan and Belchers (2004) model to describe airflow within the canopy of a forested hill in stable conditions (stable within the canopy). The onset of stability within the canopy after sunset was discussed earlier, and results in high (supercritical) gradient Richardson numbers within the canopy and consequent collapse of turbulence causing sub-canopy airflows to be decoupled from those above (Belcher *et al.* 2008). Under such conditions the only coupling is by pressure effects, and sub-canopy forces are a balance between the hydrodynamic pressure and hydrostatic pressure. This balance depends on the degree of stability within the canopy, which Belcher *et al.* (2008) describe using the Froude number,  $F_L$  (which is infinity for neutral stability and falls as stability increases). Belcher *et al.* (2008) also demonstrate that the ratio between the hydrodynamic and hydrostatic pressure forces is proportional to the hill length and not the hill slope, hence explaining why many FLUXNET sites with small slope angles experience advection problems at night, but not during the day.

Figure 1.7 shows a figure taken from Belcher *et al.* (2008) that demonstrates the evolution of sub-canopy flow in a forested sinusoidal hill as stability within the canopy increases. Until  $F_L$  passes a critical value of 1.5 the flow is similar to the neutral stability case (see figure 1.5) with convergence at the hill ridge. Then, as stability increases the convergence zone splits and starts to move down each side of the hill until an  $F_L$  of one is reached, resulting in the situation of katabatic flows descending the entire length of both sides of the hill, with convergent zones at the base and a divergent zone at the hill crest. Then, as  $F_L$  decreases further the distribution of convergent and divergent zones continues to shift.

The consequence of this analysis is that the locations at which air is emerging from the canopy (convergence zones), or being entrained into the canopy (divergence zones), will shift across a hilly landscape if stability varies. This means that if such a convergence or divergence zone crosses the location of an eddy covariance tower,

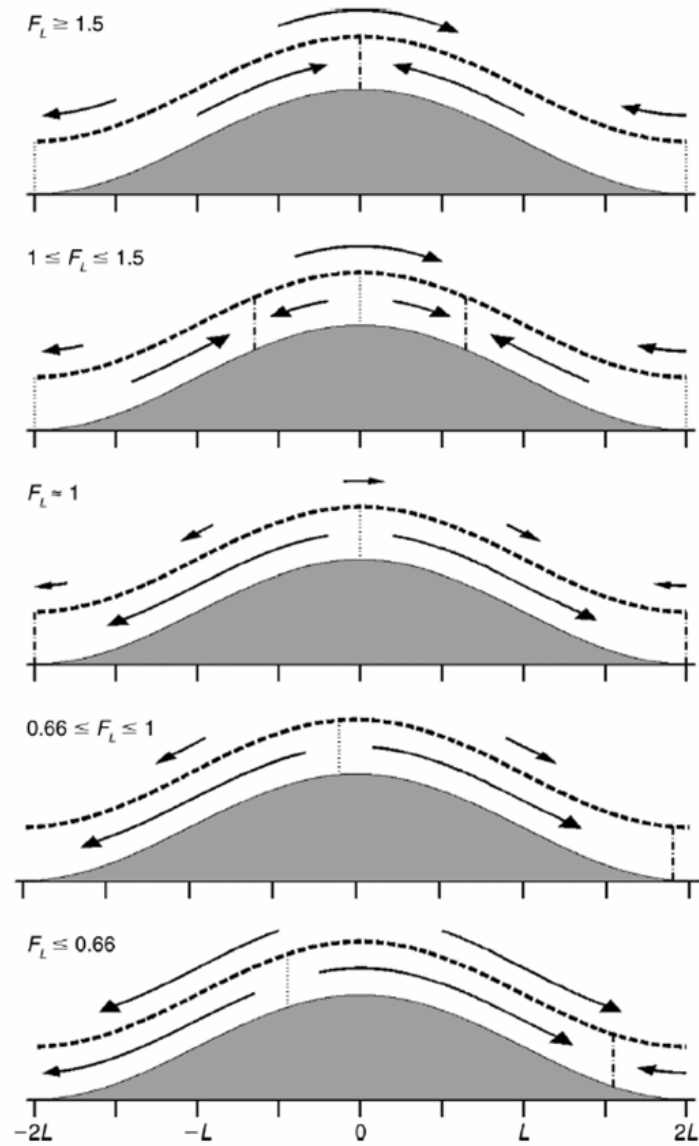


**Figure 1-7** Schematic taken from Belcher *et al.* (2008), showing forces above and below a canopy on a sinusoidal hill as a function of Froude number,  $F_L$  (indicating stability). The top of the forest canopy is indicated by the dashed line. Above the canopy the arrows indicate the hydrostatic pressure gradient only. Below the canopy top (dashed line) the arrows represent the balance between the hydrodynamic pressure gradient and the hydrostatic pressure gradient. The magnitudes of the forces are given by the lengths of the arrows. Vertical dotted lines show regions of divergence within the canopy, while vertical dash-dotted lines indicate regions of convergence within the canopy. Descent at the canopy top is expected over the regions of divergence, and ascent at the canopy top is expected over regions of convergence. *Figure text adapted from Belcher et al. 2008.*

that tower will be subject to a large advection term (see terms III and IV in equation 1.2). Unfortunately, no such model exists at present to predict these effects across a real 3D landscape.

The models described so far, although useful in choosing locations for potential new eddy covariance sites, also reinforce how intractable the advection problem may be for the eddy covariance method.

One possible way in which the simple models described so far, could be used in a manner leading to quantitative advection estimates for a given eddy covariance tower is to use a data driven technique described by Maidment (1993).

Maidment describes the construction of a data driven hydrological model using a geographical information system (GIS) to create a unit hydrograph for a complex landscape, consisting of topography (digital elevation model, DEM), diverse vegetation and soil (land cover map), and rainfall (rain gauge data). The mathematical rules or models used by Maidment were very simple, but interacted at the grid-cell and hydrological catchment level to produce a credible result. Would it be possible to create a similar model for katabatic flows? Certainly it would be a more complex model, as the fluid would be compressible and the problem more 3-dimensional in nature. However, it may be worth investigating only to rule it out, as it would likely be far less computer intensive than a traditional data assimilation model.

One intriguing possibility is that although the results of such a model probably would not be accurate enough to be useful for individual flux sites, they might be useful at the regional scale, echoing Foken's (2008) view that the energy balance closure problem is only solvable at the regional scale. The data layers that could be used to 'drive' such a model might include, in addition to a digital elevation model, land cover data, and synoptic wind data; remotely sensed data such as thermal radiance images that are provided by the ASTER sensor onboard the Terra satellite. ASTER thermal images were used by Golden *et al.* (2006) in their study of nocturnal drainage and pooling in the Amazon forest, and could be used by a GIS based model

to constrain canopy and surface temperatures. If such a model could be made to work, it might be possible to ‘iterate’ it to assimilate the eddy covariance data. However, such ‘iteration’ would be very inefficient if done using a GIS.

### **1.7 Data assimilation models**

Examples of data assimilation models in use today are the global and mesoscale numerical weather prediction (NWP) Eulerian models used by weather forecasting agencies. Such models are able to continually ingest or assimilate weather station observations and information derived from weather satellite images, in order to provide a ‘now-cast’ of current weather conditions. These models provide weather forecast information by simply letting them ‘run’ into their own ‘future’ for a few days of simulated time.

If data assimilation models are ever constructed for use with eddy covariance towers in complex terrain, they will probably be Eulerian models using a Cartesian grid, with each of the many thousands of cells in the model grid constituting an independent control volume (CV) across which the advection terms can be evaluated (see figure 1.2).

The models task will be simpler than NWP in that only ‘hind-casting’, i.e. the modelling of past conditions, will be required. However, other aspects of the data assimilation models required to address the problem of advection at eddy covariance sites will be far more challenging, as are listed below:

- 1) The required model grid cell size will be small, possibly as small as 10 to 100 m, compared with 5 to 10 km for mesoscale NWP models. This small cell size is essentially a guess based on a qualitative consideration of the micro-topography observed in the vicinity of typical eddy covariance towers, and its effect on katabatic flows.
- 2) The required data assimilation models will probably need to be nested (Finnigan 2008), rather like a Russian doll, with a mesoscale NWP model handing atmospheric flow information down to a boundary layer model

and that model handing data to a regional (say 10 km to 50 km square) advection model, and that regional model driving a very detailed advection model centred on the eddy covariance tower in question. Such an approach would be required to avoid massive computational overheads caused by the small grid cell size. The boundary condition problems between such a model hierarchy would be challenging as they would be inherently scale dependant in both space and time.

- 3) The background gridded data layers such as terrain (DEM) and vegetation cover, would need to match the smallest model grid size, at least in the vicinity of the eddy covariance.
- 4) If a nested hierarchical approach is used for the advection model, it may greatly complicate data assimilation for a multiple tower situation.

Finnigan (2008) comments that the data processing procedures used for eddy covariance data today (the  $u^*$  threshold method) is in effect a simple data assimilation model based on the implicit assumption that the data is ‘compatible with a one-dimensional flow and transport model that does not include advection’.

This review of the data assimilation approach suggests that it will be several years, at least, before the data assimilation approach could provide useful nighttime advection term estimates for FLUXNET sites. For comparison the first usable NWP data assimilation models took around 30 years to develop (Shuman 1989).

### **1.8 Chapters 2 and 3 of this thesis**

The following two chapters of this thesis describe field investigations relevant to the advection problem, that were carried out at two temperate forest eddy covariance sites situated in complex terrain.

Respectively, they are an advection study carried out at the Tumbarumba OzFlux site in Australia during 2005 (chapter 2), that resulted in the publication of Leuning *et al.* (2008), and a study of airflow in a forest under anti-cyclonic conditions, that took

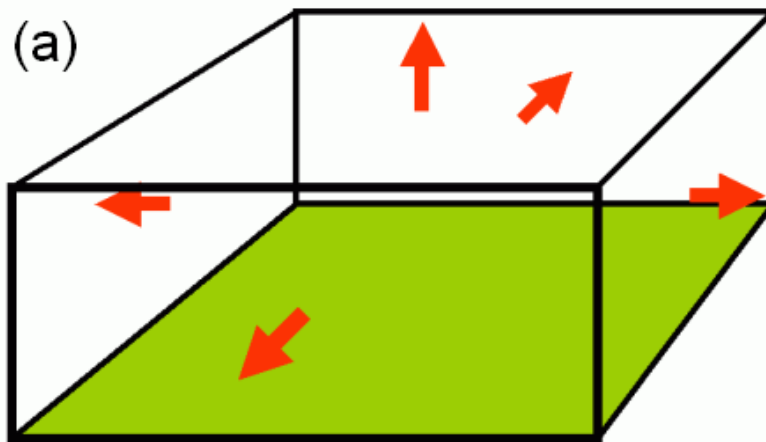


place during 2005 and 2006 at the Griffin forest eddy covariance site in Scotland, UK, resulting in a qualitative model of above canopy and in canopy air flow for that site (chapter 3).

Figure 1.8a shows a cartoon illustration of the “box budget” concept that measured the vertical advection, horizontal advection, change in storage and vertical eddy flux of carbon dioxide from the control volume (CV) or box situated beneath the tree canopy at the Tumbarumba forest site as is described in chapter 2. The CV represents a “virtual chamber” over a 50 by 50 metre plot through the calculation of the net ecosystem exchange (NEE) of carbon dioxide from its aerodynamic components measured on the walls of the box (CV) using instrumentation, these components being diagrammatically represented by the red arrows in figure 1.8a.

The two Griffin forest experiments described in chapter 3, took the form of a horizontal transect, and vertical profile of sonic anemometers respectively in addition to the existing flux tower. The air velocity data from these two experiments was processed to investigate wind flow coupling effects from above to below the tree canopy over gently sloping terrain, vertical advection, and possible flow divergence effects within the canopy, with special reference to the possible presence of katabatic flows. Figure 1.8b shows a cartoon representation of this set of experiments.

## Box Budget



## Coupling

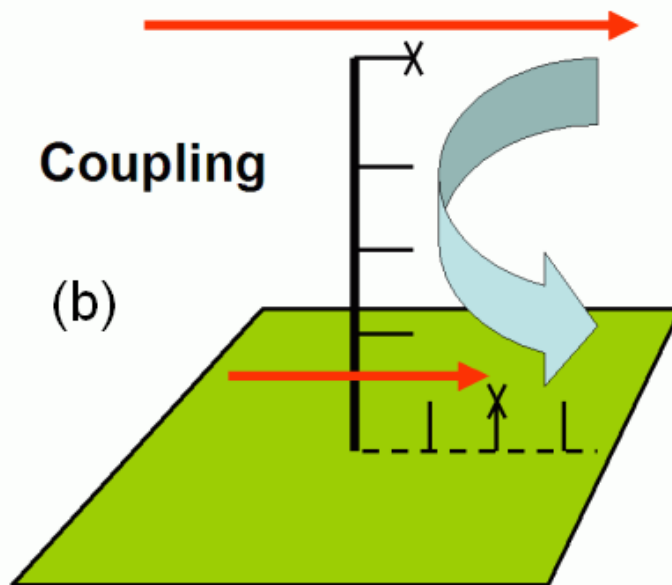


**Figure 1-8** (a) Cartoon representing the Box Budget concept employed at the Tumbarumba site (the detail of the forest canopy and central tower are not shown). (b) Cartoon representation of the two Griffin Forest experiments (one using a tower profile and the other a horizontal transect of ultrasonic anemometers) investigating coupling of wind flow from above to below the canopy (details of the tree canopy have been omitted). Detailed diagrams of both the Tumbarumba and Griffin Forest experimental setups are given in chapters 2 and 3 respectively.

## 2 The Tumbarumba Advection Experiment

### 2.1 Experimental Setting

As discussed in chapter 1 of this thesis, concern has been expressed in the eddy covariance literature (Raupach and Finnigan 1997, Finnigan, 2003, Katul *et al*, 2003) that horizontal and vertical advection effects under stable conditions are a significant problem (causing error magnitudes of the order of 100% of signal) for the global eddy covariance tower network, FLUXNET.

The purpose of the experiment reported in this chapter, was to directly measure all the CO<sub>2</sub> flux terms affecting a 50 by 50 m area within a Eucalyptus forest, up to a height of 6m above ground level (agl), henceforth referred to as the control volume (CV).

These flux terms consist of a change in storage term, horizontal advection terms (for the x and y directions), and a term for vertical eddy covariance and vertical advection. Taken together these terms can be used to calculate the net ecosystem exchange of CO<sub>2</sub> (NEE) between the area under consideration (below 6 m agl) and the surrounding atmosphere. NEE can be written as:

$$\begin{aligned}
 \overline{F_c} = & \frac{\overline{c_d}}{\Delta t} \left[ \int_0^h \overline{\chi_c} dz \Big|_{t=\Delta t} - \int_0^h \overline{\chi_c} dz \Big|_{t=0} \right] \\
 & + \frac{\overline{c_d u_h}}{L} \left[ \int_0^h S(z) \overline{\chi_c}(z) dz \Big|_{x=L} - \int_0^h S(z) \overline{\chi_c}(z) dz \Big|_{x=0} \right] \\
 & + \frac{\overline{c_d v_h}}{L} \left[ \int_0^h S(z) \overline{\chi_c}(z) dz \Big|_{y=L} - \int_0^h S(z) \overline{\chi_c}(z) dz \Big|_{y=0} \right] \\
 & + \overline{c_d} \left[ \overline{w \chi_c} + \int_0^h \left( \overline{w \frac{\partial \chi_c}{\partial z}} \right) dz \right]
 \end{aligned} \tag{2-1}$$

where  $\overline{F_c}$  represents NEE,  $\chi_c$  is the mole fraction of CO<sub>2</sub> (ppm),  $c_d$  is the concentration of dry air (mol m<sup>-3</sup>),  $\Delta t$  represents the length of the averaging time period,  $h$  is height of the CV (6 m),  $L$  is the length of the CV sides or faces (50 m),  $u$



**Figure 2-1** Location of the Tumbarumba field site within Australia, and with respect to nearby towns and cities (inset). *Map of Australia, public domain, courtesy of the University of Texas Libraries, The University of Texas at Austin. Inset map courtesy of the OzFlux website (<http://www.cmar.csiro.au/ozflux/>).*

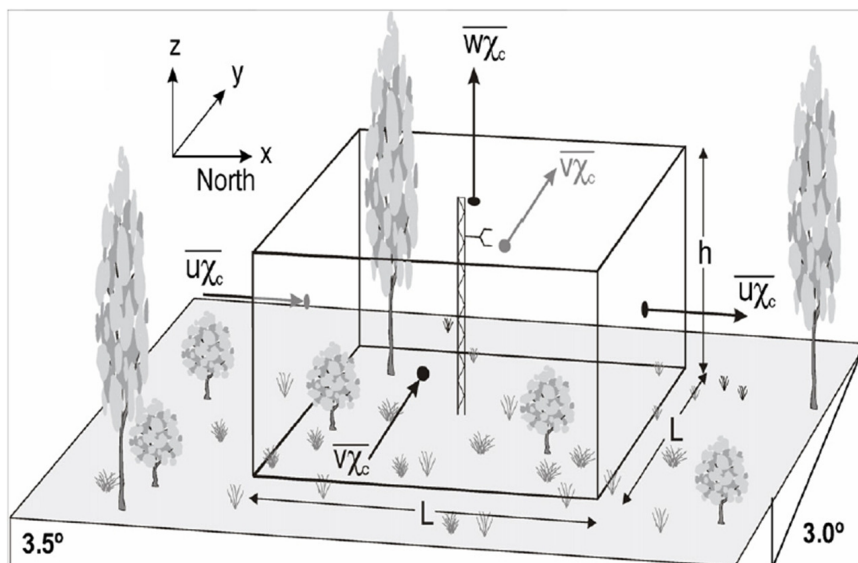


**Figure 2-2** Schematic diagram of the horizontal advection experimental set up in relation to the forest canopy/over-storey and the underbrush/understorey, showing the advection control volume (CV). The rectangular volume is formed by the four CV faces each of which is 50 m in length and 6 m high, comprised of perforated horizontal sampling tubes, and a ‘lid’ consisting of an eddy covariance system situated 6 m above ground level. The topographic slope components of the ground surface are indicated as 3.5 degrees and 3.0 degrees in the x and y directions. The annotations on the CV faces refer to equation 2.1. *From Leuning et al. (2008).*

and  $v$  are wind velocities ( $\text{ms}^{-1}$ ) in the  $x$  and  $y$  directions respectively,  $w$  the wind velocity ( $\text{m s}^{-1}$ ) in the  $z$  direction (vertical), and  $S(z)$  is a normalised horizontal wind profile between the ground and  $h$  (6 m). The Reynold's notation is used with overbars ( $\bar{\quad}$ ) indicating a mean taken over the averaging period  $\Delta t$ , and the dash notation ( $'$ ) indicating an instantaneous value.

The experiment was carried out in a temperate Eucalyptus forest near the Tumbarumba OzFlux flux tower site situated 1230 m above sea level in New South Wales, Australia, see figure 2.1. Figure 2.2 shows the relationship between the instrumented experimental control volume (CV) and the forest elements, understorey and canopy/overstorey. The height of the understorey vegetation within the CV was around one metre. The bottom of the Eucalyptus tree canopy started at about 25 m and had its top at around 40 m above ground level (agl) (Jupp, 2008; *pers comm.*). The experimental site has a topographic slope of 4.6 degrees towards the northwest. This experiment took place in collaboration with CSIRO. A diagrammatic 3D view of the experimental set is shown in figure 2.3 and an annotated photograph of the instrument mast in the centre of the CV is shown in figure 2.4.

### 2.1.1 Methodology

In order to determine horizontal advection fluxes of  $\text{CO}_2$  using a relation of the type given by the second and third terms of equation 2.1, horizontal wind speeds were first measured on a vertical profile for a period of three weeks, on the central 6 m mast shown in figures 2.2 and 2.3. These wind measurements shown in figure 2.5, took place one month before the commencement of the main experiment and the erection of the control volume faces, and were used to produce a representative wind speed profile for the location up to 6 m above ground level (agl). The 50 by 50 m wide by 6 m high CV was centred on the 6 m mast. The gas sampling tubing was then erected along the sides of the CV at 0.2, 0.4, 0.8, 1.6, 3.2 and 6.0 m agl, forming the CV faces, as shown schematically in figure 2.3. The air from the gas lines in a given face was sampled in proportion to the wind speed at their particular heights, and then combined (see figure 2.3). These weighted air samples for each face of the

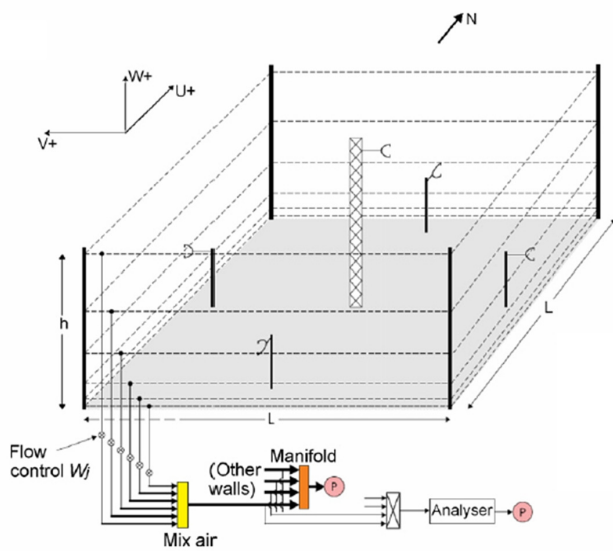


**Figure 2-3** The Tumbarumba advection experiment control volume (CV), showing a diagrammatic representation of the gas sampling walls. The dashed lines represent the perforated tubing through which air was sampled. The mast and 6 m sonic anemometer is shown in the centre of the CV. Also shown are sonic 1.65 m anemometers near the middle of each face of the CV. Note: intermediate support poles have been left out for clarity. *Modified from Leuning et al. (2008).*

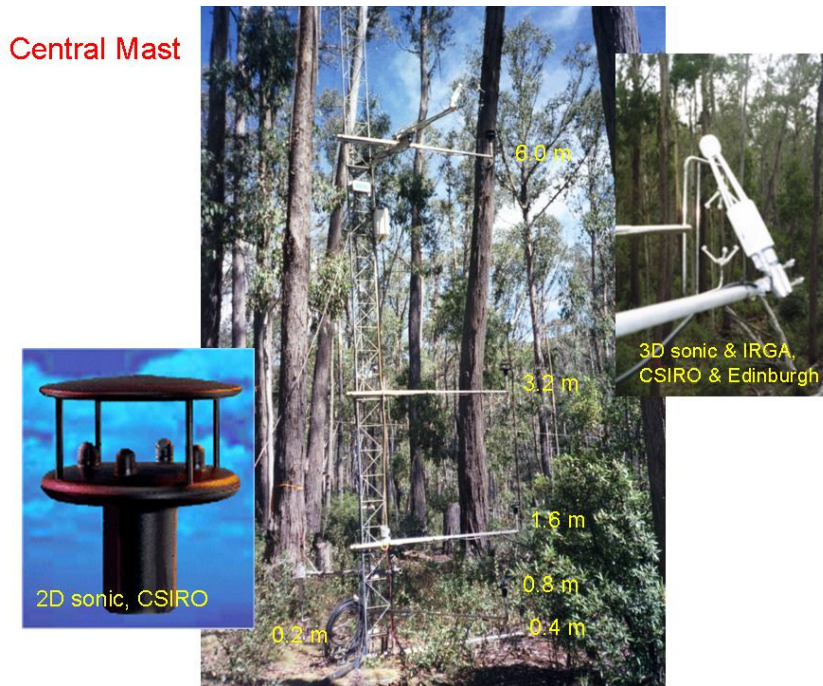


**Figure 2-4** Annotated photograph of the central 6 m mast, showing detail of the 2D sonic anemometers provided and logged by CSIRO, and the 3D sonic anemometer, open path IRGA combination (6 m agl) provided by CSIRO. 2D anemometer heights are 0.2, 0.4, 1.6, 3.2 and 6 m agl.

CV were then passed in turn through the gas analyser. The principal reason for obtaining the wind profile shown in figure 2.5d was to obtain the weighting functions,  $W_j$ , used to combine the airflow from each of the six levels on each CV face. Figures 2.5a to 2.5c show cross plots between 15 minute interval observations of horizontal wind speed measured at the lower levels on the 6 m mast, and wind speeds measured at the top of the mast at 6.4 m. Also shown are regression lines forced to pass through the origin for each of the cross plots. In figure 2.5d the slopes of these regression lines have been used to directly plot a normalised wind profile,  $S(z)$ , up to 6.4 m. This normalised wind profile is modelled using an exponential function:

$$S(z) = a[1 - \exp(-bz)] \quad (2-2)$$

which generates the curve through the data points in figure 2.5d. Figure 2.5e shows normalised wind speed values calculated using equation 2.2 at heights corresponding to the gas sampling tubes heights (0.2, 0.4, 0.8, 1.6, 3.2 and 6.0 m agl) used for the CV faces. These normalised wind values are then used to calculate the weighting functions,  $W_j$ , using the equation:

$$W_j = S(z)\Delta z_j \quad (2-3)$$

where  $\Delta z_j$  is the domain height of each gas sampling level, calculated as the mean of the distances to the sampling tubes below and above the current tube level. Figure 2.5f shows the resultant profile of normalised  $W_j$  values with height. These normalised weighting functions were used to set the flow valves on the gas lines taking air from the perforated sampling tubes to each of the six sampling levels (0.2, 0.4, 0.8, 1.6, 3.2 and 6.0 m agl), on each of the four CV faces. After passing through the flow control valves, the six gas lines for each CV face were combined in to one at a manifold, resulting in just four gas lines, one for each CV face. The calculation of the weighting functions,  $W_j$ , and their use to set the flow control values is crucial for this type of experimental set up, and must be completed before the commencement of the main experiment.

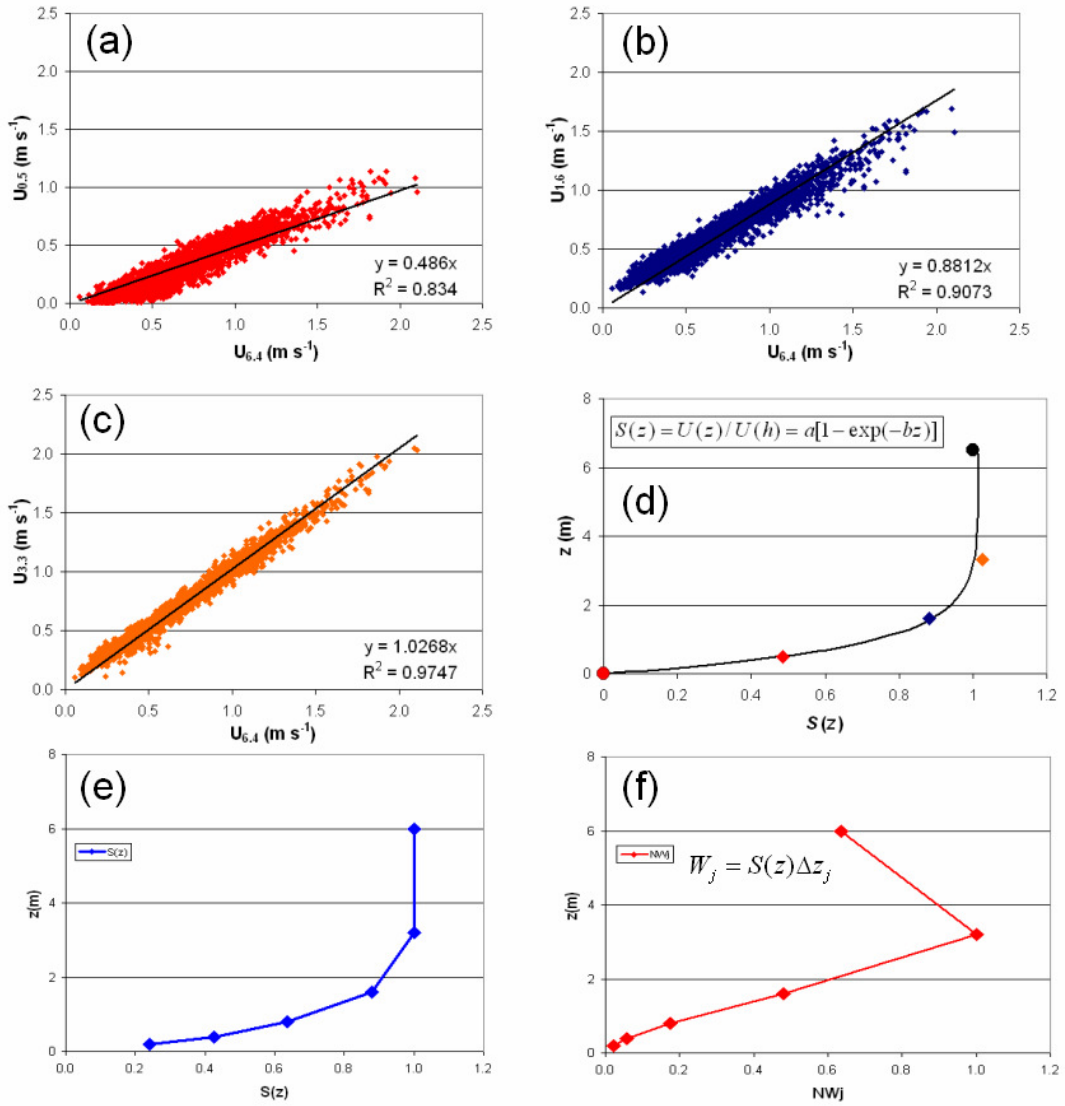


**Figure 2-5** Wind data collected on the 6 m mast in the month before the main experiment, that was used to calculate the weighting functions  $W_j$ . (a) scatter plot of horizontal wind at 0.5 m against 6.4 m, (b) 1.6 m against 6.4 m, (c) 3.3 m against 6.4 m. (d) is a normalised wind profile derived from the regression slopes, and modelled using an exponential function. (e) is normalised winds at the heights of the CV face sampling tubes, derived from the exponential model. (f) shows the corresponding weighting functions,  $W_j$ , in normalised form.



The four gas lines (one for each face) were sampled in turn by a single closed path infrared gas analyser (IRGA) via a gas line switching unit. This approach results in a gas sampling cycle time of just four minutes and so requires a steady wind direction of just this duration. This is a big improvement on previous techniques that required up to 45 minutes of constancy of wind direction.

Five 2D sonic anemometers on the central 6 m mast at the same height agl as the gas sampling tubing in the CV faces allowed the shape of the vertical wind profile,  $S(z)$ , within the CV to be monitored.

The 2D sonic anemometer at 6 m on the central mast allowed evaluation of the weighted integrals of the CO<sub>2</sub> concentrations to give the horizontal advection fluxes.

Leuning *et al.* (2008) provide an expression for  $\overline{F_c}$  in finite-difference form:

$$\begin{aligned}
\overline{F_c} = & \frac{\overline{c_d}}{\Delta t} \left[ \sum_{j=1}^6 \overline{\chi_{c,j}} \Delta z_j \Big|_{t=\Delta t} - \sum_{j=1}^6 \overline{\chi_{c,j}} \Delta z_j \Big|_{t=0} \right] \\
& + \frac{\overline{c_d u_h}}{L} \left[ \sum_{j=1}^6 \overline{W_j \chi_{c,j}} \Big|_{x=L} - \sum_{j=1}^6 \overline{W_j \chi_{c,j}} \Big|_{x=0} \right] \\
& + \frac{\overline{c_d v_h}}{L} \left[ \sum_{j=1}^6 \overline{W_j \chi_{c,j}} \Big|_{y=L} - \sum_{j=1}^6 \overline{W_j \chi_{c,j}} \Big|_{y=0} \right] \\
& + \overline{c_d w \chi} \Big|_h + \overline{c_d} \int_0^h \left( \overline{w \frac{\partial \chi_c}{\partial z}} \right) dz
\end{aligned} \tag{2-4}$$

the second and third terms of which are those used to calculate the horizontal advection terms for the  $x$  and  $y$  directions respectively. These horizontal advection terms can be calculated from the weighted mole fractions of CO<sub>2</sub> directly measured from the four CV faces, and horizontal wind components measured at 6 m agl on the central mast.

CO<sub>2</sub> concentrations in air were also sampled at locations adjacent to the 2D sonic anemometers on the central mast, the sampled gas being taken to a second closed path IRGA via gas lines and a gas switching box. The data from the five 2D sonic anemometers were logged by CSIRO staff using LabView software (National

Instruments, Austin, Texas, USA) and the data from the two closed path IRGASs recorded on to a Campbell logger (Campbell Scientific, Inc., North Logan, Utah, USA).

A 3D sonic anemometer and open path IRGA were also provided at 6 m agl on the central mast to provide a ‘lid’ to the 50 by 50 by 6 m CV, in order to calculate the eddy flux of CO<sub>2</sub> through the 6 m plane. Data from this 3D sonic anemometer and open path IRGA were logged to the Edinburgh University laptop computer via an RS-422 to USB converter box. The fourth term in equation 2.4 gives this eddy flux term.

An additional four 3D sonic anemometers (Gill R3-50s) were provided by Edinburgh University, four of them being deployed at 1.65 m agl near the centre of each of the CV faces as shown in figure 2.3. The purpose of these four sonic anemometers was to overcome problems accurately measuring the vertical air velocity ( $w$ ) using the single 3D sonic anemometer at 6 m agl on the central mast. These four sonic anemometers deployed around the edge of the CV enabled vertical air velocity at the top of the CV to be evaluated using the method of continuity as outlined in Vickers and Mahrt (2006) and Heinesch *et al.* (2007). Essentially, the continuity approach calculates the vertical velocity using the horizontal flow divergences through the walls of the CV, the principle advantage being that one no longer has to make the choice of which rotational reference frame to use to calculate  $w$ . Also, the continuity method benefits from a reduction in  $w$  signal noise as the result of the combination of four horizontal air velocity measurements (one for each face of the CV). Leuning *et al.* (2008) shows that using the continuity method, differences in horizontal velocities across the CV only need to be measured to an accuracy of 10 mm s<sup>-1</sup> in order to obtain vertical velocities accurate to the required 1 mm s<sup>-1</sup>.

Leuning *et al.* (2008) gives an expression for the vertical velocity at any particular height within the CV,  $\bar{w}(z)$ , derived from continuity as:

$$\bar{w}(z) = \frac{-1}{L} \left[ \bar{u}_h \Big|_{x=L} - \bar{u}_h \Big|_{x=0} + \bar{v}_h \Big|_{y=L} - \bar{v}_h \Big|_{y=0} \right] \int_0^z S(\zeta) d\zeta \quad (2-5)$$

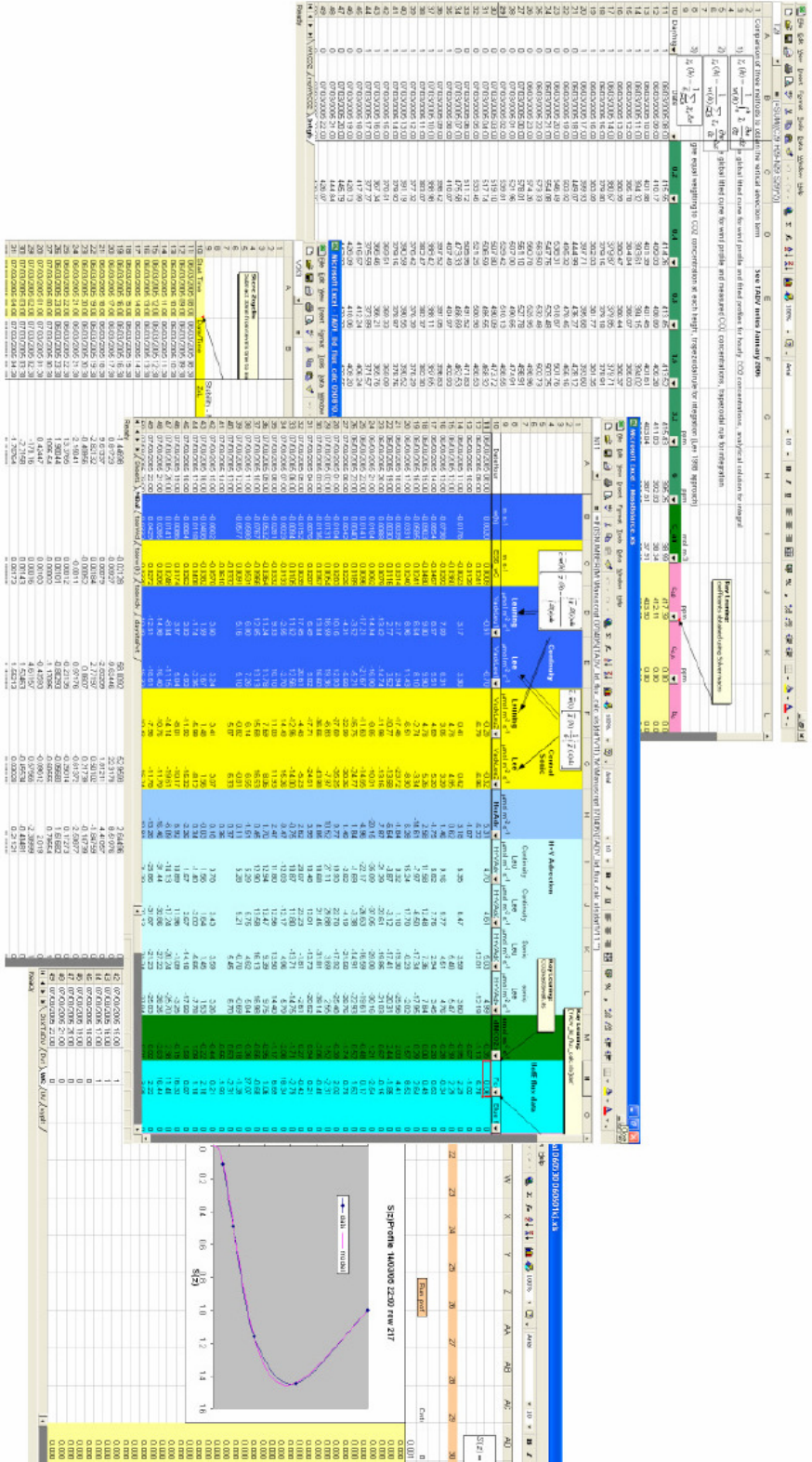


**Figure 2-6** An example of some of the Microsoft Excel spreadsheets used to process the Tumbarumba data. Preprocessing of the high frequency data from the University of Edinburgh's ultrasonic anemometers and IRGA into hourly means, was done using EditRe software (Clement, R., 2005; *pers comm.*) before exporting into Excel. Preprocessing of CSIRO data from their ultrasonic anemometers and closed path IRGAs was done using LabView (National Instruments, Austin, Texas, USA) and Fortran.

where  $\zeta$  is a dummy variable to replace  $z$  within the integration. In addition Leuning *et al.* (2008) demonstrates that the vertical advection term (the later part of the forth term in equation 2.1) is given by:

$$\int_0^h \left( \overline{w} \frac{\partial \overline{\chi_c}}{\partial z} \right) dz = \overline{w}(h) \overline{\chi_c}(h) - \int_0^h \left( \overline{\chi_c} \frac{\partial \overline{w}}{\partial z} \right) dz = \overline{w}(h) \left[ \overline{\chi_c}(h) - \frac{\int_0^h \overline{\chi_c}(z) S(z) dz}{\int_0^h S(z) dz} \right] \quad (2-6)$$

which once a value of  $\overline{w}(h)$  is obtained can be calculated from CO<sub>2</sub> mole fraction and wind speed profiles derived from the central 6 m mast.

All data from these five 3D anemometers were logged using EdiSol software (Moncrieff *et al.* 1997). Over the 20 day duration of the experiment from the 3<sup>rd</sup> to 22<sup>nd</sup> March 2005, the amount of sonic anemometer data logged on the Edinburgh University laptop was 1.4 Gigabytes, consisting of EdiSol proprietary **.slt** binary data files. After initial pre-processing with EdiRe software (Clement. R., 2005; *pers comm.*) or Lab View and Fortran (for the data collected by CSIRO), the data was processed using a large system of Microsoft Excel spreadsheets, see figure 2.6 for some screen shots.

## 2.2 Experimental results

A representative sonic temperature record for the experimental duration, measured just above the underbrush/understorey vegetation is given in figure 2.7, showing a temperature range of -3 to +27 Celsius. The two major synoptic frontal weather systems that crossed the site during the experiment can be clearly seen, separated by ten days of fair weather associated with a large high pressure system. Figure 2.8 shows the synoptic weather chart corresponding to the passage of the first cold front over the site on the morning of the 5<sup>th</sup> March 2005.

The areas of high pressure away from this isolated front are indicative of the fair weather conditions present over the site for most of the experimental duration.

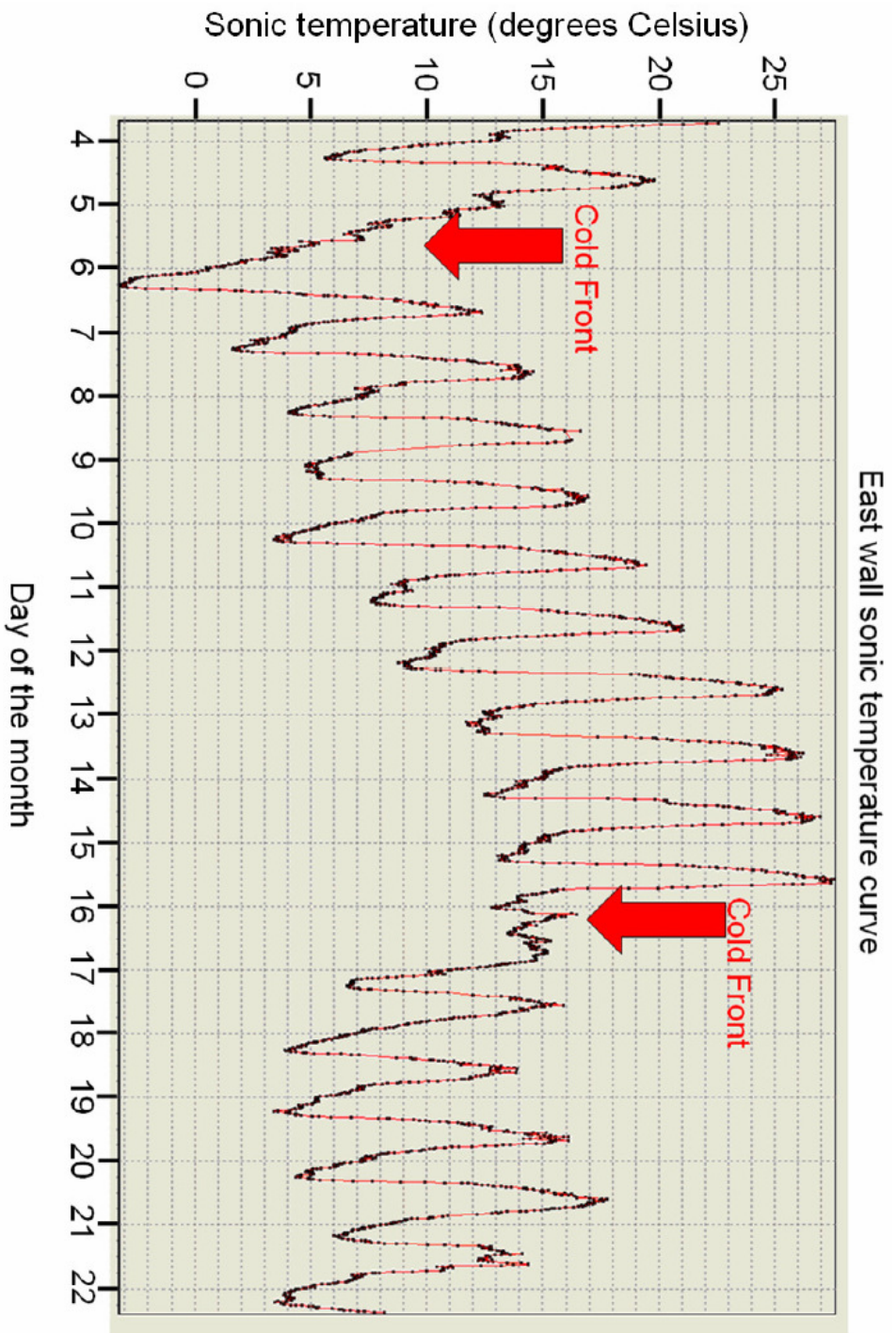


**Figure 2-7** The sonic temperature curve for the duration of the experiment (during March 2005) measured at a height of 1.65 m agl, near the centre of the east CV face, measured by a Gill R3-50 3D sonic anemometer. The day of the month labels indicate the start of a given day (0:00 hours).

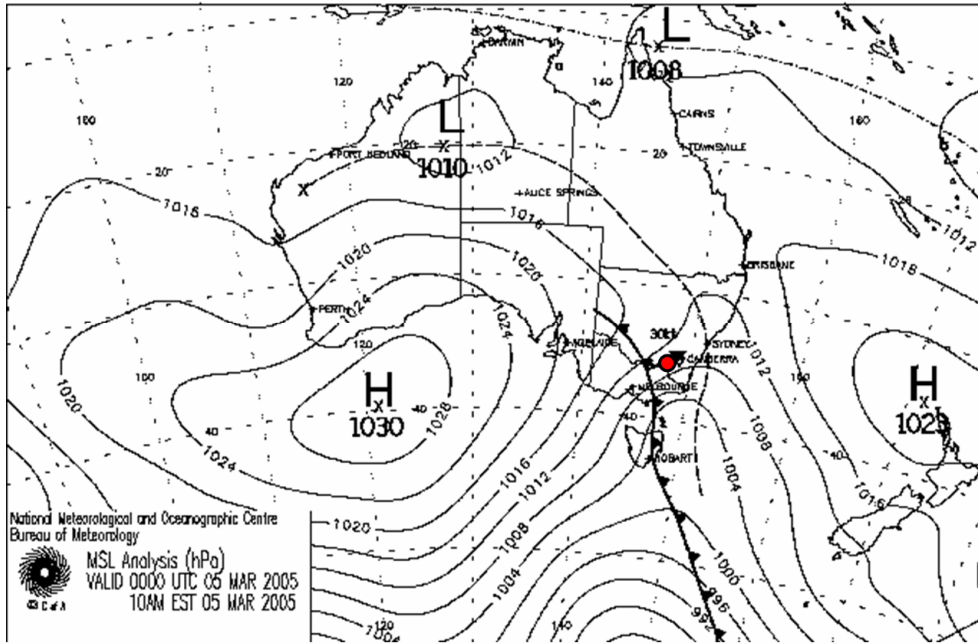


**Figure 2-8** The synoptic surface pressure chart for 10am EST on the 5<sup>th</sup> March 2005, showing a cold front approaching the Tumbarumba experimental site (indicated by the red dot). *Copyright National Meteorological and Oceanographic Centre, Bureau of Meteorology, Australia.*



Of principal interest is whether nocturnal katabatic type advection flows were indeed detected below the forest canopy during the experiment. In order to confirm this, the data from the five sonic anemometers were reprocessed using EdiRe software to provide an azimuthal distribution of the horizontal wind speed derived from the horizontal velocity components ( $u,v$ ). Figure 2.9 shows azimuthal frequency distribution plots for the five anemometers using time bins of four hours duration (the raw wind vector data having been recorded at twenty samples per second).

The plots in figure 2.9 show clear evidence of nocturnal winds blowing from South to North, during the periods 6<sup>th</sup> to 15<sup>th</sup> of March and 17<sup>th</sup> of March onwards, which correspond to high pressure systems between weather fronts. This nocturnal drainage of air in a northerly direction for the whole experimental volume from 0.2 to 6 metres agl is consistent with the expected katabatic type drainage wind direction for the Tumbarumba site, as a result of the surrounding topography shown in figure 2.10.

The experimental site shown in figure 2.10 is situated in a larger topographic basin of about 5 km<sup>2</sup> in area, bounded on three sides by low hills of 40 to 85 metres relative elevation. This basin is open to the North and hence the expected direction of katabatic type flow is to the North.

The frequency distributions of wind azimuth shown in figure 2.9 contain all the required information to plot a conventional wind rose for any desired day during the experiment. Figure 2.11 shows such a wind rose plotted for the 13<sup>th</sup> March 2005, using data from the sonic anemometer at 1.65 m agl near the centre of the east face. From figure 2.9 it can be seen the northerly nocturnal airflows are at their most distinct around this date. This is confirmed by figure 2.11, which shows a clearly defined likely katabatic flow coming from a bearing of 168 degrees during the hours of darkness, compared to an uphill flow during the day from 336 degrees. The likely katabatic flows at 19 hours, 23 hours and 03 hours have mean (over 4 hours) velocities of 0.34, 0.35 and 0.31 m s<sup>-1</sup> respectively, whereas the uphill flows at 11 hours and 15 hours have mean velocities of 0.95 and 0.79 m s<sup>-1</sup>.

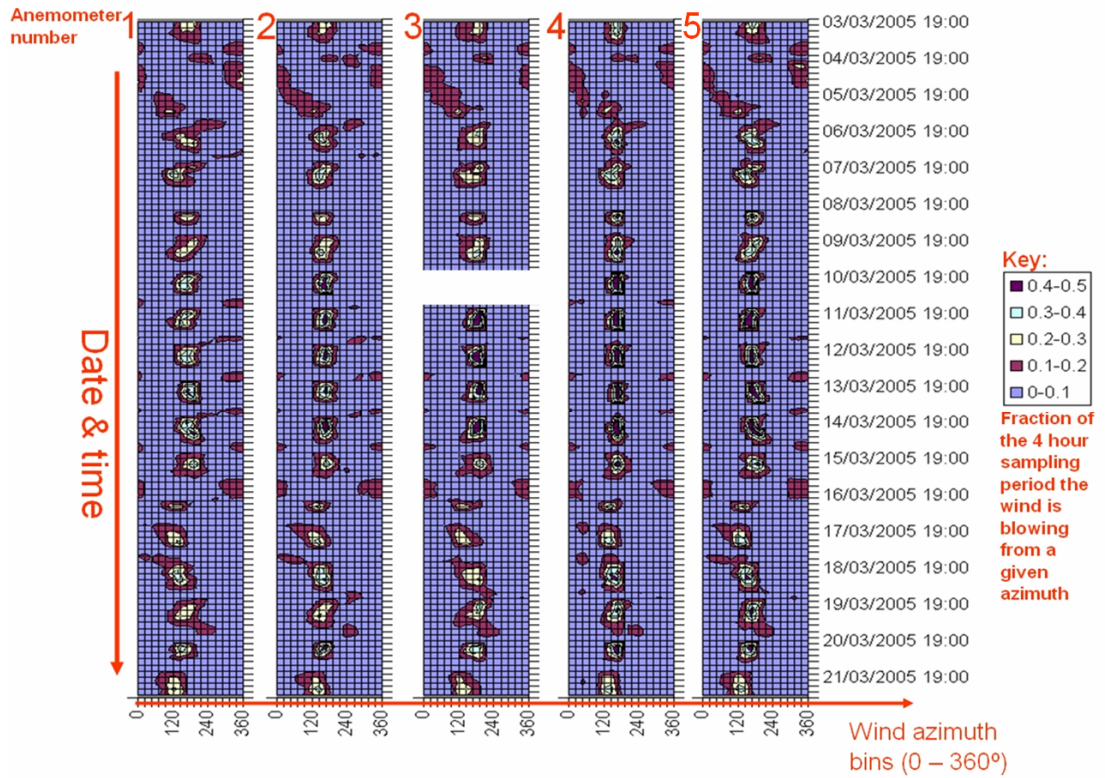


**Figure 2-9** Frequency distribution plots of wind azimuth for the sonic anemometers of the East, South, West, and North curtain walls at 1.65 m, and the central mast at 6 m (numbered 1, 2, 3, 4 and 5 respectively). Data from anemometer three is absent for the night of the 10<sup>th</sup> March due to equipment malfunction.



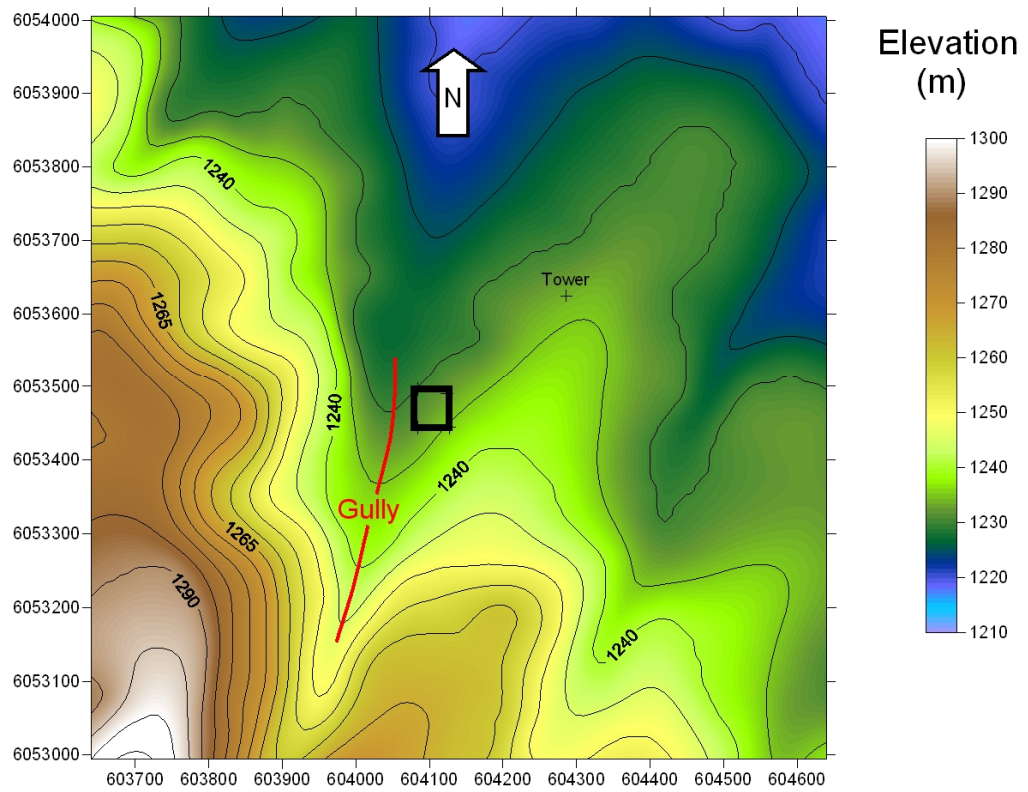


**Figure 2-10** A one kilometre square topographic map of the Tumbarumba site, showing the location of the experimental control volume (CV) (black square) and the pre-existing 70 m high OzFlux eddy flux tower. The contour interval is 5 m. *Modified from Leuning et al. (2008).*

Figure 2.12 shows that during the hours of darkness on the 13<sup>th</sup> March the prerequisite canopy temperature inversion occurred over the site that is required for katabatic flows to happen. Similar temperature inversions occurred on the other nights between the 6<sup>th</sup> and 15<sup>th</sup> March, on all of which evidence of katabatic flows were seen.

Hourly wind data from 70 m agl on the nearby (240 m away) OzFlux mast, show the wind blowing from 12 degrees at  $2.8 \text{ m s}^{-1}$  at 03 hours, 13 degrees at  $1.8 \text{ m s}^{-1}$  at 19 hours and 9 degrees at  $3.3 \text{ m s}^{-1}$  at 23 hours on the 13<sup>th</sup> March. These directions are roughly 160 degrees away from the possible katabatic flow directions seen at 1.65 m agl in figure 2.11 for the same times (03 hours, 19 hours, 23 hours), suggesting that these near surface flows are indeed decoupled sub canopy katabatic flows.

Hourly daytime winds for 70 m agl measured on the OzFlux mast for 11 hours and 15 hours on the 13<sup>th</sup> March are  $3.7 \text{ m s}^{-1}$  blowing from 305 degrees, and  $1.9 \text{ m s}^{-1}$  from 279 degrees respectively. Figure 2.11 shows the 1.65 m agl wind blowing from between 288 degrees and 360 degrees at 11 hours and 15 hours EST (wind speeds being around  $1 \text{ m s}^{-1}$ ). This suggests that the daytime airflows seen in figure 2.11 for 11 hours and 15 hours are not uphill anabatic flows, but simply veered and slacked surface winds driven by the overhead geostrophic wind.

Figure 2.13 shows a comparison of wind azimuth histograms valid for 23 hours EST on the 13<sup>th</sup> March 2005 (created using data for the period between 21 hours on the 13<sup>th</sup> and 01 hours on the 14<sup>th</sup> of March). The histograms shown are for 1.65 m agl in the middle of the North, East, South and West faces of the CV, see figure 2.3. Also shown is a histogram for 6 m agl on the mast in the centre of the CV.

All the histograms in figure 2.13 show a probable katabatic flow is occurring, blowing from a Southerly direction for the night of the 13<sup>th</sup> March. The histograms have most of their energy between 144 degrees and 192 degrees, but peak at 168 degrees and 192 degrees.

For the four hour period centred around 23 hrs EST on the 13<sup>th</sup> March, the mean horizontal wind directions derived from the five anemometers mentioned in figure

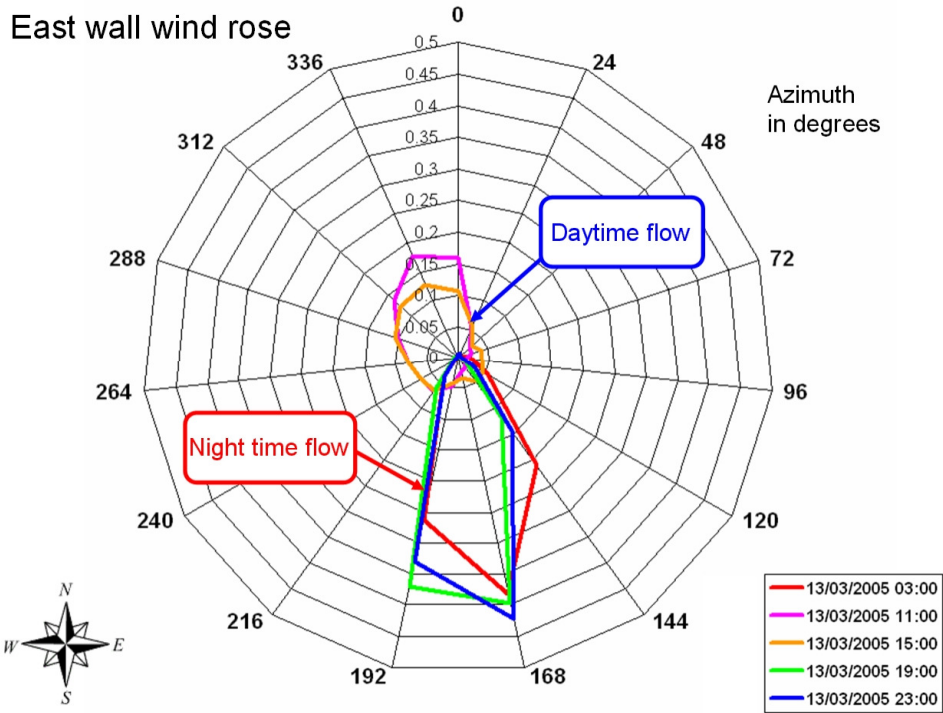


**Figure 2-11** Wind rose for 1.65 m near the centre of the East CV wall, for the 13<sup>th</sup> of March 2005. The wind data was processed using time bins of four hours.

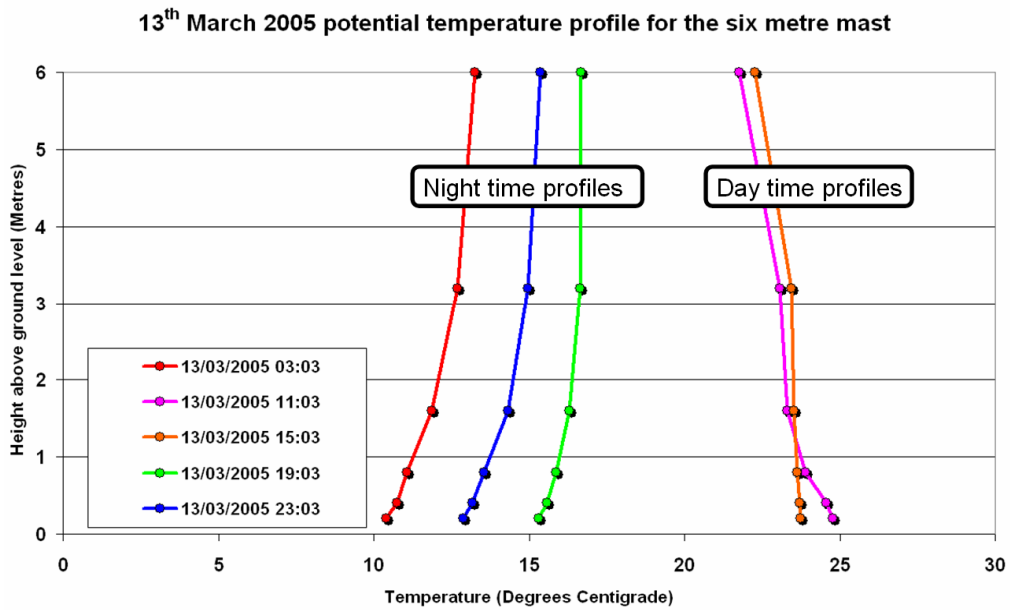


**Figure 2-12** 13<sup>th</sup> March 2005 potential temperature profiles for the central six metre mast, calculated from thermocouple data for heights of 0.2, 0.4, 0.8, 1.6, 3.2 and 6.0 m agl, showing the temperature inversions that occurred.

2.13, were between 175 degrees and 196 degrees, with associated standard deviations of around 30 degrees. Mean vector wind velocities were between 0.3 and 0.4 m s<sup>-1</sup> with a standard deviation of just over 0.1 m s<sup>-1</sup>. Maximum vector wind velocities were around 1 m s<sup>-1</sup> and minimum velocities near zero.

In figure 2.13 all the wind azimuth distributions apart from the west wall anemometer, have maxima for winds blowing from 168 degrees. The azimuth distribution for the west wall by contrast has a maxima for winds blowing from 192 degrees, one azimuth bin or 24 degrees further west than for the other walls. This may be caused by the presence of a small gully situated about 20 m to the west of the CV, that is oriented north-northeast, see figure 2.10.

The effect of this gully on the west end of the CV may be to direct low level katabatic type wind flows in a slightly more north-easterly direction compared to similar wind flows effecting the other three walls of the CV. This possible flow distortion across the CV at night may contribute to errors in estimations of horizontal and vertical (derived via continuity) advection values across the CV.

### **2.2.1 The eddy flux 'lid' calculation for the control volume**

Fluxes through the top surface of the 50 x 50 x 6 m experimental control volume (CV) were determined by the conventional eddy covariance methods (Moncrieff *et al*, 1997).

In order to determine what length of averaging interval would be required to calculate the means of vertical wind speed ( $w$ ) and CO<sub>2</sub> concentrations ( $c$ ) needed in the eddy flux calculations to give satisfactory fluxes, an ogive plot analysis of the cospectrum of  $w$  and  $c$  was carried out as described in Barcza (2001) and Moncrieff *et al* (2004). Figure 2.14 shows such  $w$ - $c$  ogive plots derived from 4 hour data blocks taken from the 'lid' anemometer and IRGA at 6 m agl on the central mast (see figure 2.4). The nocturnal ogive curves in figure 2.14 converge to constant values at frequencies corresponding to averaging times of between 66 seconds and 16 minutes.

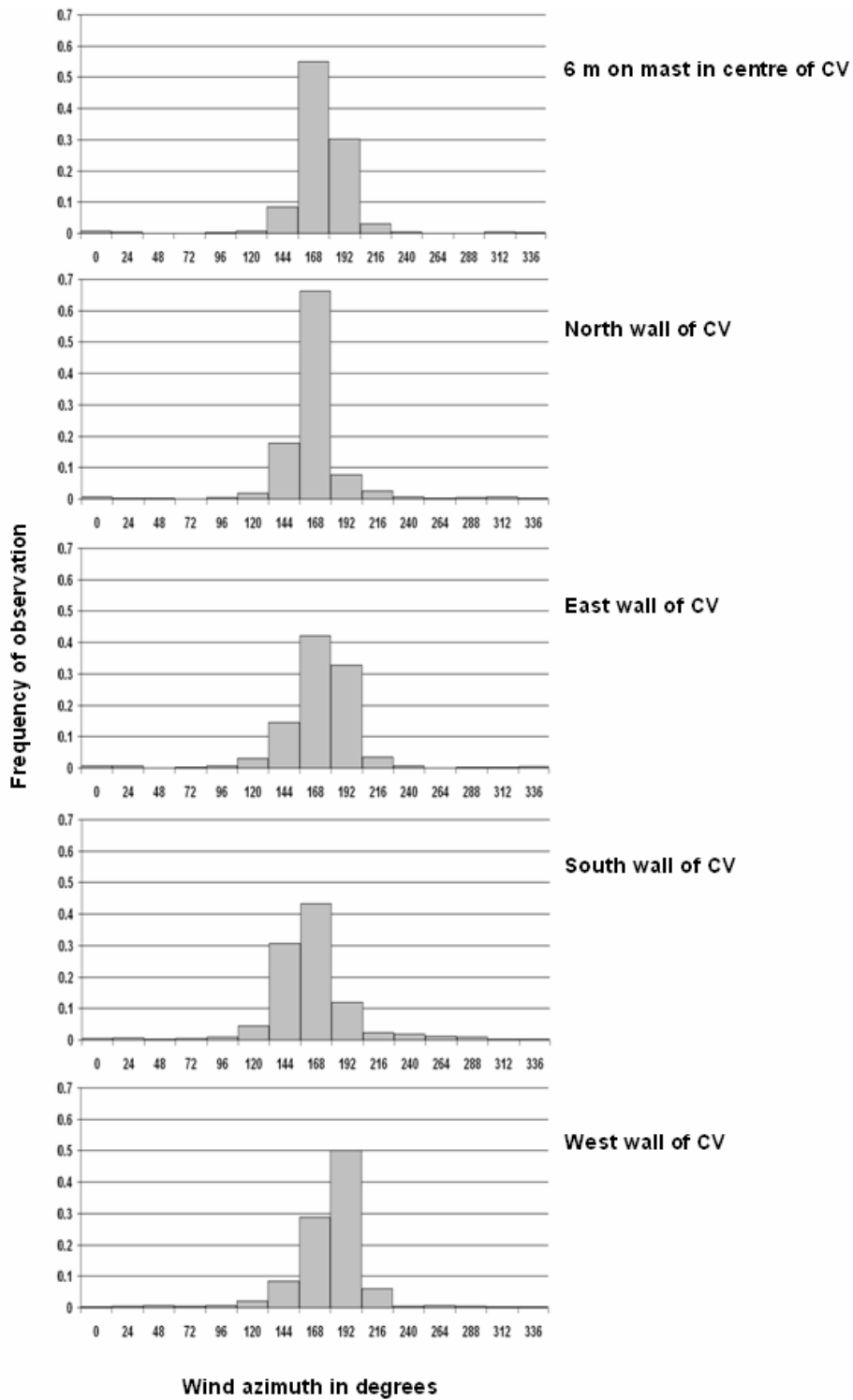


**Figure 2-13** Wind azimuth histograms for 23 hrs EST on the 13<sup>th</sup> March 2005, for sonic anemometers of the North, East, South, and West faces (walls) of the control volume (CV) at 1.65 m, and the central mast at 6 m. The sonic anemometer wind data has been processed using time bins of four hours, centred on 23 hours, to produce each histogram.

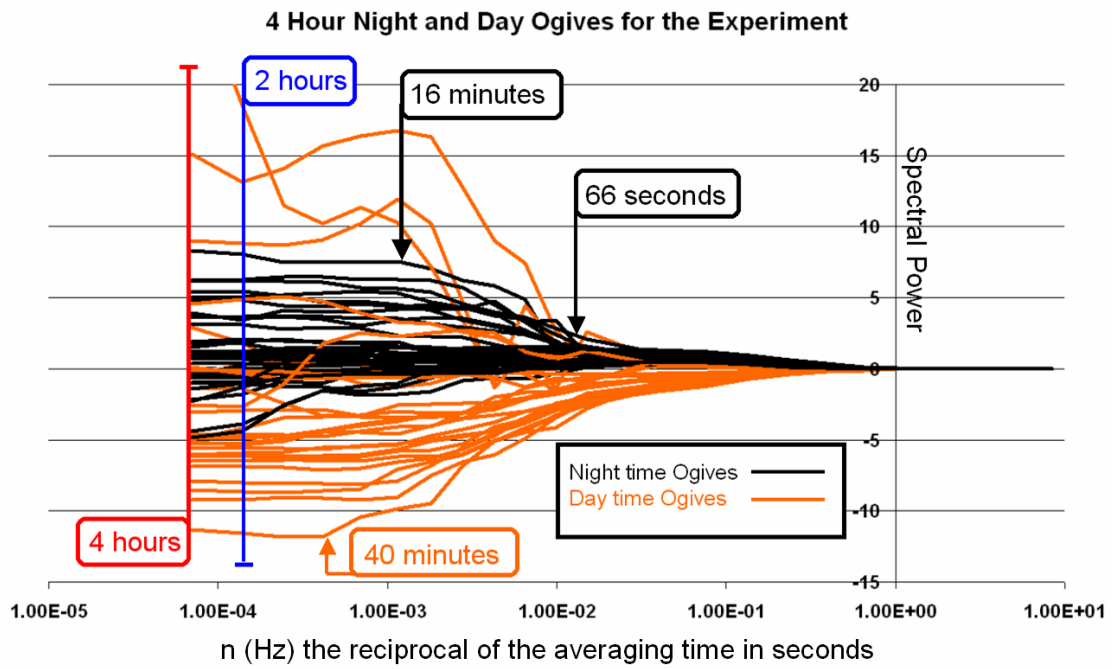


**Figure 2-14**  $w-c$  Ogive plots for the experimental duration derived from 4 hour blocks of data for the 6 m agl 3D anemometer and open path IRGA. Ogives for the transit of synoptic frontal systems over the site have been omitted.

For the daytime ogive curves, convergence occurs at averaging times of around 40 minutes. Only a small subset of the ogive curves for day and night have not converged after an averaging period of one hour, indicating that use of a one hour averaging period for the eddy flux calculation would capture most of the lowest frequency contribution to the 'lid' flux.

Figure 2.15 shows CO<sub>2</sub> and latent heat fluxes for six metres on the central tower, calculated using the eddy covariance method using an averaging period of one hour. In the eddy covariance processing sequence the commonly used 'two coordinate rotation' approach (Tanner & Thurtell, 1969) was used making use of two rotation coefficients (Alpha and Beta) calculated for each averaging period.

Eddy fluxes were also calculated using a single set of two rotation coefficients calculated using the 'planar fit method' (Wilczak *et al.* 2001) for the ten days of settled weather between the two cold fronts, however the results were similar to those obtained using the 'two coordinate' method, and so will not be referred to further. In both cases corrections were made for the effect of variations in air density on the fluxes of water vapour and CO<sub>2</sub> (Webb *et al.* 1980).

In figure 2.15, filtering out of implausible results has already been done based on micrometeorological considerations (Clement. R., 2005; *pers comm.*). However, despite this both fluxes look very noisy, and it was decided to add the observed daily signals to each other, for the less noisy period between the two synoptic weather fronts (shown on figure 2.15), in an attempt to get a usable diurnal flux curve.

The resulting diurnal flux curves are shown in figure 2.16, which shows the latent heat flux curve as expected having values close to zero at night and positive values during the daylight hours (peaking at around 125 W m<sup>-2</sup> at 1pm EST). The sign convention used in figure 2.16 is positive values indicate a net upward flux from the surface into the atmosphere. The situation with respect to the CO<sub>2</sub> flux is more problematic with the diurnal curve showing a 'double humped' appearance, peaking around 5 and just under 6 μmol m<sup>-2</sup> s<sup>-1</sup> in the morning and afternoon respectively. The CO<sub>2</sub> flux curve shows a minimum of almost -3 μmol m<sup>-2</sup> s<sup>-1</sup> (a downward flux)

CO2 and Latent Heat fluxes for the Experiment, at 6 Metres on the Cental Tower

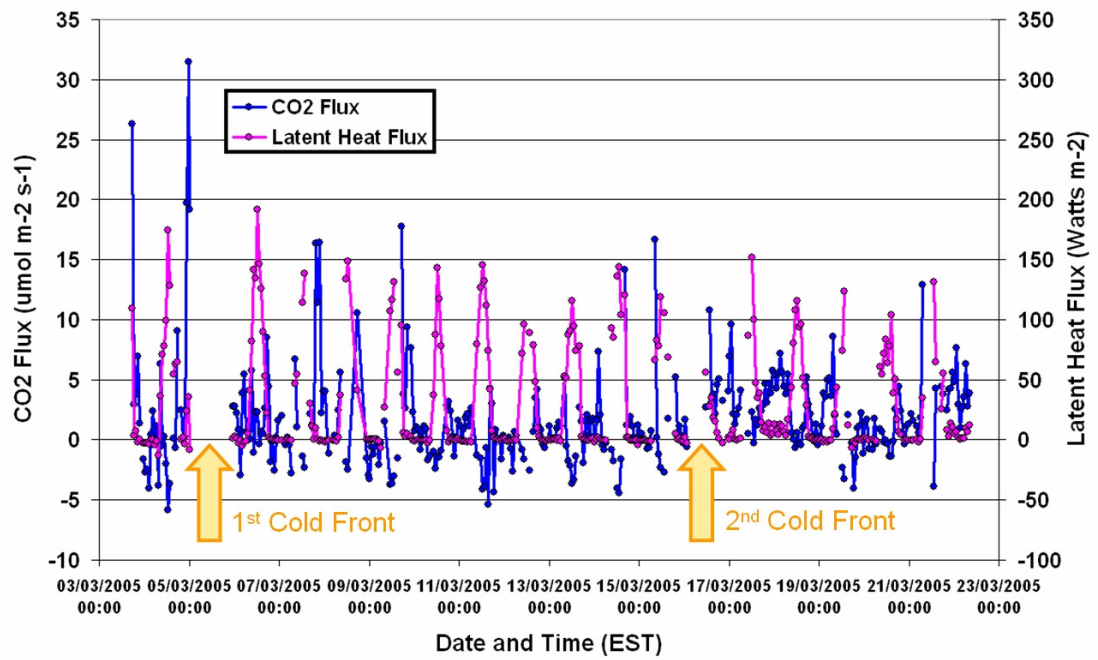


**Figure 2-15** Carbon dioxide and latent heat fluxes calculated for 6 m agl on the central tower, using the eddy covariance method, with an averaging time of one hour. Removal of ‘bad’ data points based on micro-meteorological considerations has already been carried out.



Mean Daily Fluxes for 6 Metres Above Ground Level (6th - 15th March 2005)

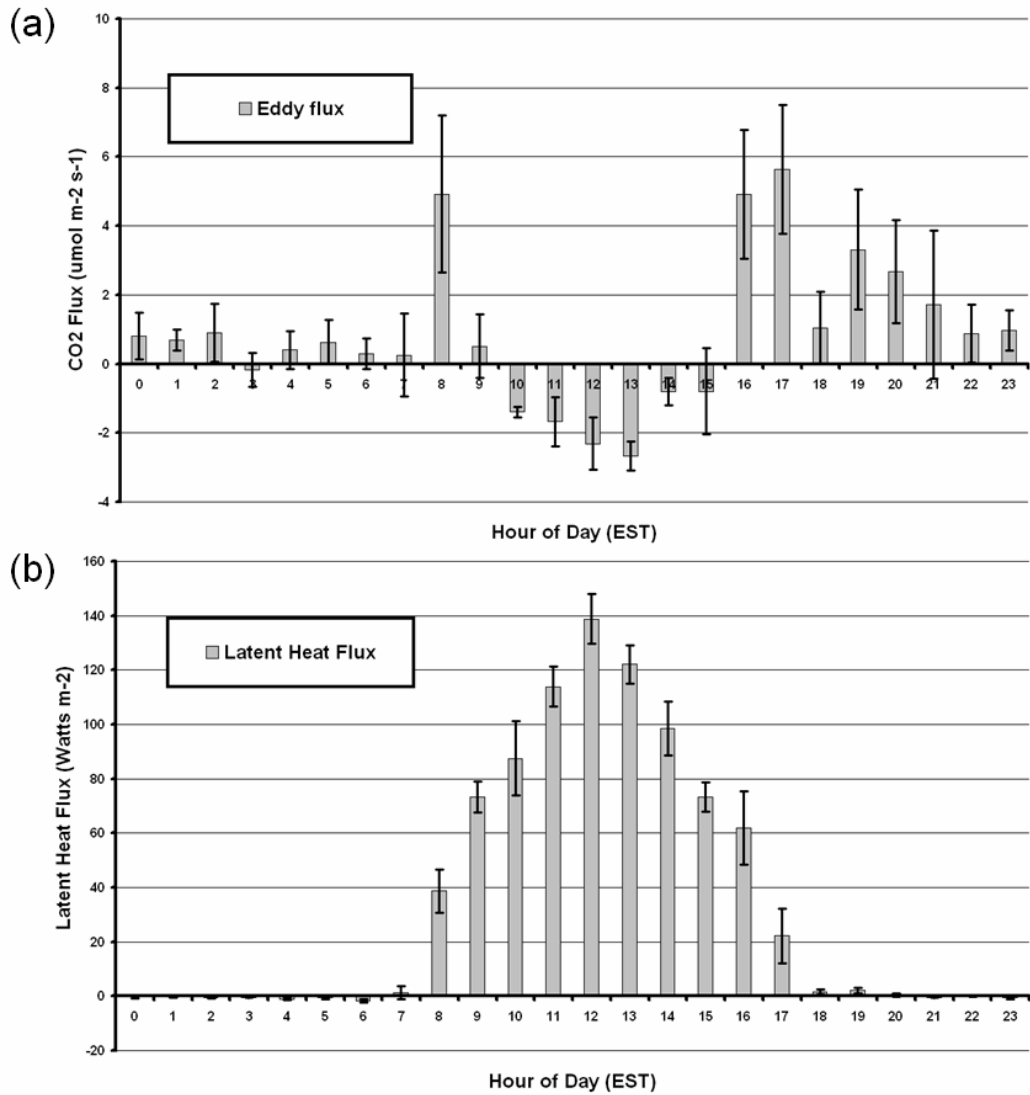


**Figure 2-16** Mean diurnal flux curves for CO<sub>2</sub> (a) and latent heat (b), derived from eddy covariance fluxes derived for the period 6<sup>th</sup> – 15<sup>th</sup> March 2005 inclusive, at 6 m agl on the central mast. The error bars on the individual CO<sub>2</sub> and latent heat curves represent plus and minus one standard error.

around midday. The night time CO<sub>2</sub> flux is around 1 μmol m<sup>-2</sup> s<sup>-1</sup> for most of the night, apart from between 19 and 21 hours when it is between 2 and 3 μmol m<sup>-2</sup> s<sup>-1</sup>.

The mean CO<sub>2</sub> flux derived from the diurnal curve was 1.4 μmol m<sup>-2</sup> s<sup>-1</sup>, suggesting that between the 6<sup>th</sup> and 15<sup>th</sup> March a net upward movement of CO<sub>2</sub> occurred through the 6 m flux plane (this does not necessarily mean the whole depth of the forest was a CO<sub>2</sub> source during this period).

Initially it was thought that a possible explanation for the low observed respiration flux during the nighttime was that the forest structure was acting as a collimator allowing bright sunlight to illuminate the under storey during the middle of the day but causing deep shade in the morning and afternoon (Clement. R., 2005; *pers comm.*).

Such a situation might result in the CO<sub>2</sub> flux curve seen in figure 2.16, photosynthesis dominating around midday (negative/downward CO<sub>2</sub> flux values), and respiration dominating (positive/upward CO<sub>2</sub> flux values) during the warm morning and afternoon, with night time respiration being suppressed by comparatively low night time temperatures.

However, as will be discussed later in this chapter, analysis of wind profiles measured between 0.2 and six metres agl on the central mast within the CV during the experiment, strongly suggest that decoupling of the forest understorey from the eddy flux system at six metres was occurring during the nighttime.

Figure 2.17 shows CO<sub>2</sub> flux measurements carried out by Black *et al* (1996) during June 1994 in a boreal aspen forest in Canada giving results comparable with figure 2.16, despite the different time of year (mid summer instead of early autumn) and latitude. Black *et al.* (1996) made flux measurements at 4 m agl above a hazelnut understorey about 2 m tall, and beneath aspen trees of height 21 m (canopy base was at 15 m). Daytime latent heat fluxes (not shown) peaked at values between 50 and 150 W m<sup>-2</sup>, and were close to zero at night. These latent heat results are of a similar magnitude to those seen at 6 m agl at the Tumbarumba site (see figures 2.15 and 2.16).

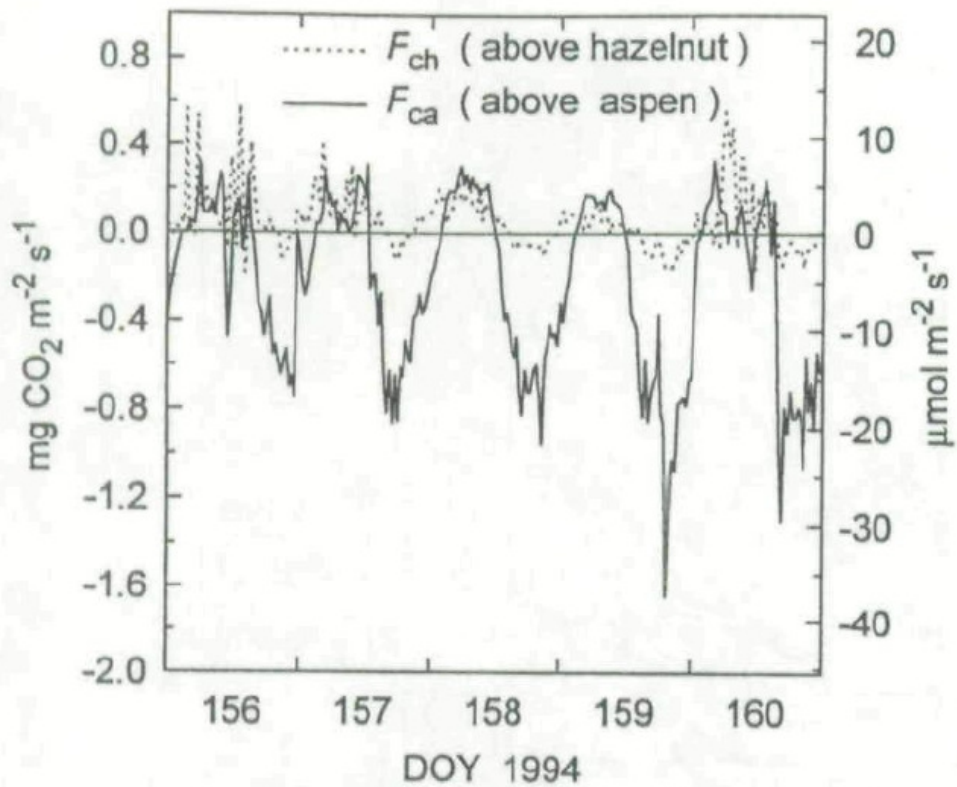


**Figure 2-17** Comparison of half-hourly eddy-correlation CO<sub>2</sub> fluxes measured above an aspen overstorey ( $F_{ca}$ ) and above a hazelnut understorey ( $F_{ch}$ ). From Black *et al* (1996).

For CO<sub>2</sub> flux curves at 4 m agl on the Canadian site, minima occurred near midday with fluxes of -1 to -3  $\mu\text{mol m}^{-2} \text{s}^{-1}$ . Afternoon and morning fluxes were around 2  $\mu\text{mol m}^{-2} \text{s}^{-1}$ , and maxima occurred at night with fluxes of 3 to 5  $\mu\text{mol m}^{-2} \text{s}^{-1}$ . Again the Canadian and Tumberumba CO<sub>2</sub> fluxes between the under storey and over storey are broadly similar in shape and magnitude with one notable exception, that the Australian CO<sub>2</sub> fluxes drop back close to zero at night, whereas the Canadian ones remain high and in fact attain their maximum diurnal values.

### 2.2.2 The discovery of a maxima in the nighttime wind profile

Figure 2.18 shows hourly horizontal wind and CO<sub>2</sub> profiles up the central mast in the CV for the night of the 12<sup>th</sup> March 2005. A maxima or 'jet' in the horizontal wind speed of 0.3  $\text{m s}^{-1}$  (1.5 times the wind speed at six metres) is seen at three metres above ground level. CO<sub>2</sub> mole fractions in the forest understorey (< 1m agl) increase from around 480 ppm at 19 hours EST up to around 600 ppm for the hour starting at 23 hours EST. The mean CO<sub>2</sub> mole fraction falls from 580 ppm at 0.2 m to 430 ppm at the 6 m level, with a break in slope at just below 1m agl that may indicate the top of a CO<sub>2</sub> enriched layer within the understorey.

In addition the wind speed curve shown in figure 2.18 may show a zero plane displacement of around 0.2 metres caused by the understorey vegetation. During the time period shown in figure 2.18 there was a positive potential temperature gradient within the CV indicating stable conditions. A similar situation of a temperature inversion and a horizontal wind maxima or 'jet' was observed on all the nights between the two synoptic weather fronts. During the daytime, wind velocity within the CV increased monotonically with height and no maxima was observed.

Figure 2.19 show examples of profiles of hourly average CO<sub>2</sub> mole fractions, potential temperature and normalised wind speed on the CV's 6 m central mast, for both nighttime and daytime conditions (modified from Leuning *et al.* (2008)), for the period between the two synoptic weather fronts that affected the site.

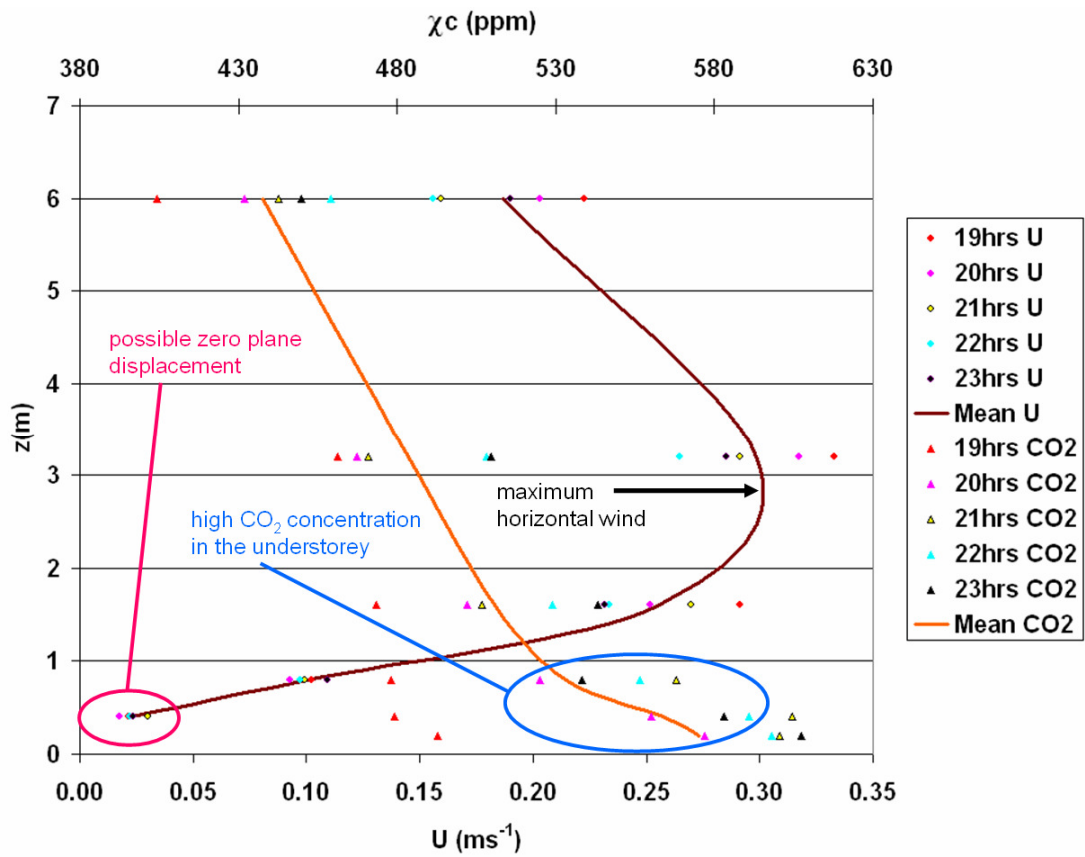


**Figure 2-18** Vertical variations of hourly average horizontal wind speed measured at 0.4, 0.8, 1.6, 3.2 and 6 m and  $\text{CO}_2$  mole fractions measured at 0.2, 0.4, 0.8, 1.6, 3.2 and 6 m on the CV central mast between 19 and 23 hours (inclusive) on the night of 12<sup>th</sup> March 2005. The mean profiles are drawn using splines to link the means of the hourly values.

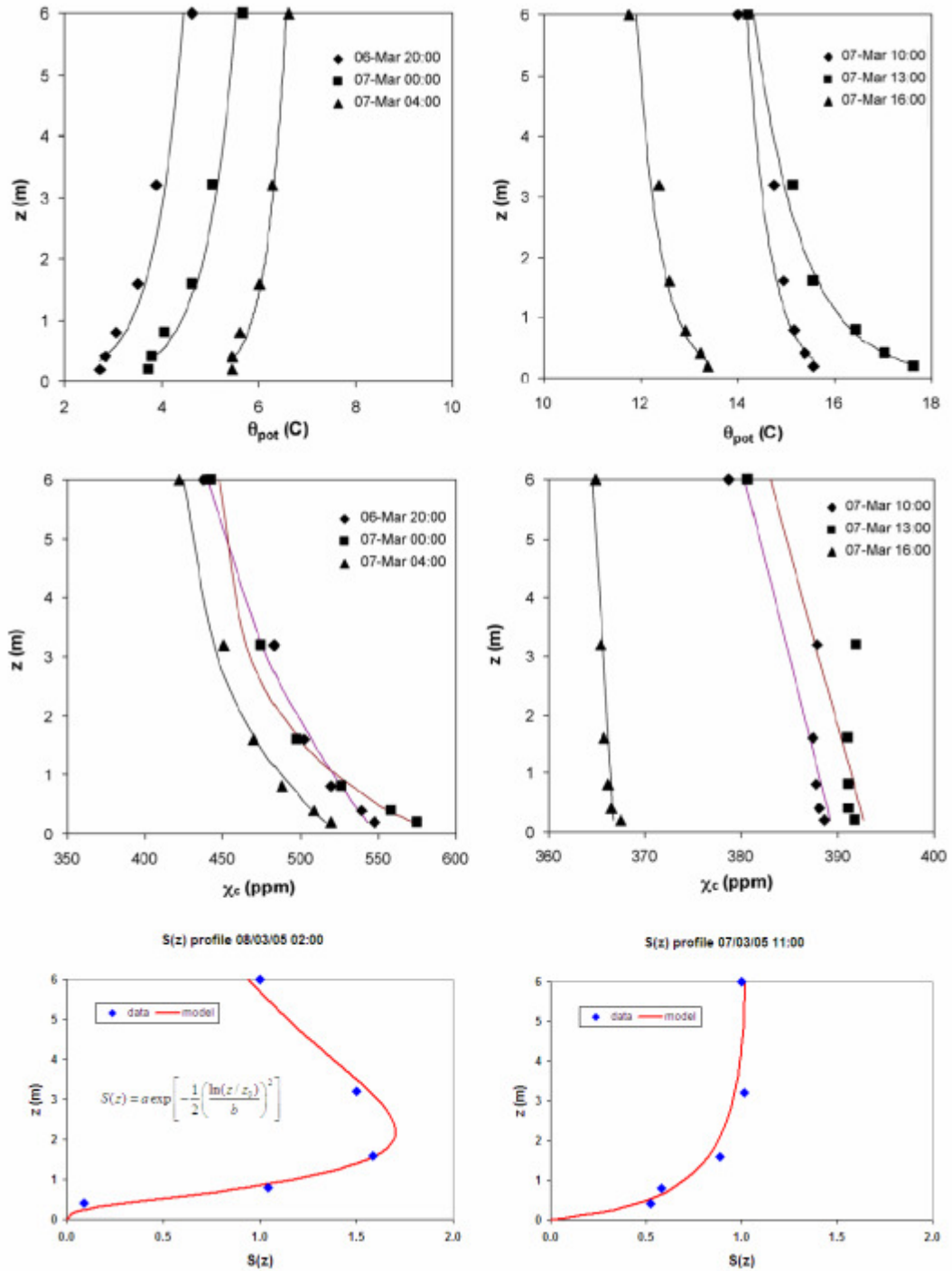


**Figure 2-19** Examples of average CO<sub>2</sub> mole fractions, potential temperatures and normalised windspeed profiles observed on the central 6 m mast within the CV, for nighttime (lefthand side of figure) and daytime (righthand side of figure). *Modified from Leuning et al. (2008).*

Leuning *et al.* (2008) have modelled the normalised wind speed profile using a log-normal function:

$$S_1(z) = a_c \exp \left[ -\frac{1}{2} \left( \frac{\ln(z/z_c)}{b_c} \right)^2 \right] \quad (2-7)$$

that is able to fit both the maximum ‘jet’ within the nighttime wind profile, and the monotonically increasing daytime profile (see figure 2.19). Where  $S_1(z)$  is normalised wind speed as a function of height,  $z$ , within the CV, and  $a_c$ ,  $b_c$  and  $z_c$  are parameters determined for each one hour interval. Leuning *et al.* (2008) describes how  $S_1(z)$  was calculated for each hour using wind speed values measured on the central 6 m mast, in order to provide a correction factor that was applied to the horizontal advection terms (the second and third terms in equation 2.4). This was required because under the stable stratification conditions existing within the CV at night, significant variations in the shapes of the hourly profiles were observed.

Figure 2.19 shows that an inversion of potential temperature ( $\theta_{pot}$ ) exists within the CV during the night but is absent during the day, and that nighttime CO<sub>2</sub> mole fractions within the CV are substantially greater than those observed in daytime, the lower 2 m of the CV at night being particularly enriched in CO<sub>2</sub> compared to the upper 4 m (a similar pattern of enrichment is seen in figure 2.18).

The potential temperature ( $\theta_{pot}$ ) is defined as the temperature a parcel of air would attain if adiabatically transferred to 1000 hPa (approximately the pressure of sea level). Since  $\theta_{pot}$  is conserved for adiabatic processes, a parcel of air will retain its  $\theta_{pot}$  value at all pressures (and altitudes), unlike temperature which varies with height due to decreasing pressure (Foken *et al.* 2008, Garrat 1994). Figure 2.19 uses  $\theta_{pot}$  rather than temperature profiles so a direct estimate of stability can be made from the profile gradient, and so comparison can be made with  $\theta_{pot}$  profiles measured on the 70 m high mast of the Tumbarumba flux station given in Leuning *et al.* (2008).

The normalised nighttime wind profile shown in figure 2.19 shows an obvious maxima or ‘jet’ at around 2 m agl, with a value  $S(z)$  of about 1.7 times the wind speed at 6 m (again a similar situation is shown in figure 2.18).

If we reconsider the shape of the diurnal  $\text{CO}_2$  eddy flux curve as shown in figure 2.16, the low values of upward  $\text{CO}_2$  flux seen at night (around  $1 \mu\text{mol m}^{-2} \text{s}^{-1}$  after midnight) are probably explained by the presence of this stable layer of air that constitutes the ‘jet’ in the lower part of the CV, the effect of which is to decouple the 6 m agl level from the respiration of the understorey. The higher values of  $\text{CO}_2$  flux of between 5 and  $6 \mu\text{mol m}^{-2} \text{s}^{-1}$  seen around sunset and sunrise being explained by the ‘jet’ having yet to form, or having been dissipated by heating from below, respectively.

We believe this discovery of the effect of a nighttime sub canopy wind speed maxima or ‘jet’ on the shape of the diurnal  $\text{CO}_2$  eddy flux curve measured above the understorey but below the forest canopy proper (see figure 2.16a), is more than a mere curiosity. This is because the presence of the characteristic ‘double humped’ diurnal  $\text{CO}_2$  eddy flux curve measured in a similar situation in the gap between a widely vertically separated understorey and overstorey may be indicative of the presence of a nocturnal subcanopy ‘jet’ below the measurement level. Black *et al.* (1996) carried out just such eddy flux measurements in the canopy space of a Canadian aspen forest, but their  $\text{CO}_2$  flux curves stayed high at night (see figure 2.17) indicating that no subcanopy ‘jet’ was present below the measurement level.

Figure 2.20 shows a foliage area volume density (FAVD) profile as measured using a ground based lidar in the vicinity of the 70 m tower, which lies 240 m northeast of the CV. This figure is taken from Leuning *et al.* (2008) and based on information provided by Jupp *pers comm.* (2008). This FAVD profile is the mean of measurements made at eight locations within the eddy flux ‘footprint’ of the 70 m mast. Figure 2.20 shows two distinct peaks in FAVD one of  $0.1 \text{ m}^{-1}$  for the upper Eucalyptus canopy around 35 m agl, and a slightly smaller one around 7 m agl with a value of  $0.07 \text{ m}^{-1}$  (Leuning *et al.* 2008). The lidar was unable to provide data below 2 m agl and so the understorey is not resolved in figure 2.20.



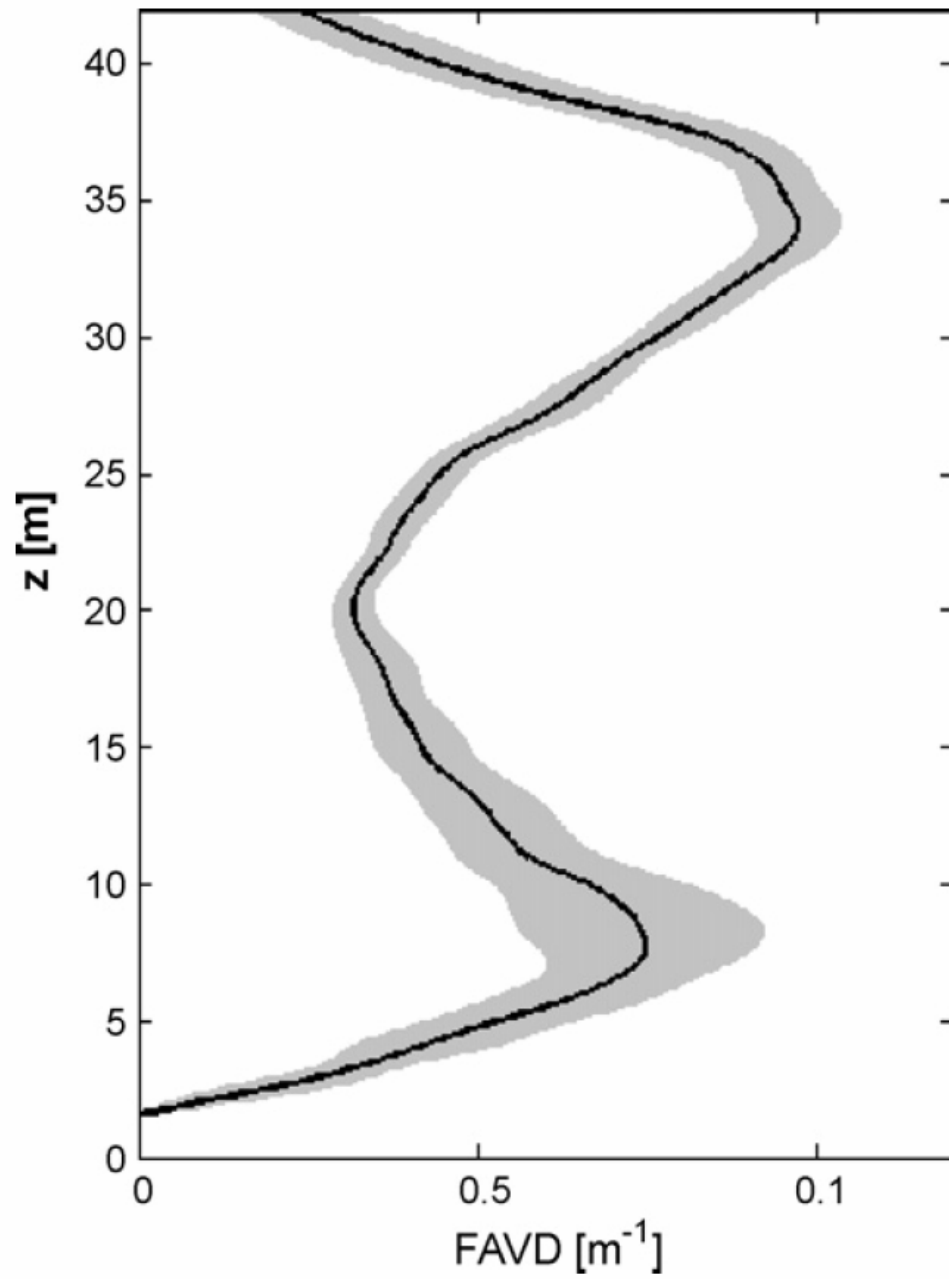


**Figure 2-20** Foliage area volume density (FAVD) profile measured for forest within the eddy flux footprint of the 70 m OzFlux tower using a ground based lidar. *From Leuning et al. (2008).*

Interestingly, the peak in FAVD at 7 m agl was not subjectively evident when one was working within the 50 by 50 m CV, although an underbrush/understorey up to around 1 m high certainly was, as was the Eucalyptus overstorey at 35 m agl.

The foliage distribution seen in figure 2.20 is relevant to the formation of relative wind speed maxima within the forest canopy. Fritschen (1985) shows how the aerodynamic drag of forest canopy elements can cause a relative wind speed maxima or 'jet' to exist in the stem space beneath a forest canopy. Fritschen describes the distribution of aerodynamic elements within his forest example in terms of profiles equivalent to FAVD, and relates observed relative 'jets' in the stem space to low FAVD values close to the ground.

An important difference between Fritschen's FAVD profiles and the one shown for the Tumbarumba forest in figure 2.20, is that Fritschen's illustrative example is a Douglas fir stand with a peak FAVD value of around  $2 \text{ m}^{-1}$  at 10 to 15 m agl, whereas the Tumbarumba has a FAVD peak of an order of magnitude less ( $0.1 \text{ m}^{-1}$  at 35 m agl). Another crucial difference between Fritschen's analysis and the situation at Tumbarumba is that the 'jet's within the Tumbarumba CV (see figures 2.18 and 2.19) are only seen at night under conditions of thermal inversion within the lower part of the canopy.

Looking at the FADV profile for the Tumbarumba forest shown in figure 2.20 it would be tempting to relate the nocturnal 'jets' seen at 2 m to 3 m agl (see figures 2.18 and 2.19) to the minima in the Tumbarumba FAVD profile at 2 m agl (see figure 2.20) that would exist if the FAVD values related to the understorey could be added below the 2 m level.

However, since the 'jet' in the CV is only seen at night this indicates it is a katabatic gravity type flow rather than one simply caused by the aerodynamic drag of the forest elements. There is still the possibility that despite being a katabatic type flow, the 'jet' seen in the CV may somehow be mechanically and/or thermally coupled to the forest vegetation elements that give rise to the FAVD profile shown in figure 2.20.

This would give rise to the interesting possibility that a second nighttime subcanopy wind maxima or 'jet' might exist at 20 m agl in the FAVD minima between the upper and lower FAVD peaks in figure 2.20. Unfortunately, the only two anemometers at a suitable height agl to measure such a mid canopy 'jet' were of the rotating cup type, situated on the 70 m OzFlux mast (at 10 m and 26 m agl), which were unable to measure wind speeds below  $0.4 \text{ m s}^{-1}$ .

Neither of these two anemometers showed evidence of a mid canopy jet during the Tumbarumba experiment. However, the possibility is still open that such a nocturnal 'jet' might exist at around 20 m agl during the nighttime, but be associated with a wind velocity below  $0.4 \text{ m s}^{-1}$  at a heights of 10 m and 26 m.

### **2.2.3 Other results from the CV faces and 6 m central mast**

The entire temporal extent of data used by Leuning *et al.* (2008) in their advection analysis was 15 days from 08 hours EST on the 6<sup>th</sup> March 2005 until 06 hours EST on the 21<sup>st</sup> March 2005. This duration was constrained by the availability of data for the CV faces and 6 m central mast recorded by the CSIRO equipment. Other time series such as latent heat and CO<sub>2</sub> eddy fluxes, and sonic temperatures were available between the 3<sup>rd</sup> March 2005 and 22<sup>nd</sup> March 2005 (see figures 2.15 and 2.7).

Figure 2.21 shows time series of data collected from the faces of the CV, and the 6 m mast in the centre of the CV. The duration of the plotted time series in figure 2.21 is 12 days from late morning on the 6<sup>th</sup> March 2005 until around noon on the 18<sup>th</sup> March 2005, the final three days of available data have been omitted for clarity but have similar characteristics to the 'calm nights' in figure 2.21c.

Figure 2.21d showing potential temperature at three selected levels on the 6 m mast, indicates that for all nights considered by Leuning *et al.* (2008), apart from the later part of the night of the 15<sup>th</sup> March when a rain bearing weather front was crossing the site, there was a temperature inversion between 0.2 m and 6 m agl in the CV.

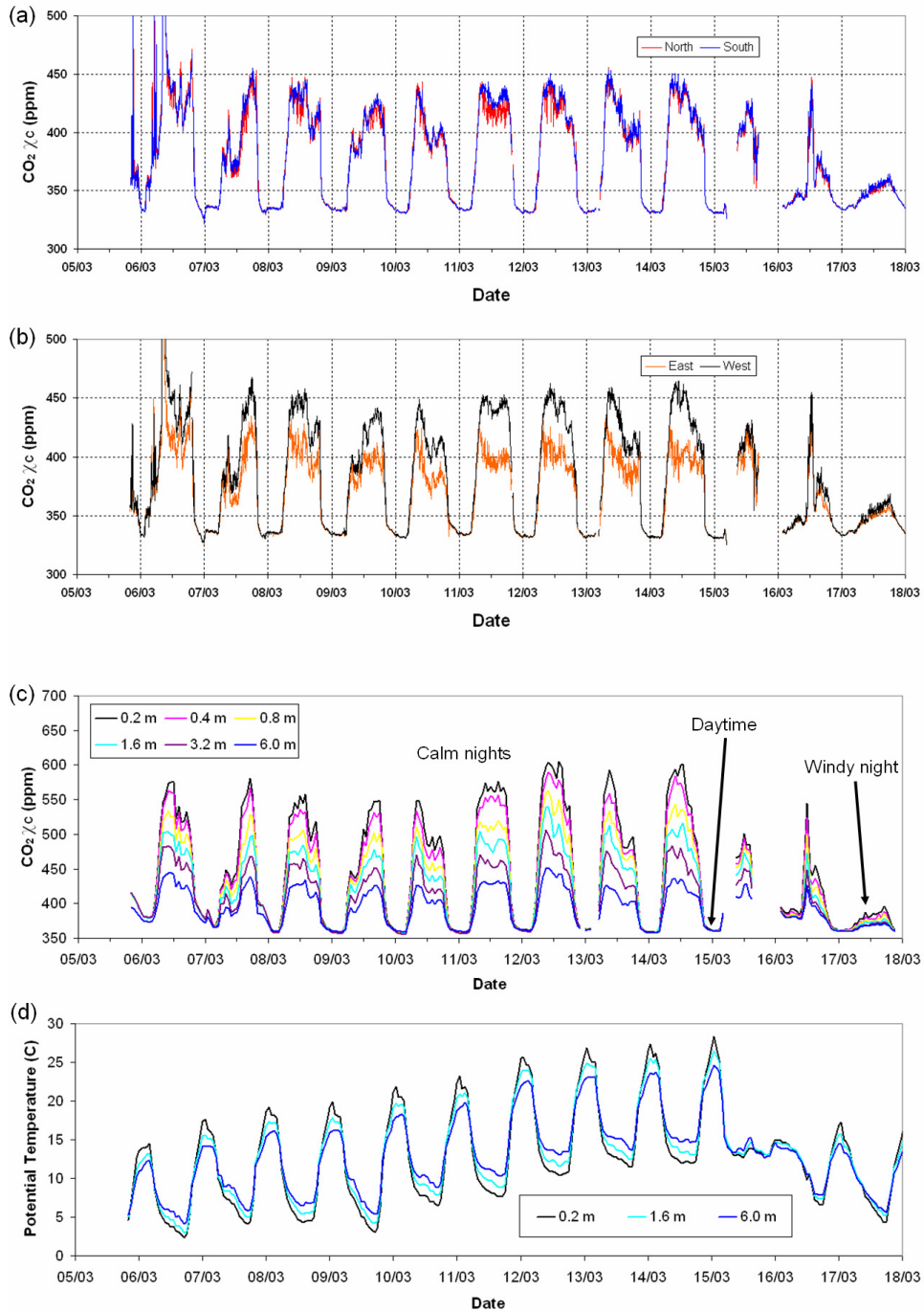


**Figure 2-21** Time series for the period 6-18 March 2005, of (a) weighted mole fractions of CO<sub>2</sub> for the north and south walls of the CV, and (b) the east and west walls. Shown in (c) and (d) are time series of CO<sub>2</sub> mole fractions and potential temperatures measured between 0.2 m and 6 m agl on the 6m mast at the centre of the CV. Date labels are centred on midday. This is an expanded version of two figures in Leuning *et al.* (2008).

Figure 2.21d also shows the progressive increase in diurnal temperatures between the 6<sup>th</sup> and 15<sup>th</sup> March associated with calm high pressure weather conditions (see also figure 2.7). The conditions within the CV on these nights were stable and stratified.

Figure 2.21c shows CO<sub>2</sub> mole fractions at six heights on the 6 m mast, indicating that for the calm nights between the 6<sup>th</sup> and 15<sup>th</sup> March, there was a vertical CO<sub>2</sub> gradient of around  $-25 \text{ ppm m}^{-1}$  (CO<sub>2</sub> mole fractions increasing by around 150 ppm from the top of the CV at 6 m, down to 0.2 m agl, as also seen in figure 2.18). During the calm days by contrast, all the CO<sub>2</sub> mole fractions at the various heights on the 6 m mast had similar values of around 360 ppm, indicating that the daytime CV was well mixed vertically. Figure 2.21d for the calm days shows that daytime potential temperature decreases with height within the CV, which is also consistent with the CV being well mixed during the day.

The night of the 17<sup>th</sup> March is notable for the CV being affected by windy conditions following the passing of the weather front. Although there is still a nocturnal inversion in potential temperature within the CV, the vertical CO<sub>2</sub> gradient is now only  $-3 \text{ ppm m}^{-1}$  compared to  $-25 \text{ ppm m}^{-1}$  on the calm nights. This indicates that during the night of 17<sup>th</sup> March the CV was being subjected to weak mixing caused by wind shear induced turbulence.

In figure 2.21a and figure 2.21b, the weighted mole fractions of CO<sub>2</sub> for the north and south, and east and west faces of the CV are shown respectively. Both sets of time series show the expected diurnal ‘cycling’ with higher mole fraction values present at night. Also the time series have gaps on the 15<sup>th</sup> and 16<sup>th</sup> March 2005, when the air pumps were turned off to avoid rain water associated with the passing weather front being drawn into the perforated sampling tubes (figure 2.21c shows gaps for the same reason).

In figure 2.21a, the difference in weighted mole fractions of CO<sub>2</sub> between the north and south faces of the CV are small at night, having a maximum difference of around 5 to 10 ppm on the night of the 11<sup>th</sup> March 2005, with the north face having the

lower of the two values. The differences between the north and south faces for the other nights during the experiment are considerably smaller.

The differences in weighted mole fractions of CO<sub>2</sub> in figure 2.21b between the east and west CV faces at night are more significant, being around 10 to 20 ppm for the nights of the 6<sup>th</sup>, 7<sup>th</sup>, 8<sup>th</sup>, 9<sup>th</sup> and 10<sup>th</sup> March 2005, and 30 to 50 ppm for the nights of the 11<sup>th</sup>, 12<sup>th</sup>, 13<sup>th</sup> and 14<sup>th</sup> March 2005, with the west face having the higher mole fraction value. These nine nights between the 6<sup>th</sup> and 14<sup>th</sup> of March 2005 have calm high pressure weather conditions, as discussed earlier, and it is likely that the excess in CO<sub>2</sub> mole fraction observed at the west face of the CV is associated with an enriched CO<sub>2</sub> mole fraction within the gully present just beyond the west face of the CV (Leuning *et al.* 2008). A similar effect is present for the final three calm nights (19<sup>th</sup> to 21<sup>st</sup> March 2005, not shown in figure 2.21) but with the CO<sub>2</sub> mole fraction excess of the west face over the east now reduced to between 15 and 30 ppm.

During the daytime throughout the experiment the differences in weighted CO<sub>2</sub> mole fraction between the four faces of the CV were insignificant.

Leuning *et al.* (2008) discusses the presence of the large weighted CO<sub>2</sub> mole fraction difference between the east and west CV faces at night. They conclude that because the nocturnal wind direction within the CV was overwhelmingly from south to north, the contribution of the large east west CO<sub>2</sub> mole fraction gradient to total nighttime horizontal advection would be small.

## **2.2.4 Vertical velocities within the CV**

Figure 2.22 shows plots of hourly averages of the unrotated vertical air velocity ( $\overline{w}_m(h)$ ) measured by the sonic anemometer situated at 6 m agl on the mast in the centre of the CV. This sonic anemometer was levelled using a spirit level before the beginning of the experiment. Figure 2.22a shows  $\overline{w}_m(h)$  values plotted against the mean directions (in degrees from north) the horizontal wind was blowing from during the 1 hour averaging periods. The  $\overline{w}_m(h)$  values for daytime hours plotted in figure 2.22a, are distributed over all wind directions in a roughly sinusoidal pattern.

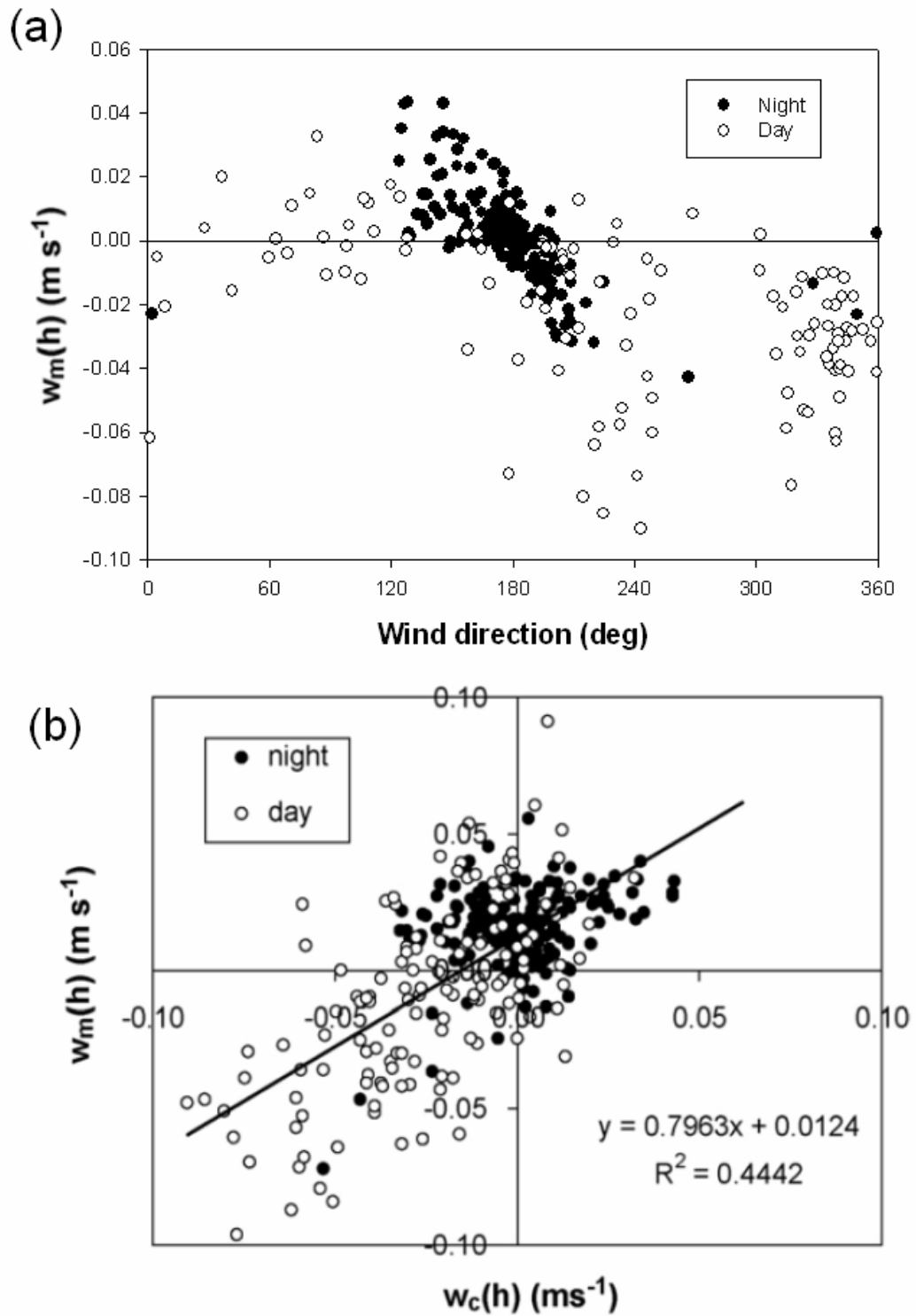


**Figure 2-22** Scatter plot of hourly mean vertical velocities ( $\overline{w}_m(h)$ ) measured at 6 m on the central mast using a 3D sonic anemometer, against (a) wind direction azimuth, and (b) vertical velocities calculated using the continuity equation ( $\overline{w}_c(h)$ ). Figure 2.19b is taken from Leuning *et al.* (2008).

This is consistent with the northwesterly direction of the downhill topographic slope within the CV. Such distribution is a result of the air movement vectors recorded by the 3D sonic anemometer being approximately parallel to the underlying topographic surface. This effect increases as the underlying surface is approached, and similar plots of data (not shown) from the four sonic anemometers situated at 1.65 m agl around the CV faces, have a much more defined sinusoidal distribution patterns.

Figure 2.22a confirms the nighttime airflow through the CV is predominantly from the south, with fringing values mostly coming from between 120 and 220 degrees. The mean of  $\overline{w_m}(h)$  at night was  $0.015 \text{ m s}^{-1}$ .

A particular difficulty with the  $\overline{w_m}(h)$  values plotted in figure 2.22a is the problem of separating ‘true’ vertical velocities useful for calculating the vertical advection term, from ‘contamination’ due to the vertical components of air flows approximately parallel to the underlying ground surface. Leuning *et al.* (2008) tried to overcome this problem by carrying out a coordinate rotation on the raw 3D vector components  $(u_m, v_m, w_m)$  recorded by the 6 m sonic anemometer. This created new vector components  $(u_n, v_n, w_n)$  with horizontal values  $(u_n, v_n)$  parallel to the underlying topography (sloping downhill at 4.6 degrees towards the northwest), and vertical components  $(w_n)$  at right angles to the topographic surface within the CV. It was hoped that this would provide hourly means of  $w_n$  at 6 m agl ( $\overline{w_n}(h)$ ) that could be used to calculate meaningful vertical advection values. Resulting hourly  $\overline{w_n}(h)$  values were plotted against hourly means of vertical velocity ( $\overline{w_c}(h)$ ) produced using the continuity equation and the new shape factor  $S_1(z)$ , see equations 2.5 and 2.7, to produce a scatter plot (not shown). Unfortunately, there was poor correlation between these plotted  $\overline{w_n}(h)$  and  $\overline{w_c}(h)$  values ( $R^2 = 0.017$  according to Leuning *et al.* (2008)) indicating that  $\overline{w_n}(h)$ , would not be suitable for vertical advection estimation.

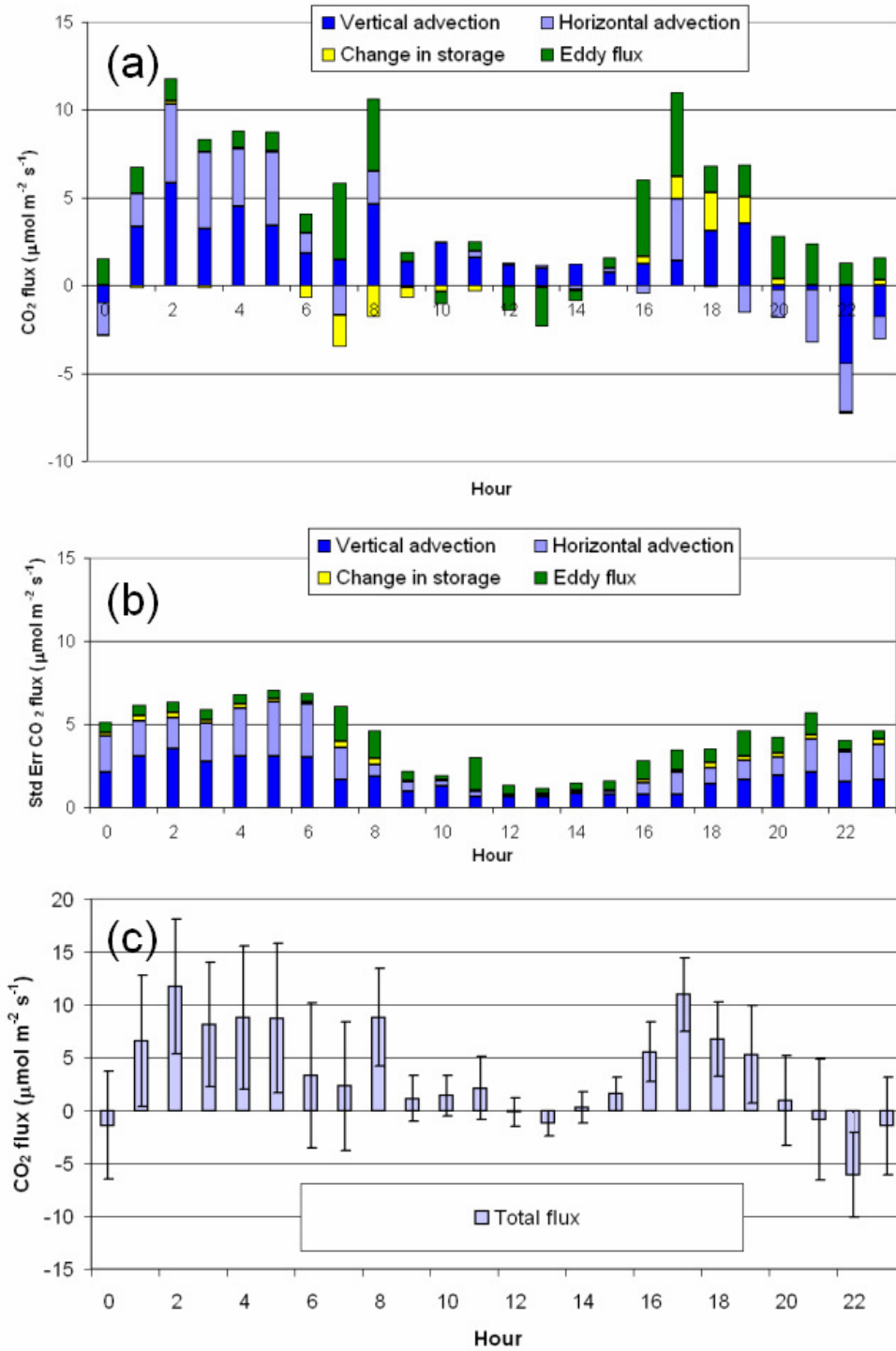


Figure 2.22b shows a scatter plot of the original  $\overline{w}_m(h)$  values from the 6m sonic anemometer against the  $\overline{w}_c(h)$  values derived using continuity. Surprisingly, the correlation is fairly good for all plotted values with an  $R^2$  of 0.444 (Leuning *et al.* 2008). However,  $\overline{w}_m(h)$  suffers from a mean value at night of  $0.015 \text{ m s}^{-1}$ , which is possibly caused by an unnoticed droop in the arm at 6 m agl that held the sonic anemometer, which may have occurred after initial levelling. Because of the large mole fraction gradients of  $\text{CO}_2$  within the CV at night this velocity offset gives rise to large negative values of vertical advection of between  $-10$  and  $-20 \mu\text{mol m}^{-2} \text{ s}^{-1}$  (Leuning *et al.* 2008) for all the calm nights. It was concluded that these large negative nighttime vertical advection values were an artefact of the velocity offset and not related to ‘real’ vertical advection velocities.

Therefore, we are left with just  $\overline{w}_c(h)$  derived from continuity, as a candidate from which to get usable vertical advection quantities. Fortunately, the  $\overline{w}_c(h)$  values shown in figure 2.22b have an average value at night of close to zero ( $0.000 \text{ m s}^{-1}$  according to Leuning *et al.* (2008)). As mentioned earlier in this chapter there are theoretical reasons to expect  $\overline{w}_c(h)$  will perform better than any directly measured vertical velocity using a single 3D sonic anemometer, both in terms of reduced signal noise and rotational coordinate system ambiguity. Therefore, after comparison of vertical advection quantities for all the individual days and nights during the experiment (not shown here but available in Leuning *et al.*(2008)), calculated using both  $\overline{w}_m(h)$  and  $\overline{w}_c(h)$  it was decided to use just those derived using  $\overline{w}_c(h)$  in the final analysis.

## 2.2.5 The final $\text{CO}_2$ flux components for the CV

Figure 2.23a shows a diurnal composite bar graph of all the  $\text{CO}_2$  flux components for the CV. This was calculated by taking the mean values of flux for each hour of the day’s flux values from the available 15 days hourly time series. Figure 2.23b shows the corresponding standard error values and figure 2.23c shows the resultant overall  $\text{CO}_2$  flux for the CV.



**Figure 2-23** Diurnal bar graphs of the four CO<sub>2</sub> flux components for the CV, calculated from hourly values derived for the 15 day experimental duration from the 6<sup>th</sup> to the 2<sup>nd</sup> March 2005. (a) shows the mean hourly diurnal values, (b) their hourly standard errors and (c) the resultant overall CO<sub>2</sub> flux for the CV (with error bars of +/- one standard error).

In figure 2.23a the horizontal advection flux of CO<sub>2</sub> is close to zero during most of the daylight hours (08 hours to 17 hours EST), with significant horizontal advection commencing around sunset and ceasing at sunrise. The horizontal flux at sunset shows an afternoon peak of around 4 μmol m<sup>-2</sup> s<sup>-1</sup>, with values then becoming negative (typically -2 to -3 μmol m<sup>-2</sup> s<sup>-1</sup>) until 01 hours EST. For the rest of the night, including sunrise, horizontal advection values are positive, with values between 2 and 5 μmol m<sup>-2</sup> s<sup>-1</sup>. The diurnal values of vertical advection are similar, but with daytime values of 1 to 2 μmol m<sup>-2</sup> s<sup>-1</sup>, and the ‘sunset peak’ occurring about an hour later. As with the horizontal flux, the vertical flux becomes negative in the early part of the night (negative peak value, -4 μmol m<sup>-2</sup> s<sup>-1</sup> around 22 hours), but is positive from 01 hours onwards with mean values around 4 μmol m<sup>-2</sup> s<sup>-1</sup>.

An important observation with respect to the horizontal and vertical advection fluxes during the night is that they appear to be ‘in phase’, having the same sign and similar magnitudes, for much of the night. Marcolla *et al.* (2005) also observed this, but other researchers have either observed (Yi *et al.* 2008), or calculated theoretically (Katul *et al.* 2006) that these advection terms should be ‘out of phase’, i.e. have opposite signs and similar magnitudes.

Finnigan (1999) theoretically considered flow in the form of spanwise vortices caused by a low hill and concluded that, in general, the advection flux terms should be equal and opposite, apart from at locations close to the terrain surface where measurements are usually made. At these close to the surface locations the signs and relative magnitudes of the advection flux terms are the result of competing effects related to the topographic and micrometeorological setting of the particular site, and the advection flux terms no longer need be equal and opposite.

At Tumbarumba, figure 2.23a shows the horizontal and vertical advection fluxes were ‘in phase’ for nine hours during the nighttime. For the hours of sunrise and sunset the advection fluxes had the same sign (both positive), but with magnitudes that were now noticeably different. For the hour before sunrise the advection fluxes were ‘out of phase’. The four hours following sunset (18 to 22 hours EST), had one of the advection fluxes being close to zero, or of opposite sign in the case of the hour

between 19 and 20 hours EST. The reason for behaviour of the advection fluxes in the hour preceding sunrise and the four hours following sunset is not known. However, considering the hours following sunset (up to 22 hours), it may indicate that a conceptually simple katabatic flow regime is not established within the forest canopy until some time between 22 hours and 01 hours EST, as by 01 hours the advection fluxes are both 'in phase' and of positive magnitude.

In figure 2.23a the CO<sub>2</sub> eddy flux shows a similar pattern to that discussed earlier in the chapter (see figure 2.16), with small or slightly negative values during the day, but having positive peaks of around 5  $\mu\text{mol m}^{-2} \text{s}^{-1}$  at dawn and dusk. During the night the eddy flux is positive (about 2  $\mu\text{mol m}^{-2} \text{s}^{-1}$ ), but unable to account for the level of nocturnal respiration from the understorey/underbrush that one would expect the eddy covariance system to observe (see the argument in section 2.2.2, suggesting 5  $\mu\text{mol m}^{-2} \text{s}^{-1}$ , corresponding to the CO<sub>2</sub> eddy flux seen around dusk and dawn). As discussed earlier (section 2.2.2) this missing CO<sub>2</sub> respiration flux of around 3  $\mu\text{mol m}^{-2} \text{s}^{-1}$  at night is thought to be related to a stratified horizontal air flow or 'jet' below the 6 m agl level of the eddy covariance system. If we consider the flux contribution of the horizontal and vertical flux components at night (see figures 2.23a and 2.23c), the 'missing' respiration now becomes accounted for between 01 hours EST and dawn, with the proviso that its true value appears to be closer to 8  $\mu\text{mol m}^{-2} \text{s}^{-1}$  (rather than 5  $\mu\text{mol m}^{-2} \text{s}^{-1}$ ) once advection fluxes are included.

Marcolla *et al.* (2005) have also described observing that horizontal and vertical fluxes at night are larger than the nighttime eddy flux, and this is indeed what figure 2.23a shows between 01 hours EST and dawn, for all but one of the hours. In magnitude terms, this is true for almost the entire night.

A problem remains in that total CO<sub>2</sub> fluxes (figure 2.23c) after the dusk peak, drop and become negative in the early part of the night before 01 hours, and what this represents is still unknown.

The change in storage values shown in figure 2.23a, have the expected diurnal behaviour. Two flux 'pulses' of CO<sub>2</sub> are evident, one at dawn and one at dusk. It

should be noted that storage flux values have a different sign convention from the other fluxes, with a positive change in storage flux contributing CO<sub>2</sub> to the CV (rather than the atmosphere). Figure 2.23a shows a storage flux of around  $-2 \mu\text{mol m}^{-2} \text{s}^{-1}$  at dawn (out of the CV) and about  $2 \mu\text{mol m}^{-2} \text{s}^{-1}$  at dusk (into the CV), the diurnal mean change of storage flux being close to zero. For a forest canopy about to experience a stable night, one expects a positive storage flux at dusk (into the canopy) and a negative storage flux around dawn (out of the canopy). This reflects the onset of nocturnal stability enabling a build up of CO<sub>2</sub> mole fraction within the canopy at night (storage flux in at dusk), and heating of the ground by the morning sun causing the stability to break down (causing storage flux out at dawn). Indeed, this appears to be the situation affecting the CV.

Figure 2.23b show the standard errors for the four flux components. The total standard error shows a clear diurnal pattern being around  $1$  to  $2 \mu\text{mol m}^{-2} \text{s}^{-1}$  during the day with higher values at night, peaking at around  $6$  to  $7 \mu\text{mol m}^{-2} \text{s}^{-1}$  after 01 hours EST. The standard error values for the individual flux components shows a similar diurnal distribution with error values being higher at night. At night the vertical and horizontal advection term errors dominate the storage and eddy flux errors by a factor of between 2 and 6. During most of the day vertical advection has the dominant error term (1 to 3 times that of eddy covariance). Both storage and horizontal advection error terms have small relative values during the day,

Figure 2.23 shows that the mean diurnal flux budget of the CV during the experiment was  $3.5 \mu\text{mol m}^{-2} \text{s}^{-1}$ , with a standard error of  $4.2 \mu\text{mol m}^{-2} \text{s}^{-1}$ . This suggests the CV was progressively losing CO<sub>2</sub> throughout the experiment. The amount of CO<sub>2</sub> lost from the CV during the 15 days of the experiment was around 11000 moles or 500 Kg (equivalent to 135 Kg of Carbon). This is equivalent to  $13 \text{ t ha}^{-1} \text{ yr}^{-1}$  of pure Carbon leaving the forest understorey, with a standard error of  $16 \text{ t ha}^{-1} \text{ yr}^{-1}$ .

Data given in Leuning *et al.* (2005) suggest that for the Tumbarumba forest, typical total ecosystem CO<sub>2</sub> flux values (NEE) for autumn (March-April), derived from the 70 m agl OzFlux mast are around  $-2 \mu\text{mol m}^{-2} \text{s}^{-1}$  (a downward flux). Our derived value of  $3.5 \mu\text{mol m}^{-2} \text{s}^{-1}$  upward out of the understorey for the same time of year, is

suggestive that large CO<sub>2</sub> fluxes may exist within the forest canopy between the understorey and overstorey canopy. However, we must be cautious about jumping to such a conclusion. Firstly, the short duration of the experiment of only 15 days makes it difficult to make such generalised conclusions. Secondly, and perhaps more importantly, the experiment only sampled dry conditions (without rain), so is unrepresentative of all conditions within the CV.

### **2.3 Conclusions**

The diurnal CO<sub>2</sub> flux budget for the 50 by 50 m by 6 m high experimental control volume (CV) gives valuable new insights into the CO<sub>2</sub> flux exchange processes affecting a forest understorey/underbrush. Specifically, the existence of a subcanopy wind profile maxima or ‘jet’ under stable stratified nighttime conditions, and the effect such a ‘jet’ can have on the shape of the diurnal CO<sub>2</sub> eddy flux curve measured in the stem space below the upper forest canopy and above the understorey/underbrush. It appears that if such a diurnal eddy flux curve has unexpectedly low values at night this may indicate the presence of a ‘jet’ below the measurement level.

Comparison of the relatively large mean upward diurnal CO<sub>2</sub> flux from the understorey ( $3.5 \mu\text{mol m}^{-2} \text{s}^{-1}$ ), compared with published values of typical fluxes in to the Tumbarumba forest during autumn ( $-2 \mu\text{mol m}^{-2} \text{s}^{-1}$ ) may indicate that large CO<sub>2</sub> fluxes may exist between the understorey (underbrush) and overstorey (forest canopy) of the Tumbarumba Eucalyptus forest. However, more work would need to be done to confirm this.

The calculation of a useable vertical advection term was only made possible by the use of the continuity method to calculate the vertical velocity within the CV. An alternative directly measured velocity estimate was found to be unsuitable.

The combined standard error values of the vertical and horizontal advection terms investigated by this experiment were large, being the same order of magnitude as the total flux signal at night. Despite this a meaningful analysis of the diurnal total flux

curve was carried out, but the large advection errors observed would make one hesitate in using the same experimental approach at other sites.

### 3 Griffin forest wind transect & profile experiments

#### 3.1 Introduction

Following the advection experiment carried out near the Tumbarumba OzFlux site in Australia during March 2005 (see chapter 2), it was decided to carry out experiments in a temperate forest in the UK, looking at issues of flux divergence within the forest canopy, and sub canopy air flow under stable conditions. Two experiments were carried out at an eddy flux tower operated by the University of Edinburgh, situated within a Sitka Spruce plantation (Griffin Forest, near Aberfeldy, Scotland). The experiments consisted of:

- 1) A transect of ultrasonic anemometers to investigate wind flow divergence within the forest canopy, in order to relate it to the horizontal advection term in the eddy covariance mass balance equation (term IV in equation 1.2). A secondary objective was to investigate the general wind climate in the lower canopy, especially in relation to the possible presence of gravity flows at night.
- 2) An ultrasonic anemometer wind profile on the eddy covariance tower to investigate the vertical air flows related to the vertical advection term in the eddy covariance mass balance equation (term III in equation 1.2). A secondary objective was to investigate the general wind climate in and above the canopy for the site, particularly in relation to nocturnal conditions.

The objective of this study was to investigate the properties of airflow within and just above the forest canopy on a so called ‘advection night’, typically under anti-cyclonic high-pressure atmospheric conditions with clear skies and light winds at night (Aubinet *et al.* 2005). Under such conditions a temperature inversion may form within and/or just above the forest canopy resulting in gravity flows that due to associated effects of advection and flux convergence or divergence, adversely effect eddy covariance measurements of scalar quantities over the forest by removing CO<sub>2</sub>



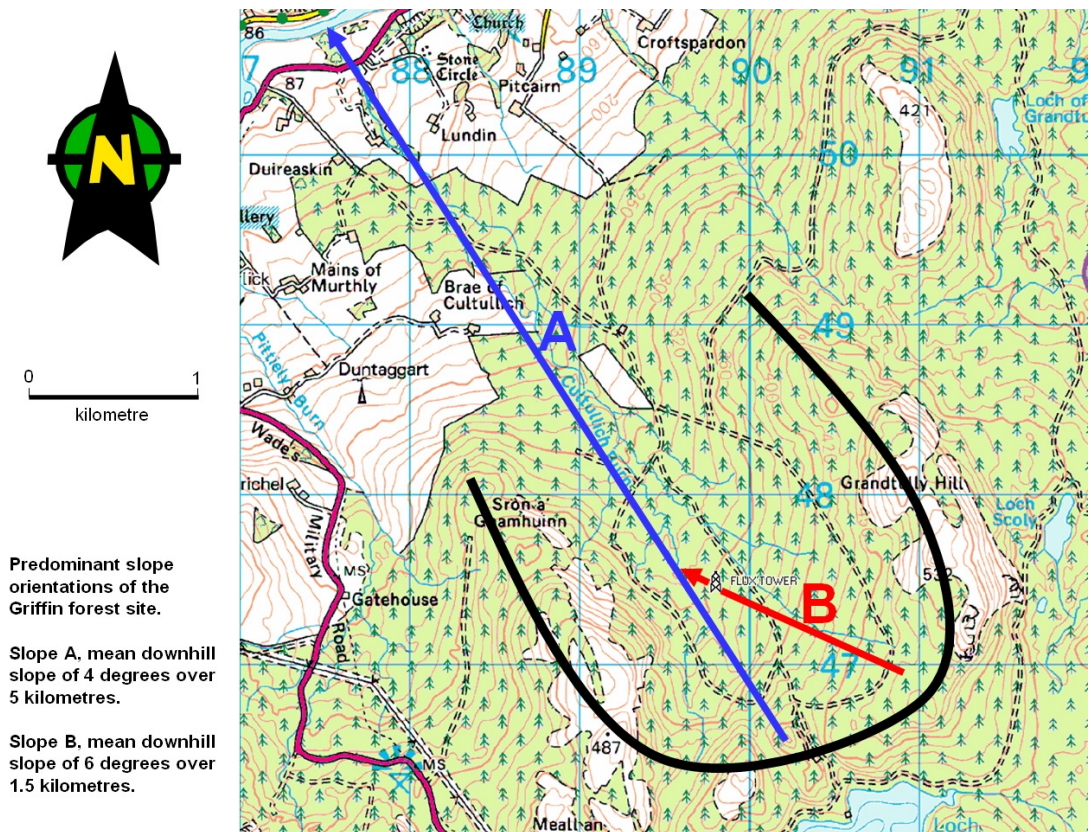


**Figure 3.1** A 5 km by 5 km topographic map of the Griffin field site showing the location of the eddy flux tower, the main downslope axis of the Cultullich valley (annotated A), and the direction and length of the hill slope present at the tower (annotated B). *Produced using Ordnance Survey 1:50 000 scale colour raster data from EDINA Digimap; <http://digimap.edina.ac.uk>, crown copyright reserved.*

from below the sensor before it has time to be mixed upwards past the eddy covariance system (Aubinet *et al.* 2005).

### **3.2 Site description**

The topographic setting of the eddy flux/experimental tower within the Griffin Forest is shown in figure 3.1. This shows the experimental tower is situated in the upper section of a side valley (henceforth referred to as the Cultullich valley) on the south side of the Tay valley. The Cultullich valley is 5 kilometres long and oriented along an axis that has a bearing of 330 degrees, being open at its northwest end with the Cultullich Burn flowing into the River Tay. At its southeast upper end the valley has the character of a closed valley head or horseshoe shaped amphitheatre, 2.2 km wide and 2.3 km long (along the valley axis). The experimental tower is situated roughly in the centre of this upper section of the valley, see figure 3.1, which is almost entirely forested apart from access roads.

Several topographic slope angles and lengths can be identified within the Cultullich valley that may be relevant when considering nocturnal katabatic type flows. The distance from the ‘lip’ of the valley head to the River Tay is 5 km with a change in elevation of 370 m, corresponding to a mean slope of just over 4 degrees along the entire length of the Cultullich valley (bearing 330 degrees). In the vicinity of the tower itself the down slope direction has been identified from Ordnance Survey maps and local survey to be 300 degrees. This local slope can be followed uphill (120 degrees bearing) from the experimental tower for a distance of around 1.2 km before reaching the ‘lip’ of the valley head in the vicinity of the southern part of Grandtully Hill, giving a change in elevation of 125 m, corresponding to a mean slope value of 6 degrees. If the local slope is followed downhill (300 degrees bearing) from the tower, Cultullich Burn is reached after only 300 m, with a drop of just 20 m, resulting in a mean slope of 4 degrees.

Near the tower the forest canopy had a representative height of around 15 m, plantation rows being oriented along an east-west axis, with every fifth row of trees having been removed by thinning (Clement, 2008, *pers comm*). The topographic

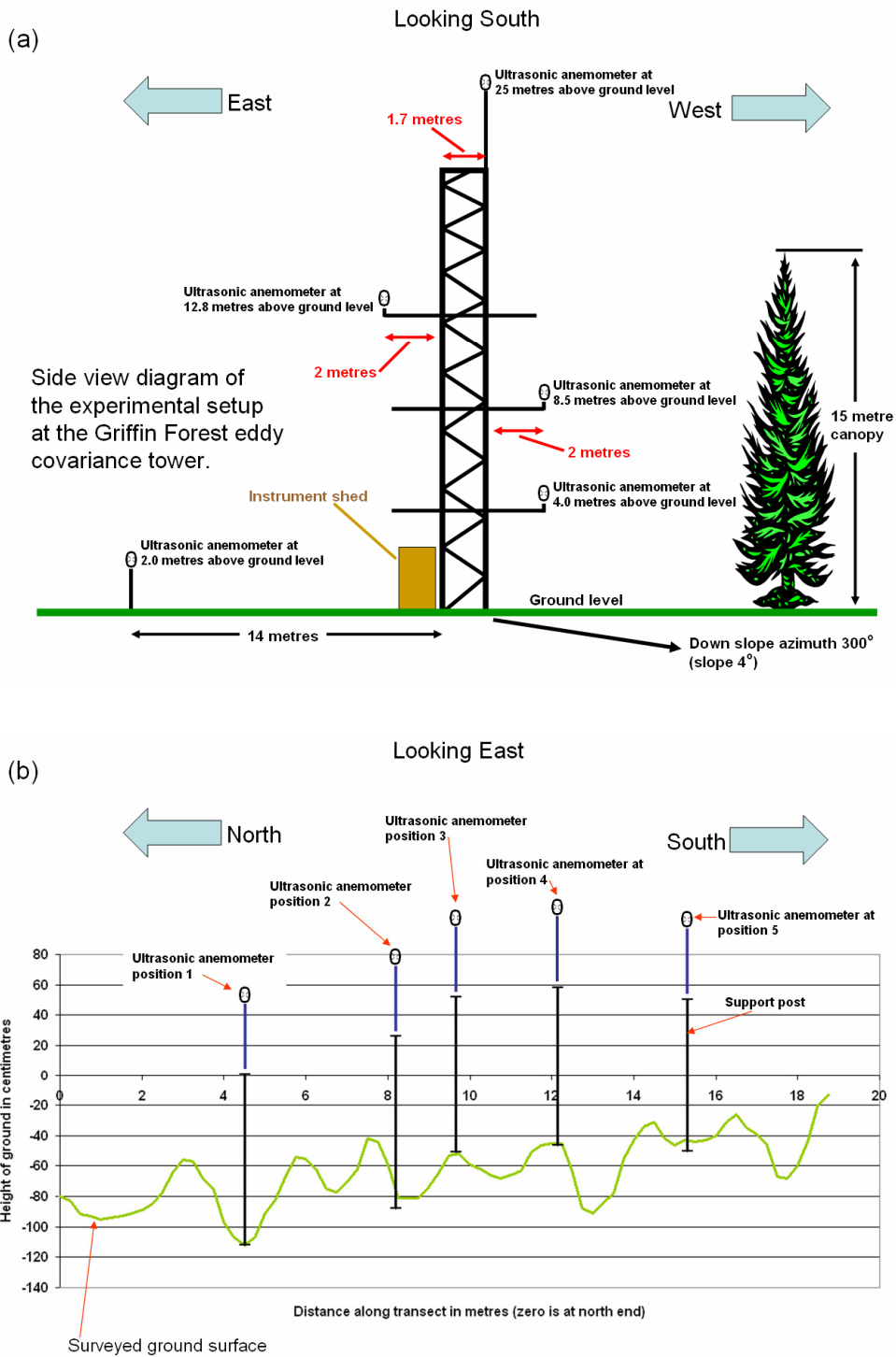


**Figure 3.2** (a) Schematic drawing of the 25 m high profile experiment tower within the Griffin forest. (b) Side view drawing of the 10.8 m long ultrasonic anemometer transect. The north end of the transect was situated 14 m east of the profile tower.

slope of the ground surface within a 20 m radius of the tower base was surveyed and found to be 4 degrees, with a down slope azimuth bearing of 300 degrees.

### **3.3 Experimental setup and results**

Between November 2005 and October 2006 two experiments were carried out at the Griffin forest flux tower site. The setups for the two experiments are shown in diagrammatic form in figure 3.2. Photographs of the locations of the experiments are shown in figure 3.3a, the eddy flux tower, and figure 3.3b the forest thinning line. Horizontal bearings were measured using a magnetic sighting compass, accuracy +/- 2 degrees. All magnetic directions were converted to Ordnance Survey grid directions. Relative heights were measured with a laser level and metre rule for the transect ground profile and anemometer post heights (accuracy +/- 5 cm), and tape measure for heights on the experimental tower (accuracy +/- 20 cm).

#### **3.3.1 The horizontal transect experiment**

The first experiment (see figures 3.2b and 3.3b) was an attempt to investigate flux divergence effects related to the horizontal divergence term (see equation 1.2, term IV). A linear transect of five 3D Gill R3-50 ultrasonic anemometers, henceforth referred to as sonic anemometers, were setup at right-angles across a forest thinning line 15 to 20 m upslope of the eddy covariance tower. The 4 m wide thinning line was orientated along an east-west axis, see figure 3.3b. The five sonic anemometers that comprised the transect were setup on steel support posts so that their measuring volumes were 1.65 m above local ground level (agl). In figure 3.2 the surveyed relative ground level is plotted along the transect, and the typical 'ploughed' surface of an artificial conifer plantation is seen, as is the north-south component of the downhill topographic slope (downhill slope 4 degrees, downhill direction 300 degrees from north). The transect was orientated exactly north south, to within the measuring accuracy of the survey equipment used.

With reference to figure 3.2b, the sonic anemometer in position 1 (henceforth referred to as sonic anemometer 1) was located within the lower part of the 15 m



(a)



(b)

**Figure 3.3** (a) Photograph of the 25 m high eddy flux tower used for the profile experiment, taken from its east side before the installation of the 2 m long anemometer support booms. (b) Looking east, up the slope of the 4 m wide forest thinning line crossed by the experimental transect. The central Gill R3-50 ultrasonic anemometer of the transect (anemometer 3), is shown installed with its measuring volume at 1.65 m above ground level.

high Sitka Spruce forest canopy, just under 4 m north of the thinning line edge. Sonic anemometer 2 was located at the northern edge of the thinning line, around 0.5 m south of the canopy proper, but in a position still in proximity to small branches from the canopy. Sonic anemometer 3 was situated in the middle of the thinning line 1.5 to 2.0 m away from any canopy elements. Sonic anemometer 4 was just beyond the southern edge of the thinning line, about 0.5 m into the canopy. Finally, sonic 5 was located in a relatively dense part of the canopy almost 4 m from the thinning line edge.

The rationale behind the setting out of the sonic anemometers along the transect was to sample the various wind environments of canopy, canopy edge and open thinning line. It was hoped to measure any cross thinning line, and approximately across downslope flow divergence effects that might occur. The expected downslope direction that any nocturnal gravity flow under stable conditions might be influenced by was 300 degrees from north (flow from 120 degrees). Alternatively the thinning line itself might steer such a flow towards 270 degrees from north (flow from 90 degrees).

Wind flow data derived from the five sonic anemometers of the transect were logged using a laptop computer and interface electronics located in the instrument shed at the bottom of the eddy flux tower, see figure 3.2a. The experimental equipment and laptop were powered by a 12 V battery array (connected in parallel), which would power the transect experiment for a maximum of around 15 hours once fully charged.

The experimental plan was to monitor synoptic weather charts of the North Atlantic and UK areas, issued by the UK Meteorological Office. Forthcoming anti-cyclonic conditions that were going to affect the experimental site at night were identified. The majority of such anti-cyclonic conditions consisted of ridges of high pressure that would typically cross the site in 24 hours or less. The site would then be visited and the battery array charged using a petrol generator, with the experiment being set running in the afternoon just before the researcher departed the site. This resulted in



an overnight dataset of 3D wind vector components from each of the sonic anemometers as the high pressure ridge crossed over the experimental transect

The duration of the experiment was from the 16<sup>th</sup> November 2005 until the 11<sup>th</sup> February 2006, with a total of 327 hours of 3D 20 Hz air flow data being collected from each of the five sonic anemometers that comprised the transect.

By default, the dataset that was obtained was expected to be biased towards anti-cyclonic conditions, in which gravity flows related to stable atmospheric conditions might be detected.

### **3.3.2 Transect experiment results and discussion**

Figure 3.4 shows histograms of wind direction and total vector wind magnitude,  $U$ , derived from data collected by sonic anemometer 3, which was positioned centrally in the thinning line (see figures 3.2b and 3.3b), and the sonic anemometer at 25 m agl on top of the eddy flux tower. In order to create the histograms, the raw 20 Hz data were processed to create mean half hourly values of wind direction and magnitude. These half hourly values were then used to construct the frequency histograms shown in figure 3.4.

Figure 3.4a is a wind direction histogram for the centre of the thinning line (anemometer 3), for nighttime during the experiment, i.e. when the centre of the sun was below astronomical horizon at the site. It shows that nocturnal winds at 1.65 m affecting the site blow predominantly from directions of between 100 and 140 degrees from north. This corresponds to a range of values that covers the local upslope direction at the site (120 degrees) to close to the direction of the up valley axis (150 degrees), see figure 3.1.

The wind direction peak is asymmetrical with observation frequency dropping abruptly for bearings over 140 degrees. Comparing figure 3.4a with the topographic map shown in figure 3.1, it seems that nighttime air flows within the lower part of the canopy (1.65 m) at the site are influenced by both the local slope which stretches uphill for a horizontal distance of around a kilometre, and some other feature on a

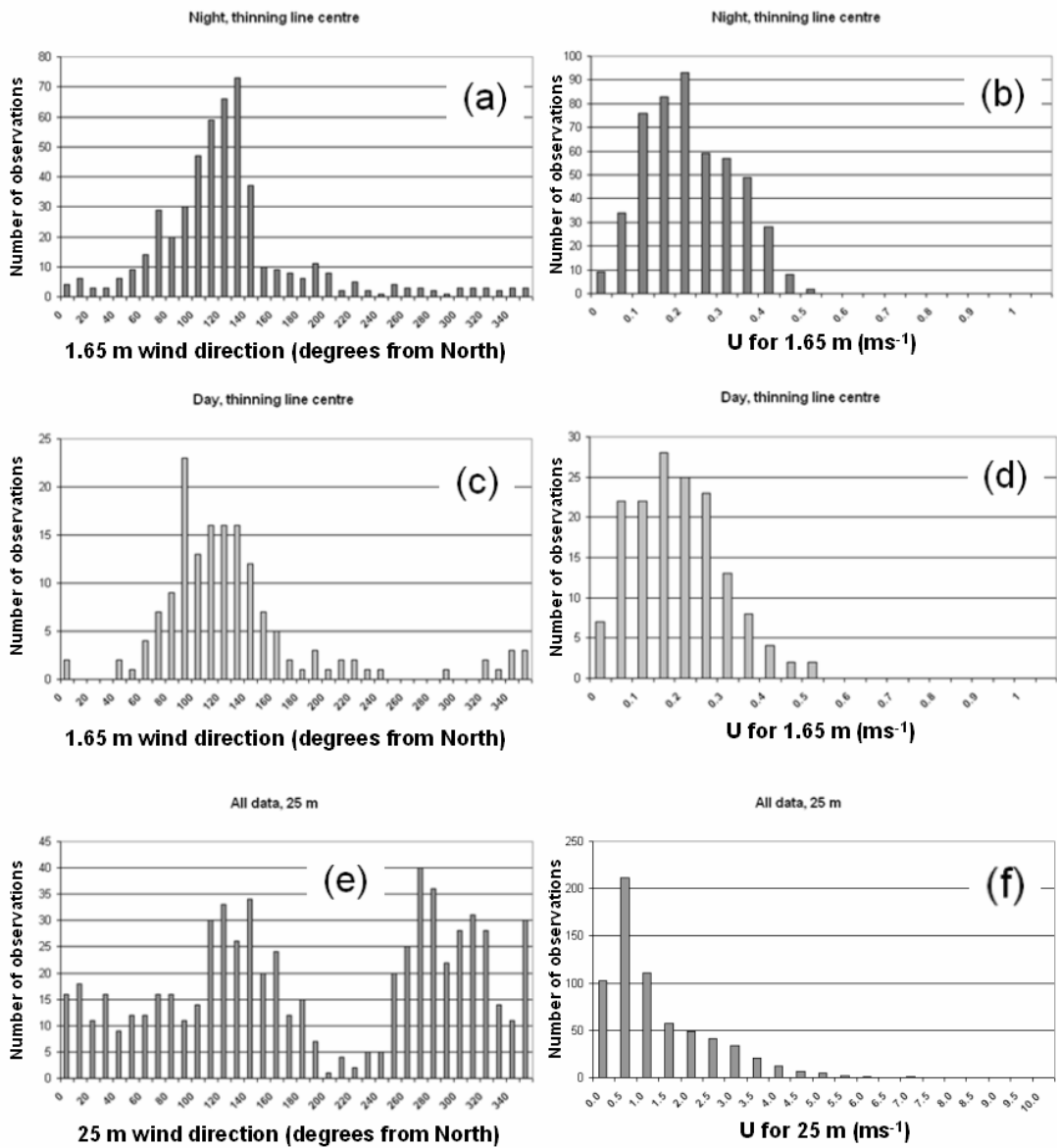


**Figure 3.4** Histograms of wind direction and total vector wind magnitude,  $U$ , derived from data collected by sonic anemometer 3, for nighttime (a and b) and daytime (c and d). (e) Histogram of wind direction from 25 m above ground level (agl) on the profile tower. (f) Histogram of  $U$  values at 25 m agl. The histograms were constructed using half hour average values.



bearing close to the valley axis. Examination of the topographic contours indicates that the slope above the eddy flux tower is terminated at its southwest extent by a several hundred metre wide 'notch' in the closed valley head that forms the upper part of the Cultullich valley. This feature is on a bearing of between 140 and 150 degrees from the site, and could explain the reduction in the wind direction frequency seen in that direction.

Importantly, figure 3.4a demonstrates that the thinning line orientated east west does not significantly effect the direction of airflow seen at night. The only feature in the nighttime wind direction histogram (figure 3.4a) that could be related to the thinning line is a small disturbance between bearings of 70 and 90 degrees. This disturbance which takes the form of a small peak between 70 and 80 degrees, and a relative minima between 80 and 90 degrees, can also be seen in nighttime wind direction histograms for the other four sonic anemometers in the transect (not shown), and a composite nighttime wind direction histogram for the entire profile (not shown). The amplitude of this feature is one seventh that of the main peak of the histogram.

Figure 3.4c shows the daytime wind direction histogram for the centre of the thinning line (anemometer 3). This daytime histogram is superficially similar to that seen at night with a main peak corresponding to flows from 110 to 140 degrees from north. The shape of the main daytime peak is noticeably flatter than the nighttime one, perhaps suggesting that at night a different mechanism is contributing to the sub canopy flow at 1.65 m.

The daytime direction histogram (figure 3.4c) has a distinctive 'spike' between 90 and 100 degrees, with a relative amplitude of around two thirds that of the main peak. Similar 'spikes' are observed at the same bearing in the wind direction histograms of anemometers 2 and 4 (not shown), situated on the north and south edges respectively, of the thinning line. These 'spikes' have smaller amplitude than the one shown in figure 3.4c.

These daytime 'spike' features seem to be associated with airflow from east to west along the thinning line. Interestingly, the shape of these daytime 'spikes' is quite

different to the equivalent nighttime feature already discussed with respect to figure 3.4a.

Figure 3.4e shows for comparison, the wind direction histogram derived using data from the sonic anemometer situated at 25 m agl atop the eddy flux tower. The derived half hour mean values used to construct figure 3.4e correspond to all the time durations of data acquired by the transect experiment (both for day and night). Figure 3.4e clearly shows two distinct peaks in wind azimuth frequency, one bearing 110 to 150 degrees, and the other bearing 270 to 330 degrees from north. These two peaks seem to be associated with the axis of the Cultullich valley (annotated A in figure 3.1), but offset from the valley axis by an anticlockwise rotation of 20 to 30 degrees.

The existence of a bimodal wind direction distribution or wind rose above the Griffin forest canopy (25 m on the eddy flux tower), and its association with the axis of the Cultullich valley was originally discovered by Clement (2004).

The wind direction histograms for day and nighttime respectively, for the 25 m agl level on the tower (not shown) show a very similar bimodal distribution to that shown in figure 3.4e.

Comparing the wind direction distributions given in figure 3.4e for the 1.65 m level and the 25 m level, it is obvious that the distribution peak corresponding to the up-valley flow at 25 m agl (270 to 330 degrees) is not detected at 1.65 m agl within the forest canopy.

By contrast, the peak corresponding to the down-slope flow seen at 25 m agl (110 to 150 degrees), corresponds well to the main wind direction peaks observed at 1.65 m agl for both day and night (100 to 140 degrees).

The implication is that down-valley wind flows at 25 m agl (10 m above the forest canopy) may be coupling to or even 'driving' the sub-canopy downslope/down-valley flow at 1.65 m, whereas up-valley wind flows at 25 m do not result in up-slope directed air flows at 1.65 m agl.

With regard to the topographic map shown in figure 3.1, it can be seen that the downslope direction at the experimental site (annotated B), and consequently the expected direction of any sub-canopy katabatic type flows that may effect the site, are in the same direction as the down-valley flow observed at 25 m (figure 3.4e). A consequence of this site geometry is that it makes it more difficult to determine if airflows seen at 1.65 m under stable nighttime conditions are indeed katabatic gravity type flows, or merely air flows driven from above the canopy or a combination of both.

The experiment described in chapter 2 relating to the Tumbarumba forest was more straightforward in this respect, as in that case the expected and measured direction of sub-canopy gravity flows were different from most of the wind directions measured above the forest canopy (at 70 m agl).

Figures 3.4b and 3.4d show total wind speed,  $U$ , frequency of observation histograms for respectively, the thinning line centre at night and during daytime. The results for the centre of the thinning line (anemometer 3) are similar for day and night, with the most frequently observed half hour mean velocity magnitude being in the range 0.15 to 0.25 m s<sup>-1</sup>. The maximum value of half-hour mean winds,  $U$ , seen at 1.65 m in the thinning line centre were 0.50 to 0.55 m s<sup>-1</sup>. Mean velocity,  $U$ , histograms constructed for the other four anemometers in the transect (not shown) showed similar values, except the maximum values of  $U$  were about 0.05 m s<sup>-1</sup> lower.

The mean velocity,  $U$ , histogram for 25 m agl on the tower for all hours (night and day) is shown in figure 3.4f, with peak values being between 0.5 and 1.0 m s<sup>-1</sup>. The maximum value of half-hour mean winds,  $U$ , seen at 25 m were 7.0 to 7.5 m s<sup>-1</sup>.

Figure 3.5 shows an along transect divergence-like quantity that has been calculated between various anemometer positions along the north-south oriented length of the transect (see figure 3.2b). This divergence-like value was calculated by taking the differences between half hourly mean north facing vector components of wind velocity derived from a pair of anemometers, subtracting them and dividing the result by the distance between the two anemometers. This resulted in a value that was

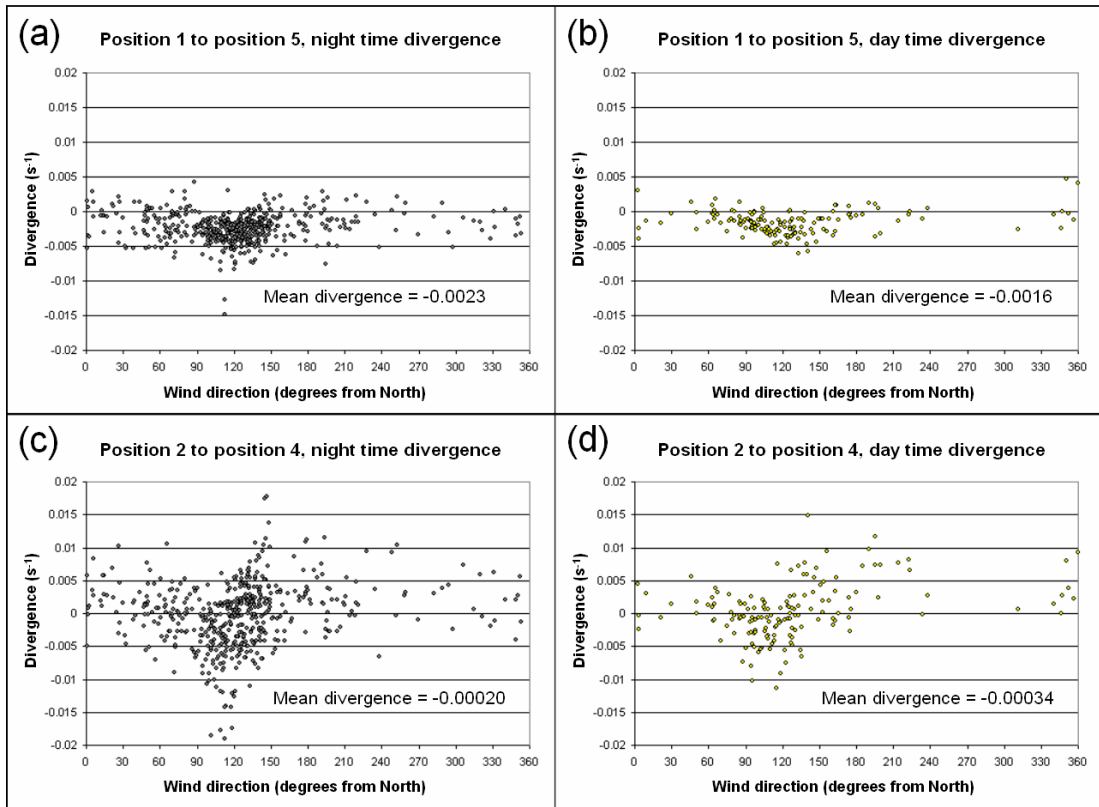


**Figure 3.5** A calculated along transect divergence like quantity for the entire 10.8 m length of the 1.65 m above ground level transect, calculated from data gathered at its north and south ends, for (a) day and (b) night. Panels (c) and (d) shown the along transect divergence like quantity calculated using data from the edges of the open transect, 3.95 m apart. Half hour mean values of the north facing vector wind components were used as the source data for the calculations. All the divergence like quantities are plotted against wind direction measured at 1.65 m agl at the north end of the transect.

positive for conditions of flow divergence along the transect, and negative for convergence along the same axis. The units of this quantity are reciprocal seconds ( $s^{-1}$ ).

The divergences shown in figure 3.5 are plotted against wind direction measured at the north end of the transect (anemometer 1). Figures 3.5a and 3.5 b show divergences calculated between the extreme north and south ends of the transect (anemometers 1 and 5, within the forest canopy, separation 10.8 m), for night and day respectively. Both these night and daytime plots indicate that flow convergence (negative values) along the transect may be associated with airflows coming from the upslope direction (around 120 degrees bearing from north).

The figures 3.5c (night) and 3.5d (day) show divergences calculated between anemometers 2 and 4, situated 3.95 m apart at the north and south edges of the open thinning line (see figure 3.2b). Here the magnitude of the divergence has a maxima associated with the bearings of 90 to 150 degrees, which ranges from the up-thinning line, to upslope, to up-valley directions. Interestingly however, when polarity is considered, there is a negative peak (convergence) around 120 degrees and positive peak (divergence) around 150 degrees bearing, seen clearly in 3.5c (night), but also discernible in 3.5d (day).

Since the divergence peak at 150 degrees is only seen in the figure using data from the edges of the open thinning line, it is possible it is some effect caused by the presence of the thinning line itself, either distorting the airflow at 1.65 m agl or allowing above canopy winds to affect the 1.65 m level.

### **3.3.3 The tower profile experiment**

Between the 2<sup>nd</sup> of August 2006 and the 18<sup>th</sup> of October 2006, three component ultrasonic anemometer data was obtained for a total of 525 hours, at five different heights above ground level (2.0, 4.0, 8.5, 12.8 and 25 m), forming a vertical profile through the forest canopy on the existing eddy flux tower, see figure 3.1.

Four of the ultrasonic anemometers (at heights 4.0 m and upwards) were situated on the eddy flux tower. The ultrasonic anemometer at 2.0 m height was situated 14 m east and upslope of the tower, at the same location as anemometer 1 in the transect experiment. This position was chosen in order to allow comparison with data from the previous transect experiment, and to avoid aerodynamic interference due to the presence of a 2.5 m high instrument shed situated at the base of the tower. A diagram showing this experimental setup is shown in figure 3.2a.

The sonic anemometers used were the same 3D Gill R3-50s as deployed previously in the transect experiment, as well as an existing Gill R3-50 anemometer at 25 m agl that comprised part of the eddy covariance flux system on top of the tower. Unfortunately, by August 2006 one of the anemometers had developed a fault and become unserviceable. It had been originally intended to deploy this sonic anemometer at 16.4 m agl on the tower in order to sample the air flow just above the tree canopy.

The data logging equipment used was the same as for the transect experiment with the three component 20 Hz data produced by the four anemometers at 12.8 m agl and below being logged onto a single laptop computer in the instrument shed (see figure 3.2a). The 20 Hz data from the sonic anemometer on top of the tower at 25 m agl, was logged using the existing computer of the eddy covariance flux system, also situated within the instrument shed.

The four sonic anemometers at 12.8 m and below were powered by the same 12 V battery array as used in the transect experiment. A similar battery charging strategy was used for this experiment as with the previous transect experiment, making sure the battery array was charged and ready in order to allow sampling of any high pressure ridges likely to cross the site.

The sonic anemometer at 25 m agl was powered from the existing 12 V electrical system of the eddy flux tower, which consisted of large 12 V lead acid battery connected via a power regulator to a number of solar panels mounted on the tower.

This system was able to power the tower eddy flux system continuously throughout the summer months.

Between the 30<sup>th</sup> of August 2006 and the 13<sup>th</sup> of September 2006, electrical power for the four sonic anemometers on the tower at 12.8 m agl and below, including their data logging electronics and laptop, was temporarily obtained from the higher capacity tower electrical system. This resulted in an almost continuous data run (with just two small breaks) of 296 hours of anemometer data from the five height levels of the profile experiment.

From the 14<sup>th</sup> of September 2006 onwards the electric power source for the lower four anemometer levels of the tower experiment reverted to the original smaller battery array, periodically charged by a petrol generator.

### **3.3.4 The profile experiment results**

Figure 3.6 shows derived half hour mean quantities ( $U$  and wind direction) cross plot between the various anemometer levels on the tower profile, using data from the 30<sup>th</sup> of August 2006 to 13<sup>th</sup> of September 2006 period.

Figure 3.6a is a cross plot of total wind vector magnitude,  $U$ , between the 2 m and 4 m anemometer levels. The plotted  $U$  values show a clear linear relationship, with the fitted regression line resulting in an  $R^2$  close to 1. Interestingly, the regression line fitted to the  $U$  values indicates that observed wind velocities at 2 m agl within the forest canopy are around 1.2 times those seen at the 4 m level. This observation is consistent with a wind velocity maximum in the lowest part of the forest canopy, possibly related to the foliage area volume density (FAVD) profile of the canopy (Fritschen 1985).

Figures 3.6c and 3.6d show similar cross plots of  $U$ , between the 8.5 and 12.8 m, and 12.8 and 25 m anemometer levels respectively. The datasets shown in these two figures again have  $R^2$  values close to 1, but this time the fitted regression lines indicate that the wind velocity drops to around one third its previous value as one descends between each of the levels.

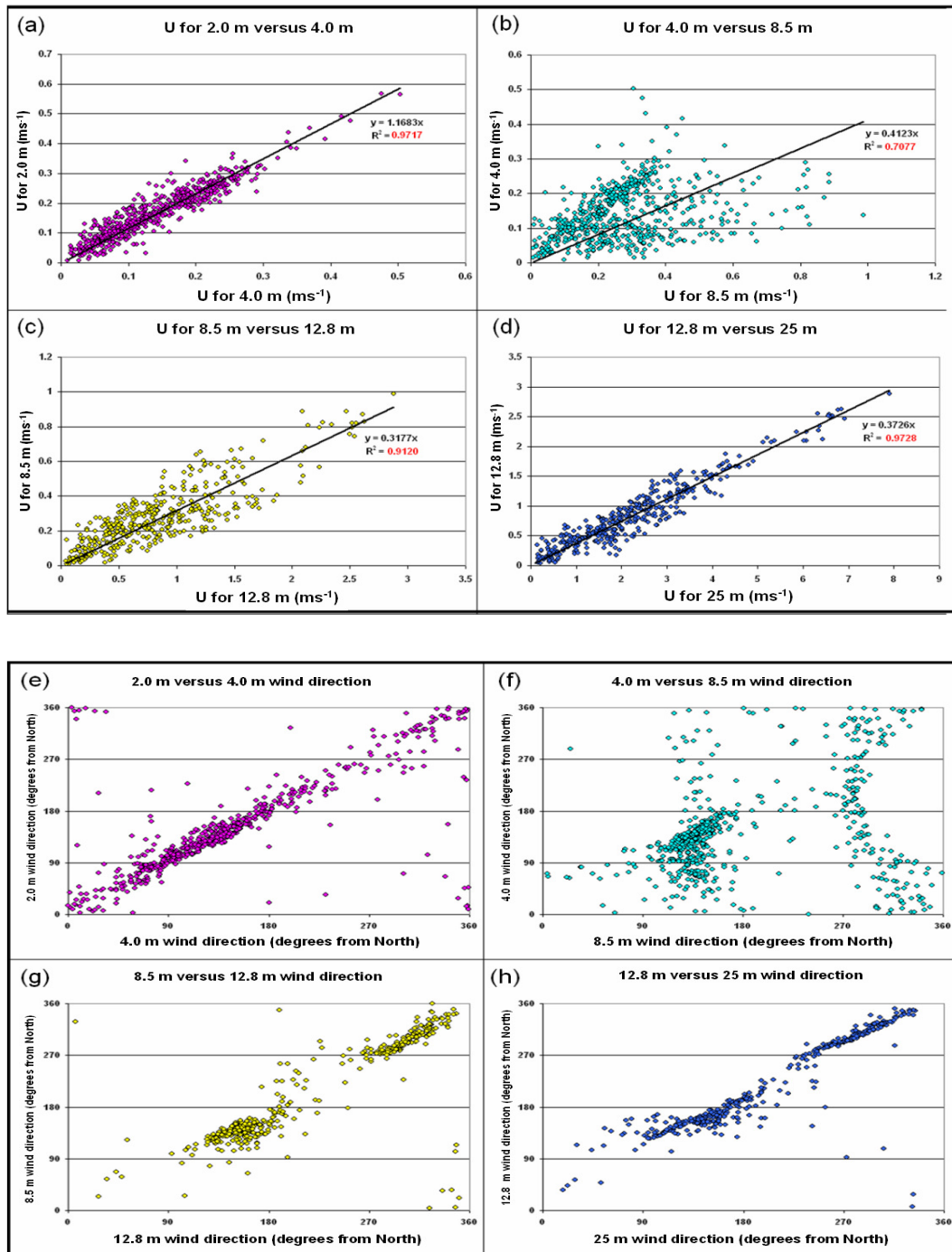


**Figure 3.6** Derived half-hour mean quantities ( $U$  and wind direction) cross plot between the various anemometer levels on the tower profile. (a, b, c, d) Are cross plots of  $U$  values between the 2 m and 4 m, 4 m and 8.5 m, 8.5 m and 12.8 m, and 12.8 m and 25 m anemometer levels, respectively. (e, f, g, h) are cross plots of wind direction values between the 2 m and 4 m, 4 m and 8.5 m, 8.5 m and 12.8 m, and 12.8 m and 25 m anemometer levels, respectively. The data used to construct the plots are from the period 30<sup>th</sup> of August 2006 until 13<sup>th</sup> of September 2006.



Figure 3.6b shows the cross plot of  $U$  values between the 4 m and 8.5 m levels on the tower. Here the  $R^2$  value of around 0.7 is significantly less than for the other graphs just described (figures 3.6a, 3.6c and 3.6d). Also, the distribution of data points present in 3.6b is suggestive of two different distributions that have been superimposed.

These two possible distributions can be investigated further by looking at figure 3.7 which shows cross plots of mean  $U$  (figure 3.7a) and mean wind direction (figure 3.7b) between the 4 m and 8.5 m levels on the tower, but this time also partitioned into daytime and nighttime values. Examination of figure 3.7a shows that two distinct distributions of  $U$  values do exist, a steeper more defined distribution for nighttime, and a more diffuse daytime distribution.

Attempts to fit straight lines going through the origin of the graph, to the nighttime distribution are shown by the two solid black lines in figure 3.7a. The steeper of the two lines with a slope of 0.77 has been simply fitted by 'eye' to the obvious axis of orientation of the distribution. The other line with a slope of 0.52 is the result of a linear regression on the nighttime data points, resulting in an  $R^2$  value of 0.78. The fact that the fitted 'by eye' line has a significantly greater slope value than that derived by regression for the nighttime data, may mean that some other form of data partitioning, for example using stability values, might separate the two distributions more effectively than a simple day night switch.

A linear regression line fitted to the daytime  $U$  distribution is shown as a dashed black line in figure 3.7a, with a slope of 0.32 and associated  $R^2$  value of 0.69.

These results in figure 3.7a clearly show that for the period 30<sup>th</sup> of August 2006 to 13<sup>th</sup> of September 2006, relative wind speeds in the lower part of the profile (4 m and below) will be higher at night than during the day when compared to wind speeds in the upper part of the profile (8.5 m and above).

The regression line slope values obtained from  $U$  cross plots in figures 3.6 and 3.7 can be utilised to create a mean relative wind magnitude profile for day and night, by simply multiplying the relevant slope values together from the top of the profile

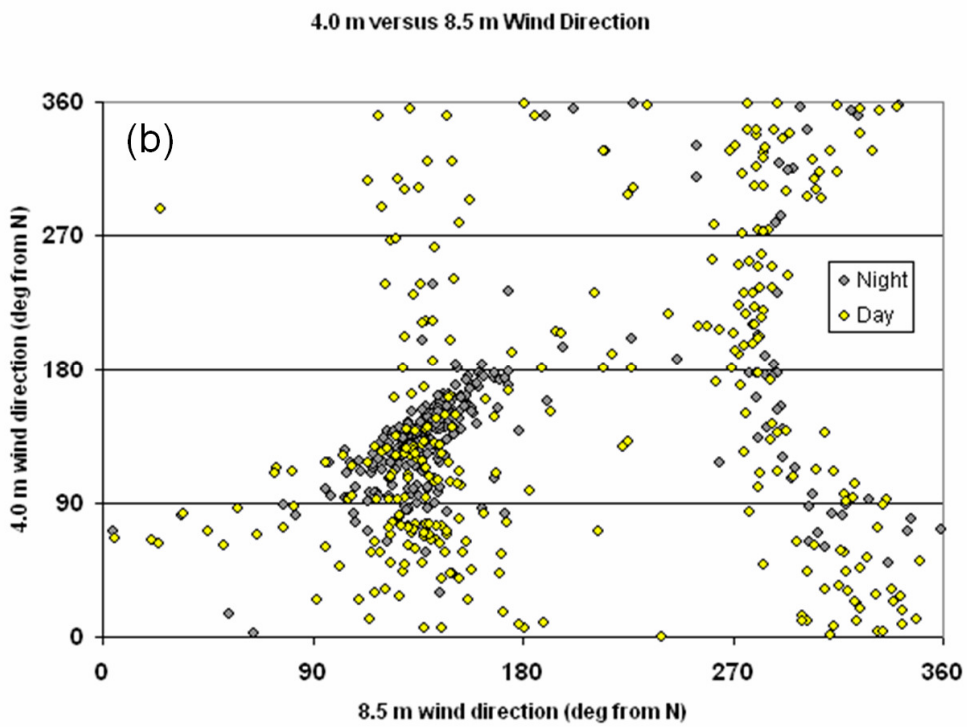
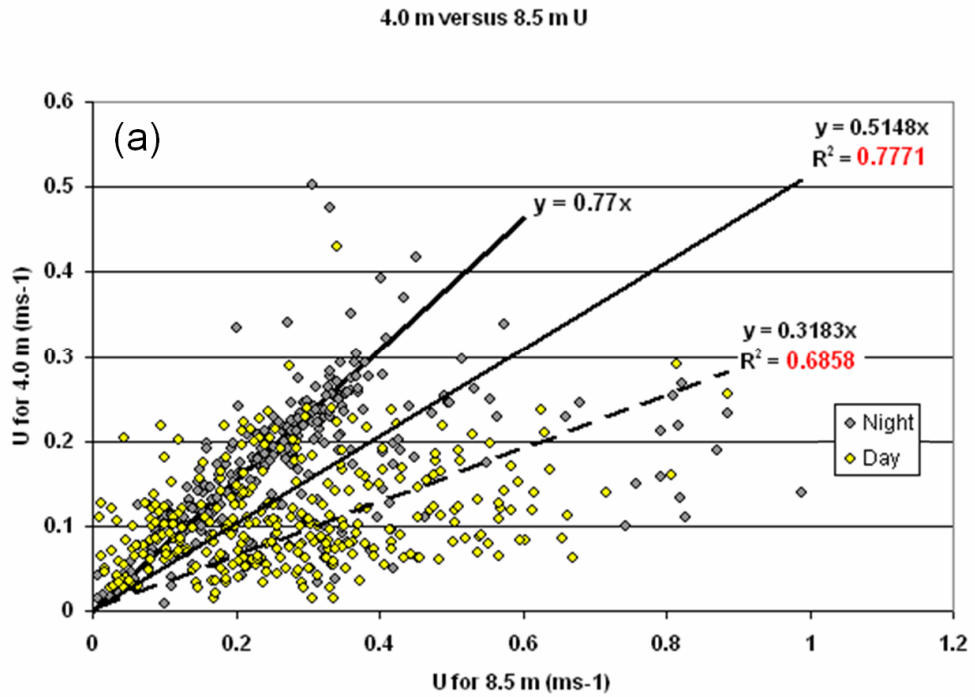


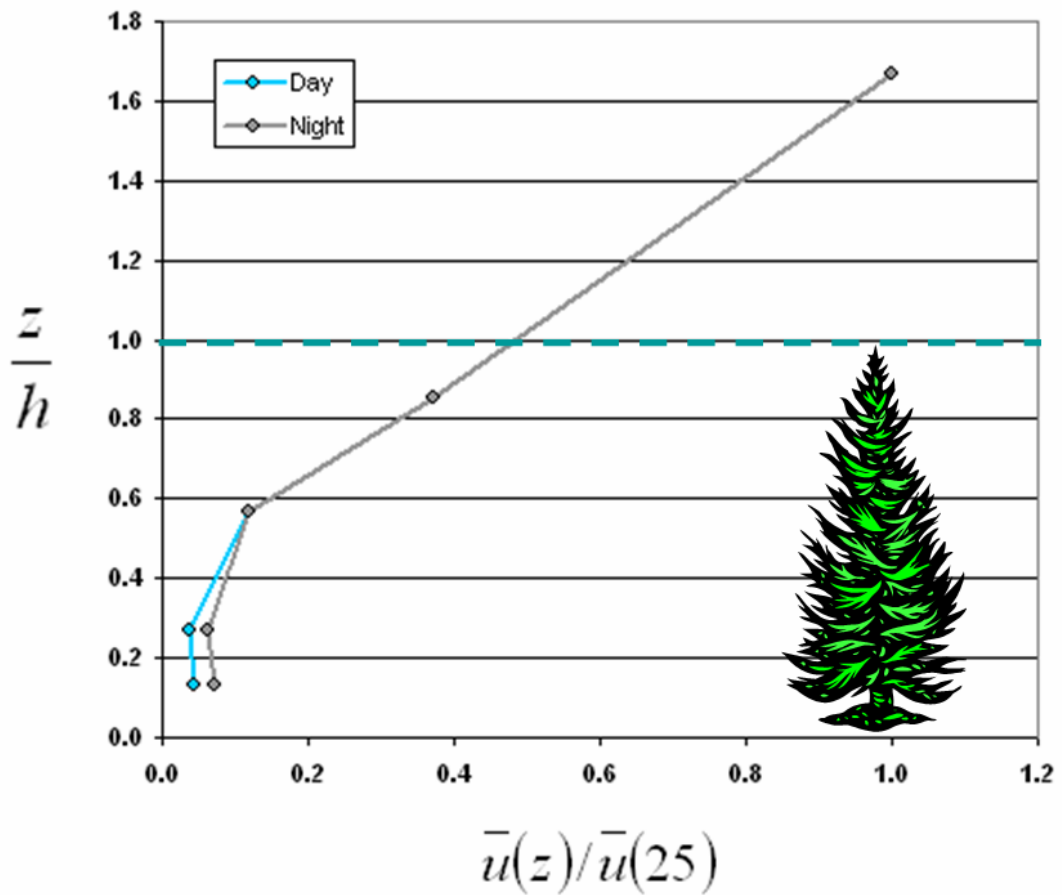
**Figure 3.7** Cross plots of mean  $U$  (a) and mean wind direction (b) between the 4 m and 8.5 m levels on the tower, partitioned into daytime and nighttime values.

downwards. Such a profile is shown in figure 3.8, which plots anemometer heights normalised by the canopy height (15 m), against mean wind vector magnitudes normalised by their corresponding value at 25 m agl.

Looking at the wind profile in figure 3.8 the higher relative wind speeds present in the lower part of the canopy (corresponding to the 2 m and 4 m anemometer levels) can clearly be seen. The mean values of  $U$  observed at the 2 m agl anemometer for the entire duration of the profile experiment (2<sup>nd</sup> of August 2006 until the 18<sup>th</sup> of October 2006) were  $0.15 \text{ m s}^{-1}$  for day and  $0.19 \text{ m s}^{-1}$  for night. Indeed, looking back at the night and day wind speed histograms obtained at 1.65 m agl in the thinning line during the transect experiment (figure 3.4b and 3.4d), it appears the most frequently observed wind speed at low level in the forest at night is around  $0.05 \text{ m s}^{-1}$  greater than that seen during the day. Thus there is evidence for both relative and absolute wind speeds being slightly higher at night in the lower part of the forest canopy than during the day.

A perusal of the upper part of the figure 3.8 wind profile indicates the considerable misfortune of the non availability of the sonic anemometer that was to have occupied the 16.4 m level on the tower (normalised height 1.09 on figure 3.8). This resulted in no information being available on the shape of the wind profile between the forest canopy top at 15 m agl and the sonic anemometer at 25 m agl on top of the tower.

In figures 3.6e, f, g and h, cross plots of wind direction between the various anemometer levels on the tower are provided. For figures 3.6e, g, and h, a linear relationship is observed, with the sonic anemometer pairs contributing to each figure experiencing wind from substantially the same direction during any given half hour averaging period. Figures 3.6g and h, which show cross plots from the upper part of the profile (8.5 m agl and above) clearly show the data points clustered around bearings of 150 and 300 degrees which correspond to the bimodal distribution in the above canopy wind direction already described in the earlier transect experiment (see figure 3.4e).



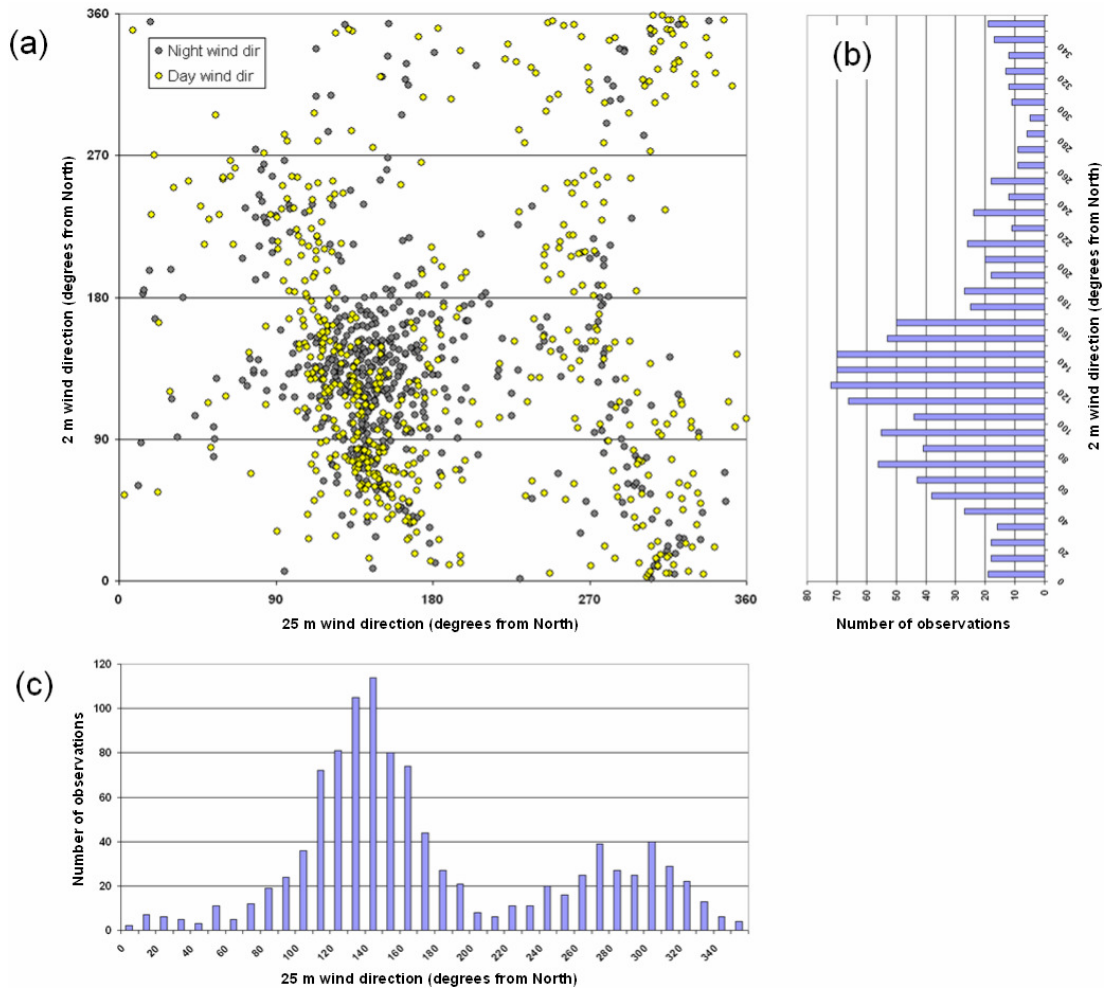
**Figure 3.8** Mean normalised wind profiles for daytime and nighttime on the main tower, valid for the period 30<sup>th</sup> of August 2006 until 13<sup>th</sup> of September 2006. Consisting of, mean wind vector magnitudes normalised by their corresponding value at 25 m agl, against anemometer heights normalised by the canopy height ( $h = 15$  m). The profile was derived using the regression line gradients in figures 3.6 and 3.7.

Figure 3.6f shows the cross plot of half hour mean wind directions between the 4 m and 8.5 m levels on the profile tower. What results is a complex scatter pattern of data points, with only the points between bearings of 90 and 180 degrees showing anything like a linear relationship. As with the previous case, involving cross plots of  $U$  values between the 4 m and 8.5 m levels (figure 3.6b) it seems something rather odd is happening between these two levels.

Figure 3.7b shows the same cross plot as figure 3.6f but with the plotted data points partitioned between night and day values (indicated by the colour coding of each point). Figure 3.7b shows that most of the nighttime values of wind direction at both the 4 m and 8.5 m levels are clustered between bearings of 90 and 180 degrees. The daytime values by contrast are scattered through two vertical bands centred at 130 and 300 degrees on the 8.5 m direction axis. Some clustering does still occur between 90 and 180 degrees on both the 4 m and 8.5 m direction axes, but it is much weaker than at night.

Figure 3.9a shows a cross plot of half hourly mean wind direction values for the 2 m and 25 m profile levels, partitioned between night and day values. This cross plot has been augmented by wind direction histograms for the 2 m and 25 m levels (figures 3.9b and c respectively) which have each been aligned with the corresponding axis in figure 3.9a. The half hourly mean wind direction values used to create figure 3.9 are derived from the 525 hours of raw data collected during the overall experimental duration of 16<sup>th</sup> November 2005 until the 11<sup>th</sup> February 2006.

A comparison of the wind direction cross plot between 2 m and 25 m (figure 3.9) and the one plotted between 4 m and 8.5 m (figure 3.7b), shows a similar pattern of data point distribution, with the clustering of nighttime values between 90 and 180 degrees on both axes, and two vertical bands of daytime data seen, centred around 130 and 300 degrees on the 8.5 m direction axis. The values plotted in figure 3.9a are however somewhat more scattered.



**Figure 3.9** (a) Shows a cross plot of half hourly mean wind direction values for the 2 m and 25 m profile levels, partitioned between night and day values. This cross plot has been augmented by wind direction histograms for the 2 m and 25 m levels (b and c respectively) which have each been aligned with the corresponding axis in (a). The figure was created using data from the period 16<sup>th</sup> November 2005 until 11<sup>th</sup> February 2006.

### 3.3.5 Discussion of the profile experiment results

Examining the cross plot in figure 3.9 in conjunction with the two histograms permits a qualitative analysis of the above canopy and near ground wind flows to be carried out.

Comparison of the position of the peaks in the wind direction histograms (figures 3.9 b and c) indicates that winds at the 25 m level blow predominantly up and down the axis of the Cultullich valley (figure 3.1), but at the 2 m level blow predominantly in the down valley down slope direction only. Now, examining the cross plot (figure 3.9a) it appears that most of the down-valley/downslope flow for day and night at 2 m agl corresponds to down-valley flows at the 25 m level. But, when an up-valley flow is occurring at 25 m agl the air flow at 2 m can be from any direction. A similar argument can be applied to the wind direction cross plot between 4 m and 8.5 m seen in figure 3.7b.

These observations lead to the following conceptual model for air flow in the Cultullich valley. When winds above the forest canopy blow down the valley there is some degree of coupling with sub canopy down-valley/downslope winds. However, when the above canopy winds blow up the valley, the down-valley/downslope winds are disrupted to be replaced by air flows from no particular direction. In addition the boundary between the 'above canopy' and 'below canopy' flow regimes seems to actually lie at a height of between 4 m and 8.5 m within the canopy.

Furthermore, the higher relative wind velocities indicated in the lower part of the canopy (4 m agl and below) at night (see figures 3.7a and 3.8), suggest that katabatic gravity type flows may be contributing to the down-valley/downslope flows in the lower part of the canopy at night; further analysis involving partition of the data using atmospheric stability within the canopy would be required to test this.

### 3.3.6 The tower profile cross correlation study

As mentioned previously, a near continuous time series of sonic anemometer data for the tower profile (2.0, 4.0, 8.5, 12.8 and 25 m agl) was recorded between the 30<sup>th</sup> of August 2006 and 13<sup>th</sup> of September 2006. During this period one night in particular met the criteria of high pressure and clear skies to be a likely ‘advection night’ (Aubinet *et al*, 2005). This was the night of the 7<sup>th</sup> to the 8<sup>th</sup> of September 2006, when a large anti-cyclonic weather system crossed the experimental site.

Since it is thought that the net ecosystem exchange (NEE) of CO<sub>2</sub> with the atmosphere has a large component coming from vertical or horizontal advection effects on such ‘advection nights’ (Aubinet *et al*, 2005), it was decided to see if the required quantities could be obtained at the tower to calculate the vertical advection term using the method of Lee (1998). Lee states the vertical advection term can be approximated by:

$$\overline{w_r}(\overline{c_r} - \langle \overline{c} \rangle) \quad (3-1)$$

Where  $\overline{w_r}$  is the vertical advection velocity at the eddy flux system on top of the tower (25 m agl in our case).  $\overline{c_r}$  is the CO<sub>2</sub> concentration measured by the IRGA of the eddy flux system on top of the tower, and  $\langle \overline{c} \rangle$  is the averaged CO<sub>2</sub> concentration between the ground and the eddy flux system IRGA.

Figure 3.10, shows a comparison of ‘raw’ 20 Hz data collected from the ultrasonic anemometer and open path infrared gas analyser (IRGA) situated at 25 m agl on the tower, with data from the ultrasonic anemometer at 12.8 m on the tower. One hour of data is shown from 00 hours until 01 hours on the 8<sup>th</sup> September. During this hour the wind at 25 m above ground level blew from a mean direction of 110 degrees, with a mean horizontal velocity of 0.9 m s<sup>-1</sup>, gusting between 0.6 m s<sup>-1</sup> and 1.2 m s<sup>-1</sup>.

Plots showing variations in carbon dioxide and water vapour concentration at 25 m height are shown, as well as sonic temperature values measured both at 12.8 m and 25 m high. Also for comparison, one minute mean values of the Obukhov stability



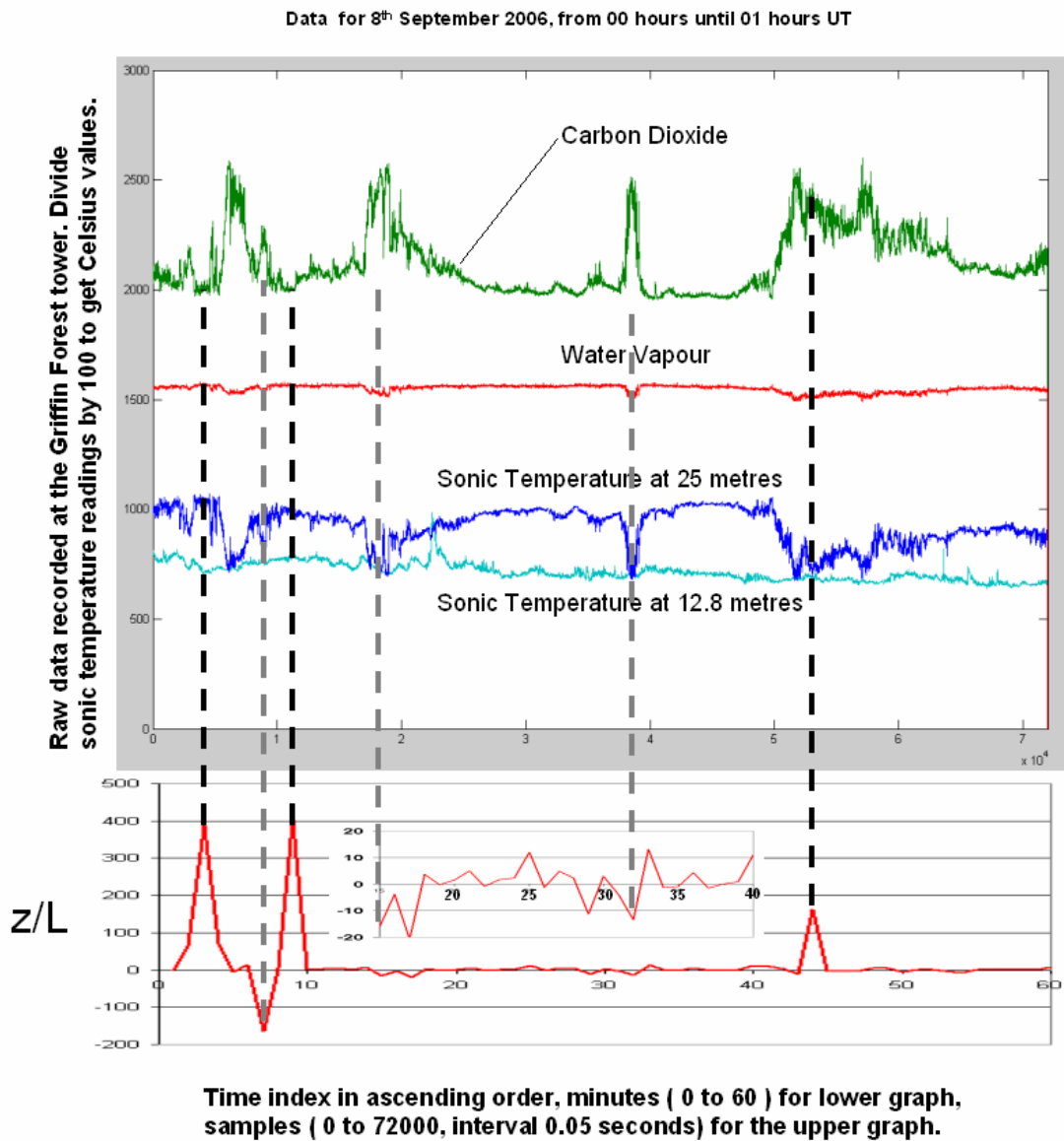


**Figure 3.10** Griffin Forest advection night data and stability values. A comparison of one hour of ‘raw’ 20 Hz data collected between 00 and 01 hours GMT on the 8<sup>th</sup> September 2006, from the ultrasonic anemometer and open path infrared gas analyser (IRGA) situated at 25 m agl on the tower, and ultrasonic anemometer at 12.8 m on the tower. The lower panel shows one minute mean values of Obukhov stability values ( $z/L$ ) calculated with data from the 25 m anemometer.

parameter,  $z/L$ , defined as observation height,  $z$ , above ground level (25 m in this case) divided by the calculated Obukhov length,  $L$ , have been calculated for each minute of the hour and are plotted in the lower graph of figure 3.10.

Monin and Obukhov (1954) used dimensional analysis to show that atmospheric turbulence statistics in a non-neutral surface layer are functions of  $z/L$ . Negative values of  $z/L$  indicate unstable conditions, and positive values indicate stability. Foken *et al.* 2008 give the Obukhov length,  $L$ , as:

$$L = - \frac{u_*^3}{\kappa \frac{g}{T} \frac{Q_H}{\rho \cdot c_p}} \quad (3-2)$$

Where  $u_*$  is the friction velocity,  $\kappa$  is von Karman's constant,  $\frac{g}{T}$  is a buoyancy parameter, given by the acceleration due to gravity divided by the absolute temperature, and  $\frac{Q_H}{\rho \cdot c_p}$  is the kinematic heat flux, given by sensible heat flux divided by the product of air density and specific heat at constant pressure.

In non-neutral conditions the Obukhov length,  $L$ , is proportional to the height at which the contributions to turbulent kinetic energy (TKE) from buoyancy and shear effects are equal (Garrat 1994), but with different constants of proportionality being used in unstable and stable situations.

Looking at figure 3.10, several interesting features can immediately be seen. Firstly, it is obvious that the shape of the carbon dioxide trace is the 'mirror image' or 'inverse' of the sonic temperature trace for 25 m. A linear regression between calibrated one minute mean values derived from these carbon dioxide and sonic temperature data from 25 m height, give an inverse relationship with an  $R^2$  of 0.9.

Secondly, the value of sonic temperature measured at 12.8 m, is consistently one to three degrees Celsius lower than the value measured at 25 m, indicating that a temperature inversion exists in the forest canopy compared to the atmosphere above.

The raw sonic temperature values given in figure 3.10 can be converted to Celsius values by dividing by 100.

However, an exception to this inversion condition occurs when peaks of carbon dioxide concentration are seen at 25 m. When these peaks occur, the value of the sonic temperature at 25 m drops to that of the cooler sonic temperature at 12.8 m agl. When the carbon dioxide peak ends, the sonic temperature at 25 m returns to a warmer value consistent with an inversion.

These observations can be interpreted as intermittent ejections or outward interactions of cooler carbon dioxide rich air from within the canopy (12.8 m level) up into the atmosphere well above the canopy (passing through the 25 m observation level on the way). Thus for the period 00 to 01 hours, it may be valid to infer the carbon dioxide values at 12.8 metres as being equal to the peak values observed at 25 m.

If this is so, a simple regression model could be constructed to predict carbon dioxide concentration at 12.8 m from the sonic temperature measured at 12.8 m. However, such a model would be likely just to be valid for just the one hour duration of the observations, and any subsequent hours of data showing the same phenomenology would each need a separate regression model. Using this approach mean CO<sub>2</sub> concentrations at 12.8 m agl within the canopy were estimated as being 16.0 mmol m<sup>-1</sup> (386 ppmv), compared to the mean value of 15.2 mmol m<sup>-1</sup> (366 ppmv) measured at 25 m agl by the IRGA, during 00 to 01 hours on the ‘advection night’ of the 8<sup>th</sup> September 2006.

An attempt can be made to calculate a vertical advection value for use with Lee’s (1998) method (see equation 3.1). Firstly, the 57 hours of sonic anemometer data from the 25 m agl sonic anemometer (corresponding to a continuous run of data from all the sonic anemometers on the profile tower) that included the ‘advection night’, was used to calculate a planar fit wind reference (Wilczak *et al.* 2001) frame for 25 m agl. The raw wind component values from the 25 m sonic anemometer for 00 to 01 hours on the ‘advection night’ were then transformed into this new planar fit

reference frame and a new hourly mean vertical velocity value calculated, and found to be  $0.024 \text{ m s}^{-1}$ , in contrast to the un-rotated mean value of  $-0.012 \text{ m s}^{-1}$ . This new vertical velocity value in the fitted planar fit reference frame is hopefully free of topographic effects on the wind and thus can be used in Lee's (1998) method. So in equation 3.1 we can use the rotated  $0.024 \text{ m s}^{-1}$  value for vertical velocity  $\overline{w_r}$ , the 12.8 m agl modelled estimate of  $\text{CO}_2$  concentration of  $16.0 \text{ mmol m}^{-3}$  for  $\langle \overline{c} \rangle$ , and the measured  $\text{CO}_2$  value at 25 m agl of  $15.2 \text{ mmol m}^{-3}$  for  $\overline{c_r}$ . This results in a calculated vertical advection term for 00 to 01 hours on the 'advection night, of  $-17 \text{ } \mu\text{mol m}^{-2}\text{s}^{-1}$ . This is a large value compared to typical respired  $\text{CO}_2$  fluxes at night which are 1 to  $4 \text{ } \mu\text{mol m}^{-2}\text{s}^{-1}$  (Moncrieff, 2008, *pers comm*). Interestingly, this is a similar magnitude to the vertical advection terms derived by Leuning *et al.* (2008) at Tumbarumba. We must exercise caution however for several reasons. Firstly, the planar fit coefficients used in the coordinate rotation to give a suitable  $\overline{w_r}$  can change dramatically depending on the length of the time period used to calculate them, to the extent that an arbitrary change in length of the period used could lead to a change of sign in  $\overline{w_r}$  and hence a change in sign of the advection term (see Vickers and Mahrt (2006) and Heinesch *et al.* (2007) for arguments about this). Secondly, earlier arguments concerning figures 3.7 and 3.9 indicate the sub canopy flow decouples from the above canopy flow at a height of between 4 m and 8.5 m agl, within the canopy. Consequently, any modelled value of  $\text{CO}_2$  concentration at 12.8 m agl during an advection night is likely to be significantly lower than concentrations below 4 m agl, and simultaneously higher than  $\text{CO}_2$  values between the canopy top and the IRGA at 25 m agl, and hence an uncertain estimate of  $\langle \overline{c} \rangle$  within the canopy. Although, some cancellation of these two opposite acting uncertainties may occur. Thus our vertical advection value obtained using Lee's (1998) method is uncertain both in polarity and magnitude. At best it should be regarded as an order of magnitude estimate.

In figure 3.10, the Obukhov stability values,  $z/L$ , throughout the hour show large apparent peaks of stability and instability ranging from values of -164 (very unstable)

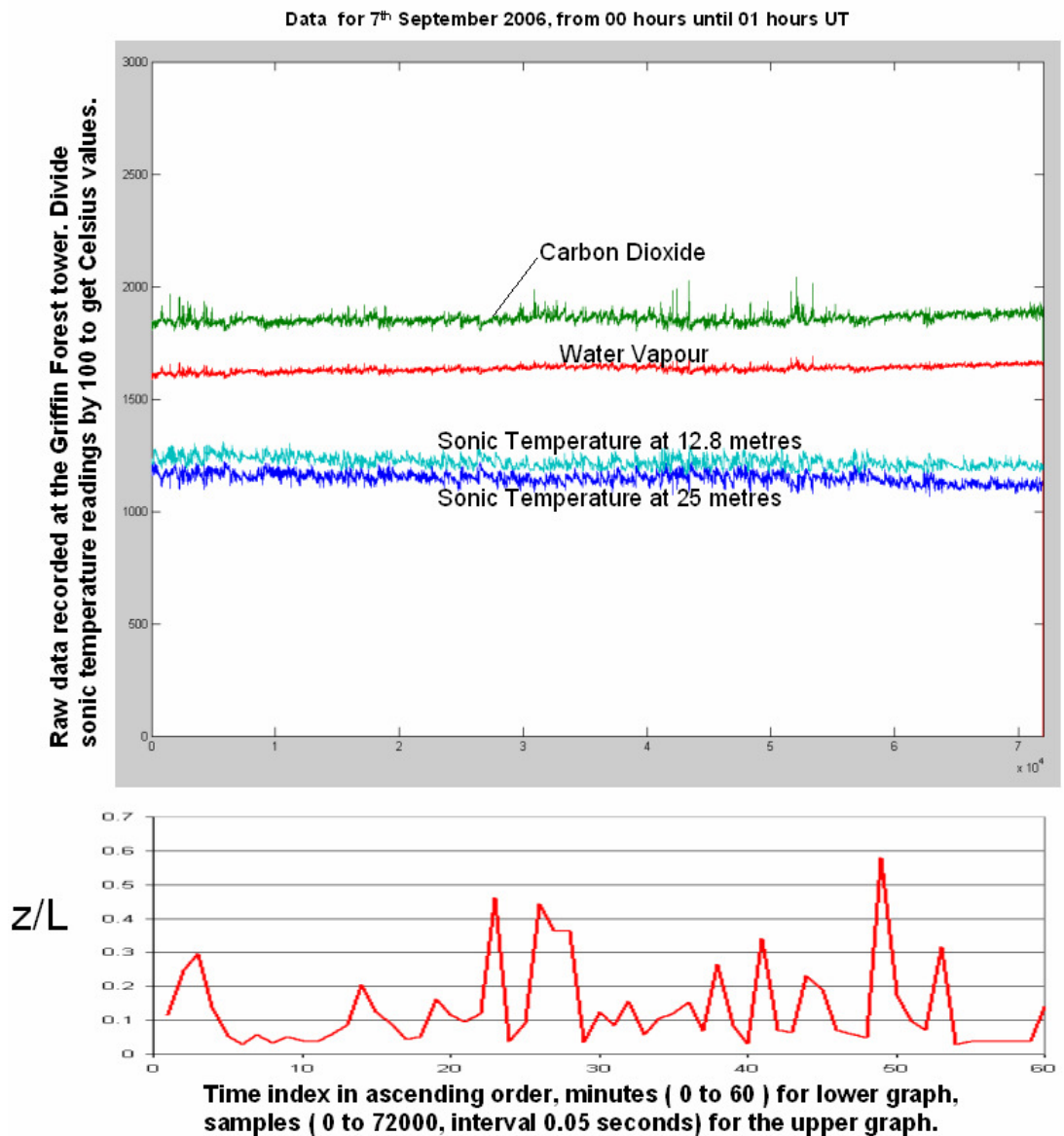
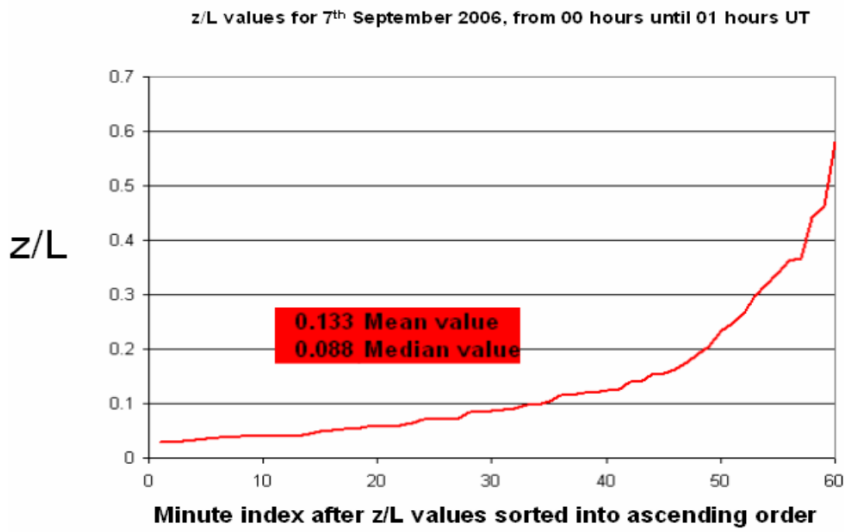


**Figure 3.11** Windy night data and stability values, in Griffin Forest. A comparison of one hour of ‘raw’ 20 Hz data collected between 00 and 01 hours GMT on the 7<sup>th</sup> September 2006, from the ultrasonic anemometer and open path infrared gas analyser (IRGA) situated at 25 m agl on the tower, and ultrasonic anemometer at 12.8 m on the tower. The lower panel shows one minute mean values of Obukhov stability values ( $z/L$ ) calculated with data from the 25 m anemometer.

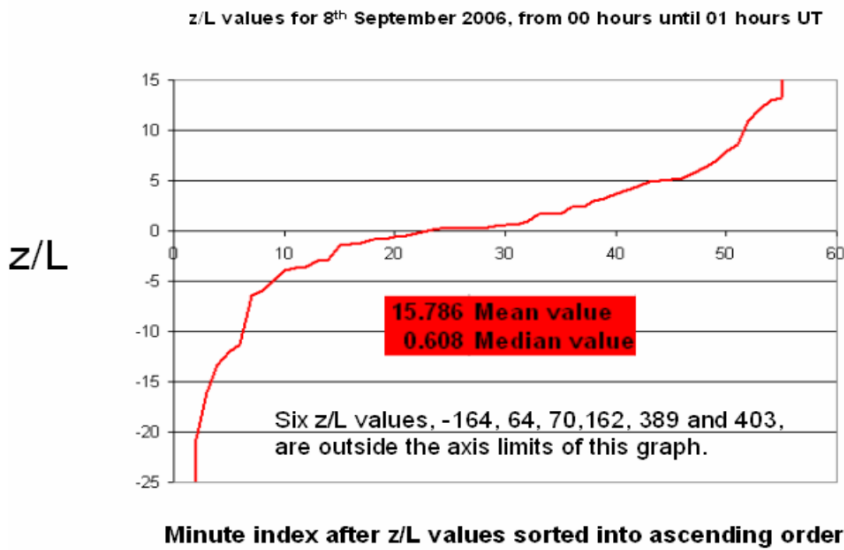
up to 403 (very stable) which may be associated with some of the carbon dioxide peaks. However, for much of the hour the stability values are closer to the 0.6 median value calculated for the hour (the mean was 15.8), and the prominent carbon dioxide concentration peaks seen at around 15 and 32 minutes into the hour seem to be associated with modestly unstable values of  $z/L$  of around -10 to -20. We may conclude that although the atmospheric situation below 25 m above ground level is stable, it is not consistently stable, but has periodic outbursts of instability. From the perspective of likely coupling between the air in the canopy and the atmosphere above, it seems likely that most of the exchange of scalars during this hour were happening during these outbursts. Finnigan and Harman (2007) discuss how intermittent turbulence can accompany the stable conditions and light winds typical of anti-cyclonic conditions, and this seems to be the situation occurring in figure 3.10.

Figure 3.11, shows the same ‘raw’ and derived plots as figure 3.10, but for exactly twenty four hours earlier, from 00 to 01 hours on the 7<sup>th</sup> September 2006. The weather conditions during this hour were as follows; no rain, but mostly overcast with atmospheric pressure increasing, and moderate winds (mean wind at a height of 25 m was  $4 \text{ m s}^{-1}$  blowing from 290 degrees, gusting between  $1 \text{ m s}^{-1}$  and  $7 \text{ m s}^{-1}$ ). Looking at figure 3.11, no large peaks are seen in the carbon dioxide concentration trace, and no corresponding large troughs are seen in the sonic temperature trace for 25 m, unlike figure 3.10. Also, there is no inverse relationship between the carbon dioxide and sonic temperature trace at 25 m. Figure 3.11 shows the sonic temperature at 25 m to be consistently lower, by about half a degree Celsius, than the sonic temperature at 12.8 m, indicating that no inversion is present within the canopy. Also, the sonic temperature traces at the two heights appear to be following each other in their movements with time, indicating that the air at 12.8 m and 25 m is well coupled throughout the hour. In figure 3.11, the water vapour trace at 25 m, tracks the carbon dioxide concentration trace, i.e. when one goes up so does the other. This is to be expected if both of these scalars have their source in the forest canopy below the sensor (as one would expect for a forest at night). The situation in figure 3.10 is surprisingly different, with the water vapour trace showing an inverse relation to the

### Windy Night



### Calm 'Advection Night'



**Figure 3.12** One minute means of Obukhov stability,  $z/L$  (sensor height / Obukhov length), values sorted into ascending order for both the 'windy night' and the 'advection night', for 00 to 01 hours GMT on the 7<sup>th</sup> and 8<sup>th</sup> September 2006 respectively. Calculated for the top ultrasonic anemometer at 25 m above ground level.

carbon dioxide concentration trace. When there are peaks in the carbon dioxide trace, there are troughs in the water vapour trace. This suggests that for 00 to 01 hours during the ‘advection night’ shown in figure 3.10, the air within the forest canopy is dryer than in the air immediately above the canopy.

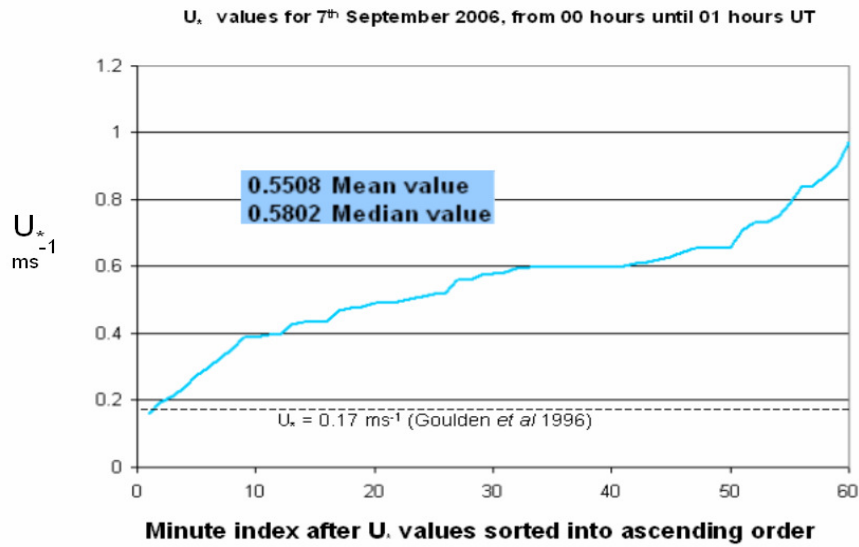
A comparison of the graphs of Obukhov stability values,  $z/L$ , from figures 3.10 and 3.11, shows marked differences. Figure 3.10, for the ‘advection night’ shows large positive and negative peaks of  $z/L$  values (in the range -164 to 403), possibly associated with the ejection of scalars from the forest canopy. Figure 3.11, which shows a relatively windy night, has entirely positive values of  $z/L$ , with a modest range of values from around 0.03 up to almost 0.6.

Comparison plots of minute mean values of Obukhov stability values,  $z/L$ , are shown in figure 3.12. These plots contain  $z/L$  values that have been sorted into ascending order for both the ‘windy night’ and the ‘advection night’. These graphs give similar information to a histogram, but without the loss of resolution caused by amalgamating the datum points into histogram bins. The range of  $z/L$  values for the ‘advection night’ is about one thousand times greater than for the ‘windy night’. The shapes of the two graphs in figure 3.12 are also very different, the ‘windy night’ one being entirely positive and almost exponential in character, while the ‘advection night’  $z/L$  graph takes the form of an inflection point linking extreme positive and negative stability values. Thus, although the mean and median values of  $z/L$  for these respective hours on the two nights are both positive, indicating stability, the stability regimes on these nights are clearly very different.

A comparison of friction velocities,  $U_*$ , measured at 25 m, for the ‘windy night’ and the ‘advection night’ are shown in figure 3.13. This figure shows two graphs of sorted one minute mean  $U_*$  values, for the period between 00 hours and 01 hours on the two consecutive nights respectively. Although both graphs are of similar shape, the values of  $U_*$  for the ‘advection night’ are ten times smaller than those of the previous ‘windy night’, i.e. 0.003 to just under 0.14, compared with 0.16 to just under 1. This indicates that production of turbulent kinetic energy by wind shear just above the forest canopy is much larger on the ‘windy night’ than on the ‘advection



### Windy Night



### Calm 'Advection Night'

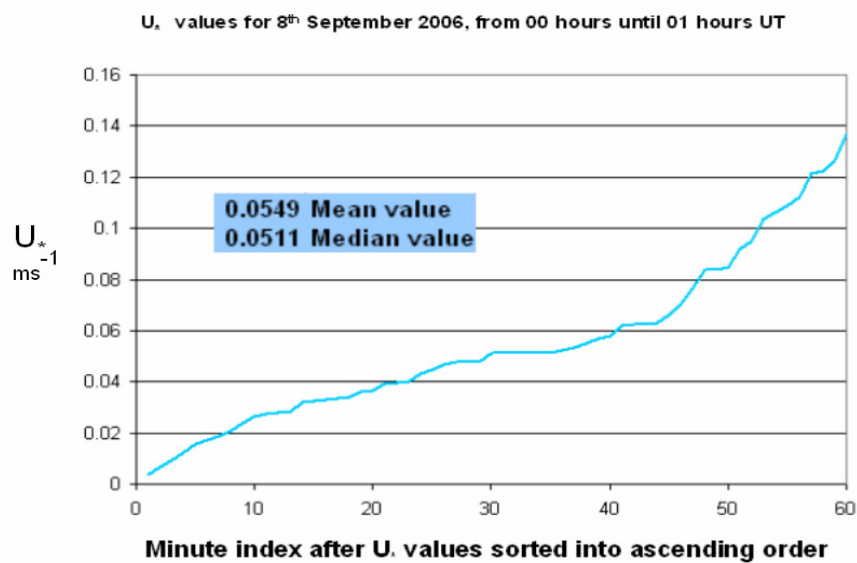


**Figure 3.13** One minute means of friction velocity ( $U_*$ ) values sorted into ascending order for both the 'windy night' and the 'advection night', for 00 to 01 hours GMT on the 7<sup>th</sup> and 8<sup>th</sup> September 2006 respectively. Calculated for the top ultrasonic anemometer at 25 m above ground level.

night', as one might expect. The friction velocity threshold of  $U_* = 0.17 \text{ m s}^{-1}$  as derived by Goulden *et al* (1996) for the Harvard Forest is shown on the graph for the 'windy night'. Although the friction velocity threshold for the Griffin Forest is probably somewhat different, it does indicate that for the 'windy night' the scalar fluxes measured by the eddy covariance system on the tower are more likely to be reliable.

In figure 3.14, the mean un-rotated vertical wind velocities ( $\overline{w}$ ) for 00 hours until 01 hours on the 'windy night' and 'advection night' respectively, are shown for four different heights on the Griffin Tower (4.0, 8.5, 12.8 and 25 m agl) and at 2.0 m agl at a location 14 m east of the tower.

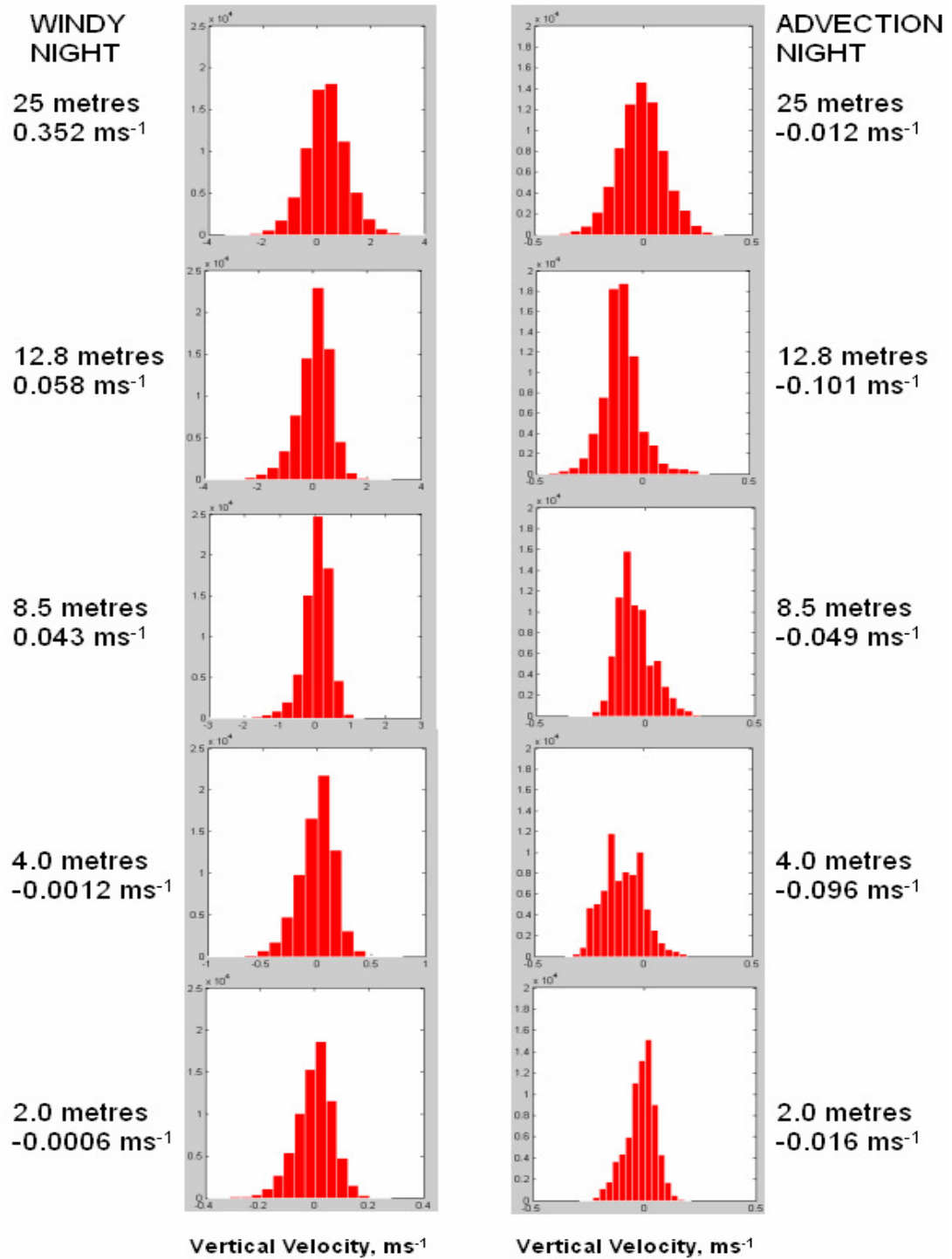
All the vertical velocities were measured by ultrasonic anemometers with their measuring centres at the quoted heights. The anemometers between 2.0 m and 12.8 m agl had all previously been levelled using 'bubble levels' to an angular accuracy of better than one degree. In addition to the mean values, histograms of vertical wind velocity were constructed and are shown in figure 3.14. Both the mean values of vertical velocity and the histograms were calculated directly from the 20 Hz values provided by the anemometers.

Figure 3.14 clearly shows that negative (downward) vertical velocities are more prevalent on the tower on the 'advection night' than on the 'windy night'. A more detailed discussion on the vertical velocities will be given later, referring to figure 3.16.

In order to provide a possibly more accurate value of vertical velocity, it was decided to make an attempt to derive vertical air velocities between anemometer levels on the tower by considering delays of cross correlation function peaks between 20 Hz vertical velocity ( $w$ ) time series measured by these anemometers. Only data from the anemometers at the 4.0, 8.5 and 12.8 m levels were used. The data from the 2.0 m level was rejected because its 14 m horizontal offset introduced an additional delay factor and the data from the 25 m level was rejected because its recording system wasn't synchronised in time sufficiently well to the other levels.

7<sup>th</sup> September 2006, from 00 hours until 01 hours UT

8<sup>th</sup> September 2006, from 00 hours until 01 hours UT



**Figure 3.14** Histograms and mean values of un-rotated vertical wind velocities ( $w$ ) for 00 hours until 01 hours on the ‘windy night’ and ‘advection night’ respectively, shown for four different heights on the Griffin Tower (4.0, 8.5, 12.8 and 25 m agl) and at 2.0 m agl at a location 14 m east of the tower.

The cross correlation algorithm used was adapted from C source code published by Bourke (1996). The cross correlation value at a lag of  $d$  samples between two time series being defined as:

$$r(d) = \frac{\sum_i [(x(i) - mx)(y(i - d) - my)]}{\sqrt{\sum_i (x(i) - mx)^2} \sqrt{\sum_i (y(i - d) - my)^2}} \quad (3-3)$$

where  $x(i)$  and  $y(i)$  are the two time series we wish to compare, and  $mx$  and  $my$  are their respective mean values. The cross correlation function was constructed by calculating the cross correlation value over a range of lags,  $d$ , which in our case was from -1000 to +1000 samples (-50 to +50 seconds).

The calculated cross-correlation functions for 00 hours to 01 hours on 7<sup>th</sup> September (the ‘windy night’) and the 8<sup>th</sup> September 2006 (the ‘advection night’) are shown in figure 3.15. Three cross-correlation functions were calculated for both the ‘windy night’ and the ‘advection night’, corresponding to cross-correlation functions between the one hour long 20 Hz time series of vertical wind velocities, at 12.8 and 8.5 m, 8.5 and 4.0 m, and 12.8 and 4.0 m agl. Displacement of the cross-correlation function peaks away from zero lag, gives the lag of signals seen at the lower height level on the tower compared to similar signals seen at the higher of the two levels on the tower used to create the cross-correlation function. These lags are annotated on figure 3.15. Time lags in seconds were obtained from these sample lags, and effective propagation velocities were calculated between the various measurement levels using the vertical distance between them.

Profiles of these effective velocities and a comparison with profiles of the directly measured un-rotated vertical velocities are shown in figure 3.16. In addition to the effective velocities derived from the Griffin forest, an additional datum point is plotted on figure 3.16 which is derived from a cross-correlation function calculated by Crowther and Hutchings (1985), using data from a tower experiment in Rivox forest, which consisted of an 11 m high Sitka Spruce canopy. In this case the anemometers were at a height of 5.9 m and 8.65 m above the ground, resulting in a

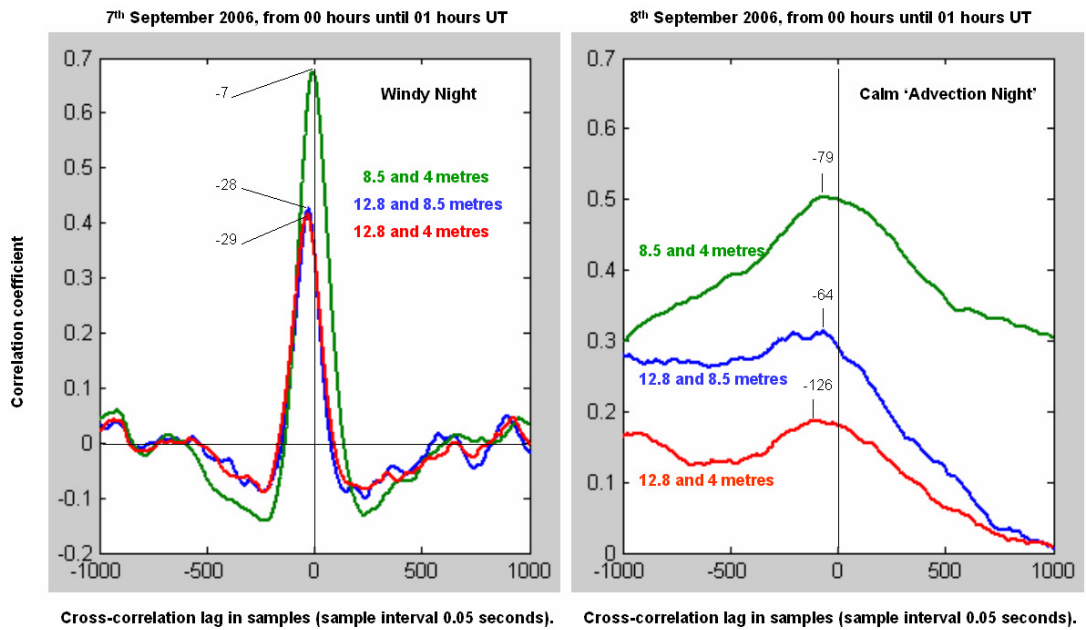


**Figure 3.15** Calculated cross-correlation functions for 00 hours to 01 hours on 7<sup>th</sup> September (the ‘windy night’) and the 8<sup>th</sup> September 2006 (the ‘advection night’). Three cross-correlation functions were calculated for each night, corresponding to cross-correlation functions between the one hour long 20 Hz time series of un-rotated vertical wind velocities, measured at 12.8 and 8.5 m, 8.5 and 4.0 m, and 12.8 and 4.0 m agl, on the Griffin Forest tower. Delay times corresponding to the displacement of the cross-correlation maxima are annotated. The sign convention used means a lower height observation lagging an observation made higher up the tower will result in a negative value.

cross-correlation lag of 1 second, which results in an effective downward vertical velocity of  $2.75 \text{ m s}^{-1}$ .

A number of issues stand out when one looks at figures 3.15 and 3.16.

Firstly, the cross-correlation function peaks are very much wider on the ‘advection night’ than on the ‘windy night’. Secondly, the magnitude of the delay lags are larger on the ‘advection night’, resulting in lower magnitude effective velocities than on the ‘windy night’. It seems that better atmospheric coupling through the canopy may be associated with higher magnitude effective cross-correlation velocities, and narrower cross-correlation peaks. This suggests that the width of the cross-correlation peak may be related to atmospheric stability within the canopy. Unfortunately, the width of such peaks are rather difficult to measure directly, unlike the lag and resulting effective vertical velocity (lower magnitude effective velocity possibly relating to higher stability).

Examining figure 3.16, a comparison of the profiles of the in situ measurements of vertical air velocity and effective vertical cross-correlation derived velocities strongly suggests they are describing two distinct and not directly related processes. The effective vertical velocities derived from cross-correlation seem to be describing some kind of ‘group velocity’ down the tower, corresponding to a ‘front’ or ‘eddy’ penetrating the canopy and hitting the tower almost from the side. Obviously, if such a ‘front’ were to pass parallel to (its normal at right angles to) the tower, then the cross-correlation lag would be zero and the effective velocity would be infinity.

Considering the un-rotated vertical velocities that were measured directly using the ultrasonic anemometers on the tower, figure 3.16 shows that between 00 and 01 hours on the ‘advection night’ downward air velocities of the order of  $0.05 \text{ m s}^{-1}$  to  $0.1 \text{ m s}^{-1}$  are present in the middle part of the forest canopy (between 4 and 13 metres above ground level). Using the method of Lee (1998) these downward velocities could be used, after a suitable coordinate rotation as discussed earlier, to estimate the NEE vertical advection term for non-zero vertical velocity, provided an estimate of carbon dioxide concentration within the canopy was available, in addition to that

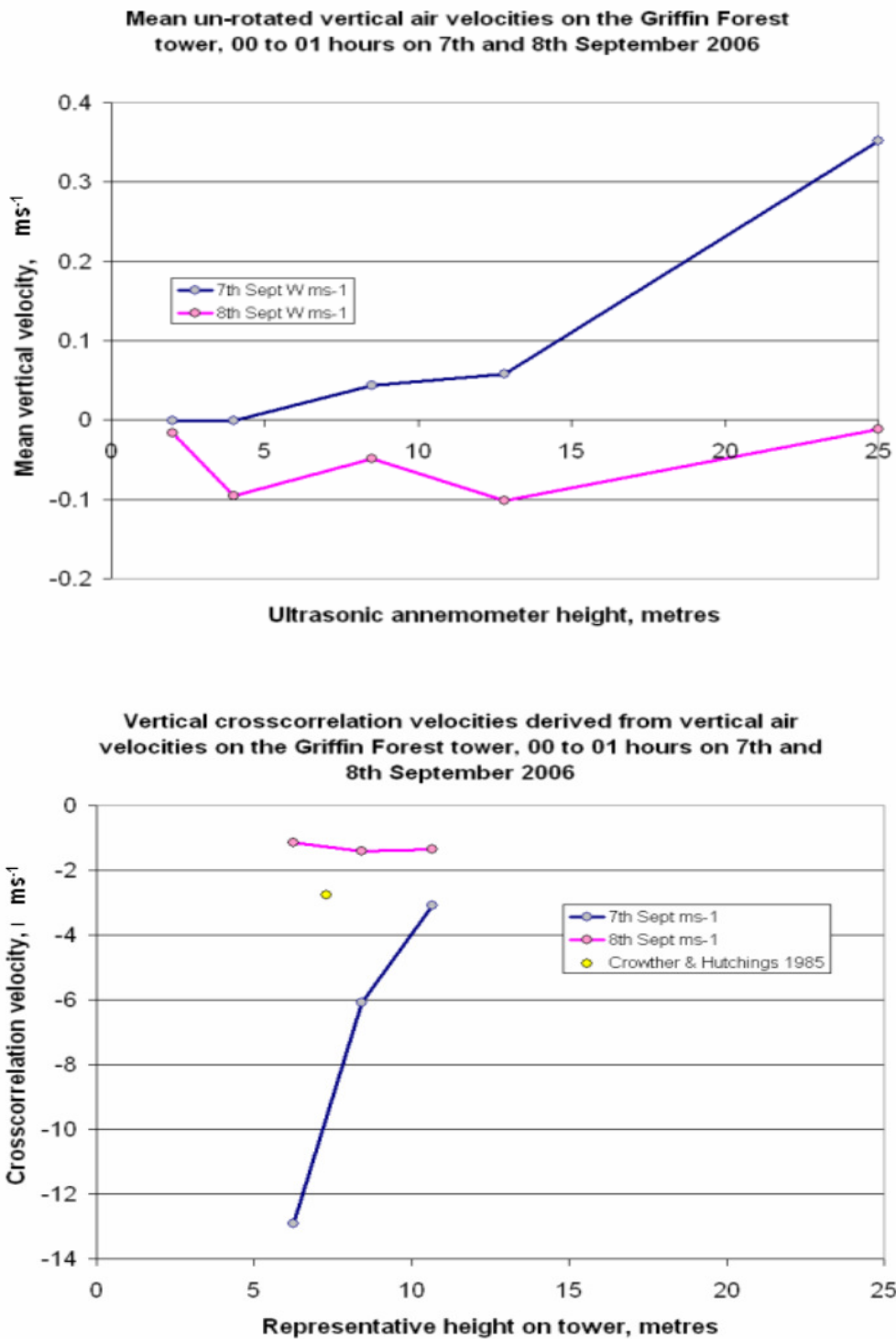


**Figure 3.16** Comparison of profiles of *in situ* measurements of un-rotated vertical air velocity and effective vertical cross-correlation derived velocities (calculated from the lags in figure 3.15) on the 25 m tower. The representative heights used to plot the cross-correlation velocities are the means of the heights of the anemometer pairs used to derive the cross-correlation functions.

measured at 25 metres height. The possible regression model for estimating the carbon dioxide concentration at 12.8 metres above ground level, discussed earlier in the text could be used to provide such an estimate of carbon dioxide concentration. Lee (1998) mentions that the sensor tilt relative to the terrain surface may contaminate the un-rotated vertical velocities, so it may be necessary to rotate the vertical velocities into a reference frame perpendicular to the terrain surface, or use a reference frame based on a long-term regression (i.e. taken over several days). For the hour of data considered for the ‘advection night’ the wind measured at 25 m above ground level is blowing in approximately the down slope direction at the experimental tower. This enables a simple trigonometric calculation to be made in order to estimate the contamination of the measured vertical velocities at the 25 m level. Given a terrain slope of 4 degrees and horizontal wind speeds of between 0.6 and 1.2 m s<sup>-1</sup>, then the expected vertical velocity contamination at 25 metres should be between -0.04 and -0.08 m s<sup>-1</sup>, if the 25 m ultrasonic anemometer is level to start with. The actual mean un-rotated vertical velocity measured at 25 metres, has a value of only -0.012 m s<sup>-1</sup> (see figure 3.14) that is three to seven times less than the expected contamination. However, this may simply imply that the 25 metre level ultrasonic anemometer is not ‘plumb’ level, and may have its base plate accidentally parallel to the horizontal flow. If this were the case, then twenty four hours earlier between 00 and 01 hours on the ‘windy night’, when the wind at 25 m was blowing in the opposite direction, up the slope, then one would not expect to see the predicted vertical velocity contamination of between 0.1 and 0.5 m s<sup>-1</sup>. However, this is not the case as the measured un-rotated vertical value is 0.35 m s<sup>-1</sup> (see figure 3.16). So, the low vertical velocity magnitude observed at 25 m on the ‘advection night’ remains a mystery.

The un-rotated vertical velocity values observed within the canopy on the ‘advection night’, of -0.05 m s<sup>-1</sup> to -0.1 m s<sup>-1</sup> at between 4 and 13 m above ground level (see figure 3.16), are of two and a half to five times the maximum magnitude of the expected vertical contamination (i.e. -0.02 to -0.04 m s<sup>-1</sup>) calculated from the ‘advection night’ horizontal wind profile, see figure 3.17. This strongly suggests that ‘real’ downward air movements are present in the canopy of the order -0.05 m s<sup>-1</sup> to



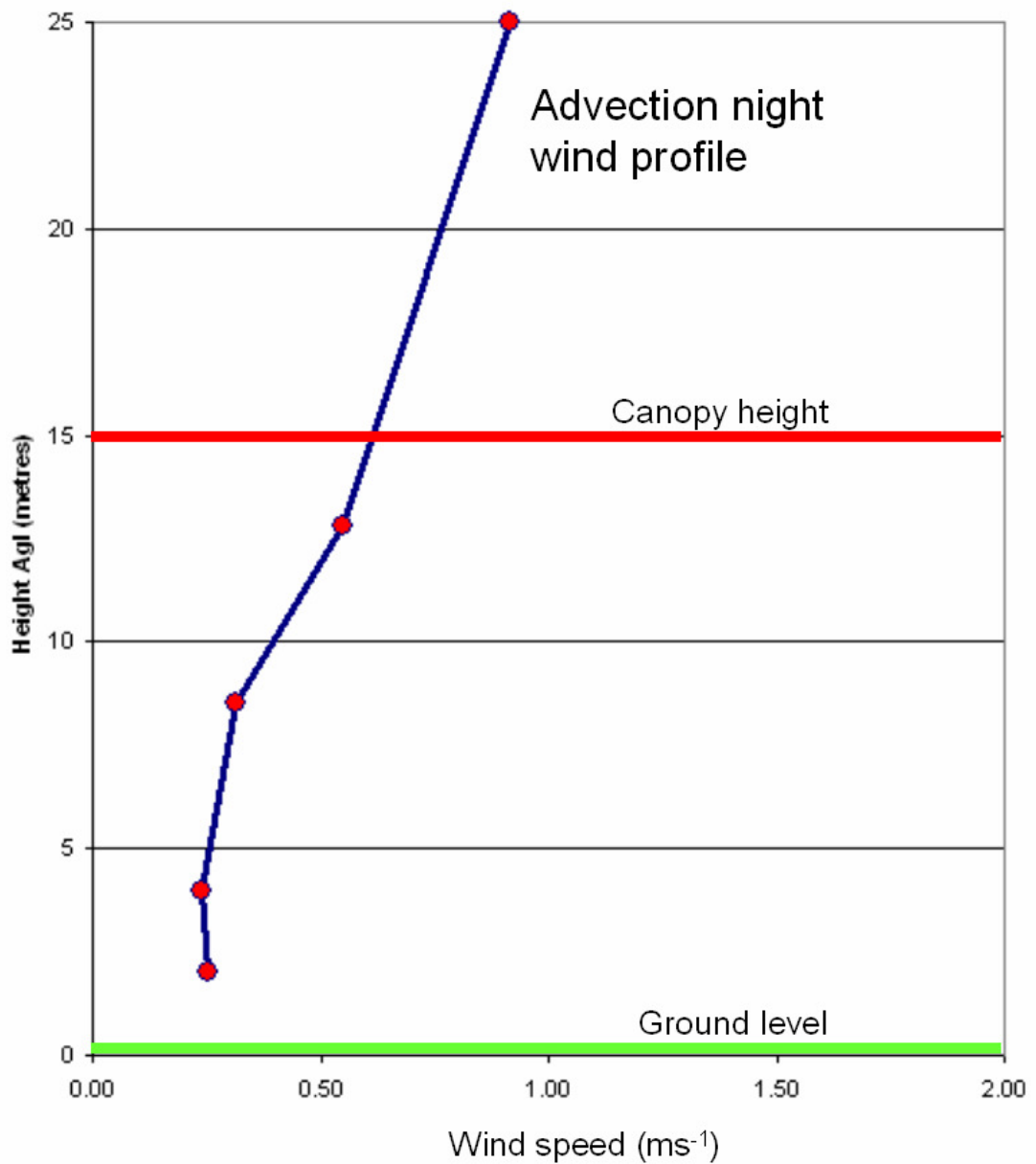


**Figure 3.17** A mean horizontal wind speed profile for (4.0, 8.5, 12.8 and 25 m agl) on the Griffin Forest tower and at 2.0 m agl at a location 14 m to the east. Calculated using data from 00 to 01 hours GMT on 8<sup>th</sup> September 2006, the ‘advection night’.

-0.1 m s<sup>-1</sup> that could be used in a Lee (1998) style of analysis, to obtain an estimate of the vertical advection term.

### 3.3.7 Discussion of the profile cross-correlation study

The effective vertical velocities within the forest canopy derived by the cross-correlation study do not seem to be simply related to the desired vertical air velocities that would be required to obtain the vertical advection term (using the method of Lee 1998) for the eddy covariance NEE estimation method. However, various other properties of the cross-correlation functions obtained, such as the width of the cross-correlation function peak, and the lag of the peak, may be an indication of the coupling between different levels in the canopy, and/or a possible indicator of the stability situation within the forest canopy.

Some of the vertical velocities measured directly by the ultrasonic anemometers on the experimental tower may be usable to estimate the vertical advection term using the method of Lee (1998). However, ‘contamination’ of these velocities by the local topography needs to be taken in to account before this can be done. The problems of using such directly measured vertical velocities with the Tumbarumba experiment data (see chapter 2) to estimate the vertical advection term, makes one sceptical that any resulting vertical advection term would be reliable. Indeed Leuning *et al.* (2008) discusses how when the corrected vertical velocity depends on both topographic slope and atmospheric stability, it is very difficult to determine if it is correct or has an unaccounted for, velocity offset. It would have been better if a vertical velocity estimate derived from the horizontal divergence method of Vickers and Mahrt (2006) and Heinesch *et al.* (2007) had been available for the profile experiment, as it had been in the Tumbarumba case (see chapter 2). However, sufficient extra sonic anemometers were not available to make the measurements required.

In order for Lee’s (1998) method to be applied, an estimation of carbon dioxide concentration within the forest canopy is required. For the ‘advection night’ an hourly regression model can probably be constructed relating CO<sub>2</sub> peaks seen at 25 m agl to the sonic temperature measured at 12.8 m, in order to estimate CO<sub>2</sub>

concentrations within the forest canopy (at 12.8 m). As discussed earlier, such an estimate of CO<sub>2</sub> concentration at 12.8 m could be used as an approximation to the mean CO<sub>2</sub> concentration,  $\langle c \rangle$ , within the canopy as required by Lee (equation 3.1).

### **3.4 Conclusions**

The horizontal transect experiment at the Griffin forest eddy flux site during winter 2005/2006, provided wind direction histograms at 1.65 m above ground level (agl) in a 15 m high Sitka Spruce canopy that indicated that under anti-cyclonic conditions the predominant wind directions near the forest floor were in the downslope/down-valley direction, during both daytime and nighttime. This was despite the presence of a significant thinning line that crossed the experimental transect at a 30 degree angle to the downslope direction. This forest thinning line was detected in the wind direction histograms only as a secondary effect, with relatively small amplitude.

Using wind vectors oriented along the long axis of the 10.8 m long experimental transect it was found that wind flow convergence occurred (at 1.65 m agl) between the ends of the transect, when the air flow was in the downslope/down-valley direction. This flow convergence might be related to the shape of the local topography out to some radius from the transect centre, however further work such as a very detailed topographic survey of the site, would be needed to confirm this.

Where the transect crossed the thinning line flow convergence was seen when air was flowing down the local slope, but divergence was seen for air flows flowing in the down the valley direction. This observed divergence is difficult to interpret but is probably associated with the presence of the thinning line.

The tower profile experiment carried out in summer and autumn 2006, as well as confirming the wind flow regime already found in the lower part of the forest canopy during the transect experiment, also allowed a qualitative model of air flow within and above the forest canopy to be constructed. Briefly, that down-valley air flows above the forest canopy appear coupled to downslope/down-valley air flows in the lower part of the forest canopy. Whilst, up-valley air flows present above the canopy

seem to prevent downslope/down-valley sub canopy flows from occurring. Further, whilst the physical height of the Spruce canopy is 15 m, the sub canopy flow regime goes from ground level to 4 m agl, followed by a transition zone from 4 m to 8.5 m agl, with the upper part of the canopy (8.5 m to 15 m agl) experiencing the same wind directions as above the canopy at 25 m agl.

In addition, the tower profile experiment demonstrated that relatively (and probably absolutely) higher wind velocities were occurring in the lower part of the canopy at night than during the day, which is suggestive of the presence of gravity flows.

A study of sonic anemometer data from the profile tower during a potentially good 'advection night' (the night of 7<sup>th</sup> to the 8<sup>th</sup> September 2006), indicated that a temperature inversion existed within the upper part of the 15 m high forest canopy (12.8 m agl), in comparison to the temperature measured 10 m above the canopy top (25 m agl). The sonic temperature and CO<sub>2</sub> concentration traces recorded during this hour indicated that features similar to 'ejections' or 'outward interactions' were taking place between the upper canopy and the atmosphere above (through the 25 m level), consistent with intermittent turbulence under conditions of light winds and stable conditions.

Obukhov stability values ( $z/L$ ) calculated at 25 m agl showed predominantly stable values (median 0.6, mean 15.8), but with outbursts of extreme positive and negative values associated with 'ejections' or 'outward interactions'. These observations along with calculated friction velocity values,  $U_*$ , were consistent with conditions under which horizontal and vertical advection flux divergences of scalars such as CO<sub>2</sub> would take place beneath an eddy covariance system on the top of the tower at 25 m agl.

For the conditions observed during the hour it was proposed that an estimate of CO<sub>2</sub> concentration could be made for 12.8 m agl in the canopy using just sonic temperatures at 12.8 m and 25 m agl, combined with CO<sub>2</sub> concentrations readings from 25 m agl, by means of a simple regression model. The measured value of CO<sub>2</sub> concentration at 25 m agl, could then be used with the estimated value within the

canopy to obtain an estimate of vertical flux divergence by means of Lee's (1998) method.

Significant vertical downward wind velocities were observed at 25 m agl and within the forest canopy (un-rotated values of  $-0.01$  to  $-0.1 \text{ m s}^{-1}$ ) during the hour of 'advection night' data considered, however issues of 'topographic contamination' make it unclear if these could be processed to yield reliable vertical advection velocities for use with Lee's (1998) method.

Cross correlation functions between vertical velocity time series ( $w$ ) measured on the profile tower were investigated to see if they could be used to directly obtain a usable vertical advection velocity that could be used directly with Lee's (1998) method. The resulting velocities appeared to be some sort of 'group velocity' not directly related to vertical velocities in the canopy, but serendipitously related to the aerodynamic coupling between the sonic anemometer observation levels, and hence indirectly stability within the canopy; a lower 'group velocity' corresponding to poorer coupling and higher stability.

It is concluded that vertical advection velocities obtained from a horizontal divergence method such as that described by Vickers and Mahrt (2006) and Heinesch *et al.* (2007), would be required to complete the vertical advection estimate using Lee's (1998) method, but unfortunately the data needed to use this approach was not available.

If further study of these datasets is to be carried out, it would be useful to perform partitioning of the data by atmospheric stability (especially stability within the forest canopy), rather than simply partitioning into daytime and nighttime values as surrogates for stability.

Calculation of the stability conditions in the lower part of the forest canopy on the 'advection night' studied (7<sup>th</sup> to the 8<sup>th</sup> September 2006) using thermocouple temperature profile data from the tower, as well as sonic anemometer data, would be particularly useful to positively determine if the air flow below 4 m agl on the tower was in fact a katabatic gravity type flow as seems likely.

## 4 Conclusions

The eddy covariance method can underestimate the nocturnal respiration fluxes of forests in complex (non flat) terrain due to the effects of katabatic/gravity flows of air in stable conditions (Goulden *et al.* 1996). These air flows can remove by direct advection (both horizontal and vertical, Feigenwinter *et al.* 2004) CO<sub>2</sub> concentrations from below the eddy covariance sensor on the tower, and if not accounted for result in a significant overestimation of the CO<sub>2</sub> sink provided by the forest. A filtering method using a friction velocity ( $U_*$ ) threshold was proposed by Golden *et al.* (1996), with the filtered data being replaced by values from a respiration model. This method is widely used across FLUXNET. However, it has been shown by Yi *et al.* (2008) that the  $U_*$  threshold filter method still seriously underestimates the nocturnal respiration flux of forests during stable conditions. As a consequence of this problem attempts are now being made to directly measure these horizontal and vertical advective fluxes inside forest canopies and use them to correct the net ecosystem exchange (NEE) estimates provided by eddy covariance (see equation 1.2). This was the subject of this thesis. The advection fluxes are estimated by making CO<sub>2</sub> concentration and wind velocity measurements around the boundaries of an instrumented ‘control volume’ (CV) enclosing the eddy covariance tower (see figure 1.2). Examples of such experimental studies to measure the full night-time mass balances at an eddy covariance tower are given in Marcolla *et al.* 2005, and Yi *et al.* 2008.

The first experiment of this MPhil was such an attempt to directly measure advection in a temperate forest. A full micrometeorological mass balance using an instrumented 6 m high Cartesian control volume (CV) covering the understorey vegetation of a 40 m high Eucalyptus forest was carried out adjacent to the Tumbaruma eddy covariance site in Australia.

At night positive (into the atmosphere) advection fluxes caused by down-slope katabatic drainage within the forest trunk space, dominated the CO<sub>2</sub> flux budget of the CV, with both vertical and horizontal advection terms having predominantly positive values. The nighttime estimates of advection were subject to large

systematic errors that were of the same order of magnitude as the advection signal. Nevertheless, the nocturnal respiration flux of the understorey vegetation was clearly resolved by the diurnal full mass balance flux curve that resulted from the experiment (see figure 2.23); this was despite anomalous results in the early part of the night that were probably due to the presence of a small gully immediately next to the CV.

The large CO<sub>2</sub> gradients that existed in the CV at night caused a requirement for vertical velocities to be known to high precision in order to calculate the vertical advection term (Leuning *et al.* 2008). It was found that only vertical velocities calculated by the continuity method (Vickers and Mahrt 2006, Heinesch *et al.* 2007) gave plausible vertical advection results, whereas vertical velocities derived from a single ultrasonic anemometer, at the top of the CV, were too imprecise to be useful. It would have been desirable to have constructed the instrumented CV to enclose the entire 40 m height of the forest, rather than just the understorey, as this would have allowed the full carbon budget of the forest to have been estimated. However, the cost and manpower required to have done this would have been excessive. Even for the experiment carried out as it was, enclosing just the understorey, the systematic errors, cost and complexity associated with the mass balance approach outweigh any advantages of the approach. The large systematic errors in the derived advection fluxes appear to be inherent with this approach (Leuning *et al.* 2008), and therefore casts doubt on the methods wider utility across FLUXNET.

A second experiment was carried out in another temperate forest, this time in the northern hemisphere to investigate flux divergence and advection effects within a forest canopy.

Horizontal transect and vertical profile wind measurements using ultrasonic anemometers were carried out at the site of an eddy covariance tower situated in a 15 m high Sitka Spruce plantation (Griffin forest) in a valley in Scotland, UK.

Wind flow divergence results obtained within the forest canopy were inconclusive. However, analysis of wind velocity data from both the profile and transect strongly suggested that sub-canopy gravity flows were occurring within the lower part of the

canopy at night, that were decoupled from the upper-canopy and above canopy flow. It was also determined that when the above canopy winds blew in an up-slope direction, the sub-canopy gravity flows were not present. During a particularly good 'advection night', consisting of anti-cyclonic conditions with clear skies, a temperature inversion existed between the upper-canopy and the above-canopy atmosphere, and indications of intermittent turbulence were present.

An attempt was made to use Lee's (1998) method to estimate vertical CO<sub>2</sub> advection, using vertical wind velocities derived from a time averaged planar fit method (Wilczak *et al.* 2001). However, the results were unreliable due to errors in the vertical velocity. If the continuity method of deriving vertical velocities (Vickers and Mahrt 2006, Heinesch *et al.* 2007) had been used instead, it is likely the vertical advection values would have been usable.

The Griffin forest experiment clearly indicates the presence of katabatic/gravity flows of the type likely to lead to horizontal advection of scalars such as CO<sub>2</sub>, which would cause eddy covariance flux estimates, if processed with the conventional  $U_*$  threshold filtering method, to underestimate nighttime respiration fluxes from the forest.

It is clear that the direct measurement of advection fluxes at eddy covariance towers using micrometeorological mass balance methods like those used at Tumbarumba (Leuning *et al.* 2008, and this thesis) and also described by Marcolla *et al.* 2005, and Yi *et al.* 2008, are not going to provide a solution to the problem of 'missing' nocturnal respiration fluxes seen at FLUXNET sites in forests, situated in complex terrain. This is simply because the approach would be too expensive and manpower intensive to deploy across FLUXNET, not to mention significant issues with systematic error.

The method described by van Gorsel *et al.* (2007) which predicts night time respiration fluxes of a forest from the maximum value of eddy covariance turbulent plus the change in storage term, that occurs after sunset, after assimilation has ended but before katabatic/gravity flows begin, might be a way forward if it can be demonstrated to work at sites other than Tumbarumba. If it works at most eddy



covariance sites, the method of van Gorsel *et al.* (2007) could provide a cheap viable alternative to the  $U_*$  threshold filter method presently used widely across FLUXNET.

An alternative way in which the advection terms for eddy covariance sites could be predicted is through the use of data assimilation models (Finnigan 2008), similar to the models that exist today for numerical weather prediction (NWP). Finnigan (2008) is optimistic that such models would be able to provide advection estimates (and hence an estimate of the missing nocturnal respiration fluxes) for those FLUXNET sites that are subject to predictable daytime and nighttime flow fields. Information presented in this thesis suggests that both the Tumbarumba and Griffin forest eddy covariance sites probably come into this category. However, there is a problem in that no suitable data assimilation models exist at present (Finnigan 2008, Belcher *et al.* 2008). The models that exist today are too simple for use in data assimilation (Belcher *et al.* 2008, Sogachev *et al.* 2008), although useful for site selection and planning measurement strategies (Finnigan 2008). Today's models are a useful starting point for development towards usable data assimilations models, but if the development of similar NWP data assimilation models for weather forecasting is used as a guide this may take many years (Shuman 1989).

## 5 References

- Anderson, D. E., S. B. Verma, and N. J. Rosenberg, 1984: Eddy correlation measurements of CO<sub>2</sub>, latent heat and sensible heat fluxes over a crop surface. *Bound.-Layer Meteor.*, vol 29, 167–183.
- Andreae, M. O., and P. Artaxo, C. Brandao, F. E. Carswell, P. Ciccioli, A. L. da Costa, A. D. Culf, J. L. Esteves, J. H. C. Gash, J. Grace, P. Kabat, J. Lelieveld, Y. Malhi, A. O. Manzi, F. X. Meixner, A. D. Nobre, C. Nobre, M. d. L. P. Ruivo, M. A. Silva-Dias, P. Stefani, R. Valentini, J. von Jouanne, and M. J. Waterloo (2002) Biogeochemical cycling of carbon, water, energy, trace gases, and aerosols in Amazonia: The LBAEUSTACH experiments, *J. Geophys. Res.*, 107(D20), 8066.
- Aubinet, M., and Coauthors, 2000: Estimates of the annual net carbon and water exchange of European forests: The EUROFLUX methodology. *Adv. Ecol. Res.*, vol 30, p113–175.
- Aubinet, M., 2008. Eddy covariance CO<sub>2</sub> flux measurements in nocturnal conditions: An analysis of the problem. *Ecological Applications*: Vol. 18, No. 6, pp. 1368-1378.
- Aubinet, M., Berbigier, P., Bernhofer, C.H., Cescatti, A., Feigenwinter, C., Granier, A., Grünwald, T.H., Havrankova, K., Heinesch, B., Longdoz, B., Marcolla, B., Montagnani, L., Sedlak, P., 2005. Comparing CO<sub>2</sub> Storage and Advection Conditions at Night at Different Carboeuroflux Sites. *Boundary-Layer Meteorology*, vol 116, p63–94.
- Aubinet, M., Heinesch, B., Yernaux, M., 2003. Horizontal and vertical CO<sub>2</sub> advection in a sloping forest. *Boundary-Layer Meteorol.* Vol 108, pp 397-417.
- Baldocchi D, and Coauthors, 2001. FLUXNET: A new tool to study the temporal and spatial variability of ecosystem-scale carbon dioxide, water vapor, and energy flux densities. *Bulletin of the American Meteorological Society* 82:2415–2434.
- Baldocchi, D.D., 2003. Assessing the eddy covariance technique for evaluating carbon dioxide exchange rates of ecosystems: past, present and future. *Global Change Biology*, 9, 479-492.
- Barcza, Z., 2001. Long term atmosphere/biosphere exchange of CO<sub>2</sub> in Hungary. *Ph.D. dissertation, Eotvos Lorand University.*
- Belcher, S. E., Finnigan, J. J., and Harman, I. N., 2008. Flows through forest canopies in complex terrain. *Ecological Applications*, Vol. 18, No. 6, pp. 1436-1453.
- Black, T. A., Den Hartog, G., Neumann, H. H., Blacken, P. D., Yang, P. C., Russel, C., Nesic, Z., Lee, X., Chen, G., Steabler, R., Novak, M. D., 1996. Annual cycles of water vapour and carbon dioxide fluxes in and above a boreal aspen forest. *Global Change Biology*. vol 2, p219-229.

- Clement, R. J., 2004. Mass and Energy Exchange in a Plantation Forest in Scotland Using Micrometeorological Methods. *Ph.D. thesis, University of Edinburgh*.
- Clement, R., Moncrieff, J. B., Jarvis, P. G., 2003. Net Carbon Productivity of Sitka Spruce Forest in Scotland. *Scottish Forestry*, Vol 57, No 1.
- Crowther, J.M., and Hutchings, N.J., 1985. Correlated vertical wind speeds in a spruce canopy. In: *The Forest-Atmosphere Interaction* (eds Hutchinson, B.A., and Hicks, B.B.), pp.543-561. D. Reidel, Dordrecht.
- de Araujo, A. C., B. Kruijt, A. D. Nobre, A. J. Dolman, M. J. Waterloo, E. J. Moors, and J. S. de Souza. 2008. Nocturnal accumulation of CO<sub>2</sub> underneath a tropical forest canopy along a topographical gradient. *Ecological Applications*, vol 18, p1406–1419.
- Feigenwinter, C., Bernhofer, C., and Vogt, R., 2004: The Influence of Advection on the Short Term CO<sub>2</sub>-Budget in and Above a Forest Canopy. *Bound.-Layer Meteor.*, Vol 113, No. 2, p 201-224.
- Finnigan, J., 1999. A Comment on the Paper by Lee (1998): On Micrometeorological Observations of Surface-Air Exchange Over Tall Vegetation. *Agr. Forest Meteorol.* vol 97: p55-64.
- Finnigan, J. J., 2003. A Re-Evaluation of Long-Term Flux Measurement Techniques, Part 2: Coordinate Systems. *Bound-Lay. Meteorol.* vol 113. no 1, p1-41.
- Finnigan, J., 2006. The storage term in eddy flux calculations. *Agricultural and forest Meteorology.*, Vol 136, Issue 3-4, p 108-113.
- Finnigan, J., 2008. An introduction to flux measurements in difficult conditions. *Ecological Applications*, vol 18:6, 1340-1350.
- Finnigan, J. J., and S. E. Belcher. 2004. Flow over a hill covered with a plant canopy. *Quarterly Journal of the Royal Meteorological Society* 130:1–29.
- Foken, T., 2008. The energy balance closure problem: an overview. *Ecological Applications*: Vol. 18, No. 6, pp. 1351-1367.
- Foken, T., and Nappo, C. J., 2008. *Micrometeorology. Translated by Nappo, C. J. Published by Springer*, pp306. [ISBN 354074665X]
- Foken, T., and Oncley, S. P., 1995. Results of the workshop ‘Instrumental and methodological problems of land surface flux measurements.’ *Bulletin of the American Meteorological Society*, 76: p 1191-1193.
- Fritschen, L. J. 1985. Characterization of boundary conditions affecting forest environmental phenomena. - In: *Hutchison, B. A. and Hicks, B. B. (eds), The forest atmosphere interaction*. Reidel, pp. 3-23.

- Garrat, J. R., 1994. The atmospheric boundary layer. *Cambridge University Press*, pp316. [ISBN 0521467454]
- Goulden, M. L., Miller, S. D., and da Rocha, H. R., 2006. Nocturnal cold air drainage and pooling in a tropical forest. *Journal of Geophysical Research* 111:D08S04. [doi: 10.1029/2005JD006037]
- Goulden, M.L., Munger, J.W., Fan, S.-M, Daube, B.C, Wofsy, S.C., 1996. Measurements of Carbon Sequestration by Long-term Eddy Covariance: Methods and a Critical Evaluation of Accuracy. *Glob. Change Biol.*, vol 2: p169-182.
- Grace J, Malhi Y, Lloyd J, McIntyre J, Miranda AC, Meir P and Miranda HS., 1996. The use of eddy covariance to infer the net carbon dioxide uptake of Brazilian rain forest. *Global Change Biology*, vol 2: p209-218.
- Harman, N. H., and Finnigan, J. J., 2007. A simplified unified theory for flow in the canopy and roughness sublayer. *Boundary Layer Meteorol.*, vol 123, p339-363.
- Heinesch, M. Yernaux and M. Aubinet, 2007. Some methodological questions concerning advection measurements: a case study, *Boundary-Layer Meteorol.* vol 122 , pp. 457–478.
- Houghton, J. T., G. J. Jenkins and J. J. Ephraus (eds.) (1990): *Climate Change*. The IPCC Scientific Assessment. Cambridge University Press, New York, 365 pp.
- Katul, G., Finnigan, J.J., Leuning, R, and Belcher, S. E., 2003. The influence of hilly terrain on canopy-atmosphere carbon dioxide exchange. *Q.J. Roy. Meteorol. Soc.* vol 118, no 1, p189-216.
- Katul, G. G., J. J. Finnigan, D. Poggi, R. Leuning, and S. E. Belcher. 2006. The influence of hilly terrain on canopy–atmosphere carbon dioxide exchange. *Boundary-Layer Meteorology*, 118: p189–216.
- Keeling, C.D. and T.P. Whorf. 2004. Atmospheric CO<sub>2</sub> concentrations derived from flask air samples at sites in the SIO network. In *Trends: A Compendium of Data on Global Change*. Carbon Dioxide Information Analysis Center, Oak Ridge National Laboratory, U.S. Department of Energy, Oak Ridge, Tennessee, U.S.A.
- Kutch, W. L., Kolle, O., Rebmann, C., Knohl, A., Ziegler, W., and Schulze, E. D., (2008) Advection and resulting CO<sub>2</sub> exchange in a tall forest in central Germany: Ecological Applications: Vol. 18, No. 6, pp.1391-1405.
- Lee,X., 1998. On Micrometeorological Observations of Surface-air Exchange over Tall Vegetation. *Agr. Forest Meteorol.* vol 91: p39-49.
- Leuning, R., Cleugh, H, A., Zegelin, S, J., and Hughes, D., 2005. Carbon and water fluxes over a temperate *Eucalyptus* forest and a tropical wet/dry savanna in Australia: measurements and comparison with MODIS remote sensing estimates. *Agricultural and Forest Meteorology.* vol 129, iss 3-4, p151-173.

- Leuning, R., Zegelin, S. J., Jones, K., Keith, H., Hughes, D., 2008. Measurement of horizontal and vertical advection of CO<sub>2</sub> within a forest canopy. *Agricultural and Forest Meteorology*, vol148, pp. 1777-1797.
- Mahrt, L., (1981) The early evening boundary layer transition. *Quart. J. Roy. Meteorol. Soc.* Vol 107, pp 329-343.
- Mahrt, L., 1999: 'Stratified atmospheric boundary layers.' *Boundary-Layer Meteorol.*, vol 90, 375-396.
- Maidment, D. R., 1993. Developing a spatially distributed unit hydrograph by using GIS. *International Association of Scientific Hydrology Publications*, 211, p181-192.
- Malhi, Y., Nobre A. D., Grace J., Kruijt B., Pereira M. G. P., Culf A. & Scott S. 1998 Carbon dioxide transfer over a Central Amazonian rain forest. *Journal of Geophysical Research-Atmospheres* 103, 31593-31612.
- Marcolla, B., Cescatti, A., Montagnani, L., Manca, G., Kerschbaumer, G., and Minerbi, S., 2005. Importance of advection in the atmospheric CO<sub>2</sub> exchanges of an alpine forest. *Agric. For. Meteorol.* vol 130, p193-206.
- Miller, S. D., and Goulden, M. L., Menton, M. C., da Rocha, H. R., de Frettas, H. C., Michela, A., Figueira, S., and de Sousa, C. A. D., 2004. Biometric and Micrometeorological Measurements of Tropical Forest Carbon balance. *Ecological Applications*, 14(4) Supplement, 2004, pp S114-S126.
- Moncrieff, J., Clement, R., Finnigan, J., Meyers, T., 2004. Averaging, Detrending, and Filtering of Eddy Covariance time series. *In Handbook of Micrometeorology, Ch 2, p7-31, (eds) X. Lee et al.*
- Moncrieff, J. B., Massheder, J. M., de Bruin, H., Elbers, J., Friborg, T., Hensinkveld, B., Kabat, P., Scott, S., Soegaard, H., and Verhoef, A., 1997. A system to measure surface fluxes of momentum, sensible heat, water vapour and carbon dioxide. *J.Hydrol*, 188-189, p589-611.
- Monin, A. S., and Obukhov, A. M., 1954. Basic laws of turbulent mixing in the atmosphere near the ground. *Tr. Akad. Nauk SSSR Geofiz. Inst.* 24(151), p163-187.
- Ohkubo, S., Kosugi, Y., Takanashi, S., Mitani, T., and Tani, M., 2007. Comparison of the eddy covariance and automated closed chamber methods for evaluating nocturnal CO<sub>2</sub> exchange in a Japanese cypress forest. *Agricultural and Forest Meteorology*, Vol 142, Issue 1, p 50-65.
- Pachauri, R.K and Reisinger, A., 2007. IPCC : Climate Change 2007: Synthesis Report. Contribution of Working Groups I, II and III to the Fourth Assessment Report of the Intergovernmental Panel on Climate Change [Core Writing Team, Pachauri, R.K and Reisinger, A. (eds.)]. IPCC, Geneva, Switzerland, 104 pp.

- Raupach, M. R., Finnigan, J. J., 1997. The influence of topography on meteorological variables and surface-atmosphere interactions. *J. Hydrol.* vol 190, p182-213.
- Reynolds, O., 1895. On the dynamical theory of incompressible viscous fluids and the determination of criterion. *Philosophical Transactions of the Royal society of London*, A174, 935-982.
- Ross, A. N., and S. B. Vosper. 2005. Neutral turbulent flow over forested hills. *Quarterly Journal of the Royal Meteorological Society* 131:1841–1862.
- Running, S. W., D. D. Baldocchi, D. Turner, S. T. Gower, P. Bakwin, and K. Hibbard, 1999: A global terrestrial monitoring network, scaling tower fluxes with ecosystem modelling and EOS satellite data. *Remote Sens. Environ.*, 70, p108–127.
- Ruppert, J., Mauder, M., Thomas, C., and Luers, J., 2006. Innovative gapfilling strategy for annual sums of CO<sub>2</sub> net ecosystem exchange, *Agric. Forest Meteorol.*, vol 138, p5–18.
- Schmid, H. P.: 1994. Source Areas for Scalars and Scalar Fluxes. *Boundary-Layer Meteorol.* Vol 67, p293–318.
- Sellers, P. J., and Coauthors, 1997: BOREAS in 1997: Scientific results, experimental overview and future directions. *J. Geophys. Res.*, 102, 28 731–28 770.
- Shuman, F.G., 1989: History of Numerical Weather Prediction at the National Meteorological Center. *Wea. Forecasting*, vol 4, p286–296.
- Sogachev, A., M. Y. Leclerc, G. Zhang, U. Rannik, and T. Vesala. 2008. CO<sub>2</sub> fluxes near a forest edge: a numerical study. *Ecological Applications*, vol 18(6): p1454–1469.
- Staebler, R. M., and D. R. Fitzjarrald. 2004. Observing subcanopy CO<sub>2</sub> advection. *Agricultural and Forest Meteorology* 122(3–4):139–156.
- Swinbank, W.C., 1951. The measurement of vertical transfer of heat and water vapour by eddies in the lower atmosphere. *Journal of applied Meteorology*, vol 8, p135-145.
- Tanner, C. B., Thurtell, G. W., 1969. Anemoclinometer measurements of Reynolds stress and heat transport in the atmospheric boundary layer. *Research and Development Technical Report ECOM-66-G22F, University of Wisconsin, Madison, Wisconsin.*
- van Gorsel, E., Leuning, R., Cleugh, H.A., Keith, H., Kirschbaum, M. U. F., Suni, T., 2008. Application of an alternative method to derive reliable estimates of nighttime respiration from eddy covariance measurements in moderately complex topography. *Agricultural and Forest Meteorology*. Vol 148, Issue 6-7, p 1174-1180.

van Gorsel, E., Leuning, R., Cleugh, H.A., Keith, H., Suni, T., 2007. Nocturnal carbon efflux: reconciliation of eddy covariance and chamber measurements using an alternative to the  $u^*$ -threshold filtering technique. *Tellus* 59B, 397–403.

Verma, S. B., D. D. Baldocchi, D. E. Anderson, D. R. Matt, and R. E. Clement, 1986: Eddy fluxes of CO<sub>2</sub> water vapour, and sensible heat over a deciduous forest. *Bound.-Layer Meteor.*, vol 36, p71–91.

Vickers, D., and Mahrt, L., 2006. Contrasting mean vertical motion from tilt correction methods and mass continuity, *Agric. For. Meteorol.* vol 138, p. 93–103.

Webb, E. K., Pearman, G. I., Leuning, R., 1980. Correction of flux measurements for density effects due to heat and water vapour transfer. *Quarterly Journal of the Royal Meteorological Society*, Vol 106, p85-100

Wilczak, J. M., Oncley, S. P., and Stage, S. A., 2001. Sonic anemometer tilt correction algorithms. *Boundary Layer Meteorology*. Vol 99, p127-150.

Wofsy, S. C., M. L. Goulden, J. W. Munger, S. M. Fan, P. S. Bakwin, B. C. Daube, S. L. Bassow, and F. A. Bazzaz, 1993: Net exchange of CO<sub>2</sub> in a mid-latitude forest. *Science*, vol 260, p1314–1317.

Yi, C., Anderson, D. E., Turnipseed, A. A., Burns, S. P., Sparks, J. P., Stannard, D. I., and Monson, R. K., 2008. The contribution of advective fluxes to net ecosystem exchange in a high-elevation, subalpine forest. *Ecological Applications*: Vol. 18, No. 6, pp. 1379-1390.

## Website References

Bourke, P., 1996. Website, Title: Cross Correlation  
URL: <http://local.wasp.uwa.edu.au/~pbourke/miscellaneous/correlate/>  
Accessed: 31 October 2008.

FLUXNET website, Figure title: Growth of Fluxnet towers as of March 30, 2008.  
URL: [http://public.ornl.gov/fluxnet/Images/Fluxnet\\_Growth\\_April2008.jpg](http://public.ornl.gov/fluxnet/Images/Fluxnet_Growth_April2008.jpg)  
Accessed: 21 October 2008.

## Appendix

The paper by Leuning *et al.* (2008) relating to the experiment described in chapter 2 of this thesis is:

Leuning, R., Zegelin, S. J., Jones, K., Keith, H., Hughes, D., 2008. Measurement of horizontal and vertical advection of CO<sub>2</sub> within a forest canopy. *Agricultural and Forest Meteorology*, vol 148, pp. 1777-1797.

The full text of Leuning *et al.* (2008) may be obtained at:

<http://dx.doi.org/10.1016/j.agrformet.2008.06.006>

Note: Kevin H. Jones is a co-author.